Screening Potential and Bound State Properties in Strongly Coupled Quark Gluon Plasma

Thesis submitted to the University of Calicut

in partial fulfillment of the requirements

for the award of the degree of

Doctor of Philosophy

in

Physics

Rethika K T

Department of Physics

University of Calicut

Malappuram, Kerala - 673635

November 2021

CERTIFICATE

Certified that the work presented in this thesis entitled 'Screening Potential and Bound State Properties in Strongly Coupled Quark Gluon Plasma' is a bonafide work done by Mrs. Rethika K T under our guidance for the award of the degree of Doctor of Philosophy in the Department of Physics, University of Calicut and that this work has not been included in any other thesis submitted previously for the award of any degree.

C. U. campus
Date:

Dr. C. D. Ravikumar
(Co-Guide)

Dr. Vishnu Mayya Bannur
(Supervising Guide)

DECLARATION

I hereby declare that the work presented in this thesis entitled 'Screening Potential and Bound State Properties in Strongly Coupled Quark Gluon Plasma' is based on the original work done by me under the guidance of Dr. Vishnu Mayya Bannur (Guide), and Dr. C D Ravikumar (Co-Guide), Department of Physics, University of Calicut, and has not been included in any other thesis submitted previously for the award of any degree.

University of Calicut

Date: Rethika K T

Publications and Presentations

Publications in International Journals

1. **K. T. Rethika**, V. M. Bannur, *Screening of a Test Quark in the Strongly Coupled Quark Gluon Plasma.*, Few-Body Syst 60, 38 (2019)

2. **K. T. Rethika**, C. D. Ravikumar, V. M. Bannur, *Heavy Quarkonium Properties at Finite Temperature in Strongly Coupled Quark Gluon Plasma,* Few-Body Syst 62, 10 (2021)

Papers Presented in International / National Conferences

1. **K. T. Rethika**, V. M. Bannur, *Acoustic Waves in the Strongly Coupled Quark Gluon Plasma*, National Conference on Fundamental and Applied Physics on 12^{th} and 13^{th} November 2019 at University College, Trivandrum

2. **K. T. Rethika**, C. D. Ravikumar, V. M. Bannur, *Temperature Dependent Screening Potential*, ESTEEM 2021 on 21^{st} and 22^{nd} January 2021, at MANIT, Bhopal

3. **K. T. Rethika**, C. D. Ravikumar, V. M. Bannur, *Binding Energies of Diquarks*, International Conference on Advanced Physics 2021 (IEMPHYS 2021) on$1^{st} - 3^{rd}$ April 2021 at IEM, Kolkata

ACKNOWLEDGEMENTS

I would like to express my sincere gratitude to my supervisor, Dr. Vishnu Mayya Bannur, who has been the cornerstone of my Ph.D. I would like to thank him for the initial direction, and the direction provided at every point. Without his support and guidance, the PhD would have been impossible to accomplish. I am indebted to my co-guide Dr. C D Ravikumar for giving me support for submitting the thesis. He has been patient and encouraging. I am grateful to him for his kind discussions. I express my heartfelt thanks to Dr. Vinodkumar, for the support during the course of this work.

I thank my co-researchers Dr. Prasanth Jayaprakash and Dr. Sebastian Koothottil for their creative discussions. Also I thank Dr. Sineeba Ramadas, Anjana A V, Jisha, Nighilnath who have been helpful in one way or another. I am thankful to the faculty members and non-teaching staff of the Department of Physics, University of Calicut.

I express my deep gratitude and love to my family for their immense encouragements.

Contents

List of Figures

List of Tables

Preface

Both experimental and lattice results show that the matter formed near and just above the transition temperature is non-ideal. There are lots of attempts to explain such a matter using various phenomenological models. The quark-gluon plasma near T_c is called strongly coupled quark-gluon plasma (SCQGP) and can be treated as the strongly coupled QED plasma with a few modifications due to color degrees of freedom. The aim of this work is to study the screening potential and the properties of bound states in SCQGP.

The thesis is structured as follows

The purpose of chapter 1 is to give a small introduction to QGP. We start with the theory of quarks and gluons and a brief description of quantum chromodynamics. We then give an introduction to the different phenomenological models of QGP.

In chapter 2, we calculate the screening potential of a test quark entering into the strongly coupled QGP using generalized hydrodynamic equations. Also, we investigate the temperature dependence of the screening potential. We try to explain the existence of bound states and the expected J/ψ suppression in connection with the potential.

In chapter 3, we calculate the binding energy of the bound states of quarks by solving the N-dimensional radial Schrödinger equation using this potential in three different methods. i.e., analytical exact iteration method (AEIM), power series method (PSM), and Nikiforov-Uvarov (NU) method. The energy eigenvalues have

been calculated in the N-dimensional space for any state (n, l).

In chapter 4, we study the binding energies of scalar diquarks using AEIM and PSM and plotted as functions of temperature. Effective masses of diquarks are calculated using the binding energies at finite temperature in the strongly coupled quark-gluon plasma.

In chapter 5, the quarkonium properties are studied in two methods. i.e. AEIM and NU Method. The variations in binding energy and mass spectra with temperature have been studied in the N-dimensional space. The dissociation temperatures for different states of quarkonia are calculated in the N-dimensional space. Also, we discuss the influence of dimensionality number on the dissociation temperatures.

In chapter 6, we study the properties of $b\overline{c}$ and $c\overline{s}$ mesons. Variations of binding energy and mass spectra with temperature have been studied for different dimensions. The dissociation temperatures for different states of $b\overline{c}$ and $c\overline{s}$ mesons are also calculated.

Chapter 7 summarizes our results and provides conclusion and an outlook regarding our future work.

Chapter 1

The Quark-Gluon Plasma

1.1 Introduction

In 1897, the electron was discovered by J.J. Thompson using a cathode-ray tube. This event set the stage for modern particle physics. The proton and neutron were discovered subsequently. These three particles were initially regarded as elementary particles. But soon there occurred propagation in the inventory of the so-called elementary particles. In 1937, the study of cosmic rays led to the discovery of muons. A decade later, pions and strange particles were discovered. In the 1950s, the study was shifted from cosmic rays to man-made particle accelerators. The use of particle accelerators helped to discover a large number of new particles including mesons of spin higher than zero and baryons of spin higher than half with various values of charge and strangeness. These new particles are generally called hadrons. Though unstable, they exhibit similar behavior to protons and neutrons. These hadrons including the nucleons are transformed into each other in many complex ways. Now the physicists had to deal with these hadrons and

their interactions. The interaction between hadrons came to be known by a new name, the strong interaction.

The rapidly increasing number of hadrons showed that they could not be elementary. Studies on the classification mechanism, mass spectra and interactions of hadrons revealed that the hadrons were made up of more fundamental elementary particles -the quarks. In the 1960s, M. Gell-Mann and G. Zweig independently proposed the quark model [1,2]. It was then necessary to understand the quark dynamics which is responsible for the composition of hadrons and hadronic interactions. The non-abelian gauge theory, first proposed by Yang and Mills [3] was later found applicable to strong interactions also [4,5]. Gell-Mann named it as Quantum chromodynamics (QCD). QCD is a gauge theory of strong interactions based on color symmetry group SU(3) in which the non-abelian gauge field called the gluon (which is a boson), belongs to the octet representation of color SU(3). The color interactions between quarks are being mediated by the gluons and hence the binding of quarks occurs. Gluons carry color charges and hence they can interact with each other even in the absence of quarks.

Quarks fall into the fundamental triplet representation of the color SU(3) group. Each quark carries a color quantum number which can have three values (red, blue, green). Properties of quarks according to the standard model are given in Table 1.1 [6]. Six types of quarks have been discovered till now. (up (u), down (d), strange (s), charm (c), bottom (b), and top (t) quarks). The electric charges for the up, charm, and top quarks are $+\frac{2}{3}e$ and for down, strange, and bottom quarks, $-\frac{1}{3}e$. All the six quarks have spin $\frac{1}{2}$ and baryon number, B=$\frac{1}{3}$. Experimentally no colored particles have been detected. So it is proposed that only uncolored particles (color singlet) are observable. This is the hypothesis of color confinement. Thus

three quarks combine to form a colorless baryon and a quark and antiquark are combined to form a meson.

In 1968, the first experimental evidence of quarks as constituents of hadrons came from the inelastic electron-proton scattering experiments performed at the Stanford Linear Accelerator Centre (SLAC). The scattering cross sections provided evidence of elastic scattering from the point-like objects inside the proton [7]. The experimental results at SLAC could be explained only if quarks inside a proton are nearly free as was proposed by Feynman. Now there emerged a paradox. The strong interaction is powerful to permanently confine the particles within the hadron. But Feynman suggested that the interaction between the quarks should be weak enough at short distances so that the quarks can behave as free particles [8]. This paradox was solved by David Gross, Wilczek, and Politzer.

The theory of strong interactions which came to be called quantum chromodynamics (QCD) was developed in the 1970's by generalizing the existing gauge theory of electromagnetic interactions - quantum electrodynamics (QED). The fundamental difference between QCD and QED is that in QCD, the generators of the symmetry do not commute with each other. Thus the theory is a non-abelian gauge field theory, which have some paculiar properties, one of which provided the solution to the paradox created by the SLAC experiment.

1.2 Asymptotic freedom and quark confinement

For QCD, when the energy-momentum transfer increases, the effective interaction between quarks decreases, and when these variables tend to infinity, the theory becomes a free field theory. This property was discovered by David Gross, Wilczek,

Table 1.1: Properties of quarks according to the standard model [6]

Quark	Charge	Mass	Baryon number	Isospin
up(u)	$+2/3$	$\approx 4MeV$	$1/3$	$+1/2$
down(d)	$-1/3$	$\approx 7MeV$	$1/3$	$-1/2$
strange(s)	$-1/3$	$\approx 135MeV$	$1/3$	0
charm(c)	$+2/3$	$\approx 1.5GeV$	$1/3$	0
bottom(b)	$-1/3$	$\approx 5GeV$	$1/3$	0
top(t)	$+2/3$	$\approx 175GeV$	$1/3$	0

and Politzer and it is called the asymptotic freedom [4, 5, 9, 10]. It results from the anti-screening of the color charges. This property explains the SLAC results where quarks behave as free particles, though they are confined.

The attractive force between quarks increases with separation and an infinitely large amount of energy is required to separate them fully. Thus they are permanently bound to hadrons. This is called quark confinement, which is another important property of QCD.

Thus at low energy, there is confinement and at high energy, there is asymptotic freedom in QCD. These two properties can be explained using the coupling constant. The effective running coupling constant in QCD can be written as [11],

$$\alpha_s(\mu) = \frac{12\pi}{(33 - 2n_f)\ln\left(\mu^2/\Lambda^2_{QCD}\right)} \tag{1.1}$$

where n_f is the number of active quark flavor and Λ_{QCD} is the QCD scaling parameter

When the momentum scale μ approaches infinity, α_s will go to zero. This phenomenon is called asymptotic freedom.

1.3 The QCD phase diagram

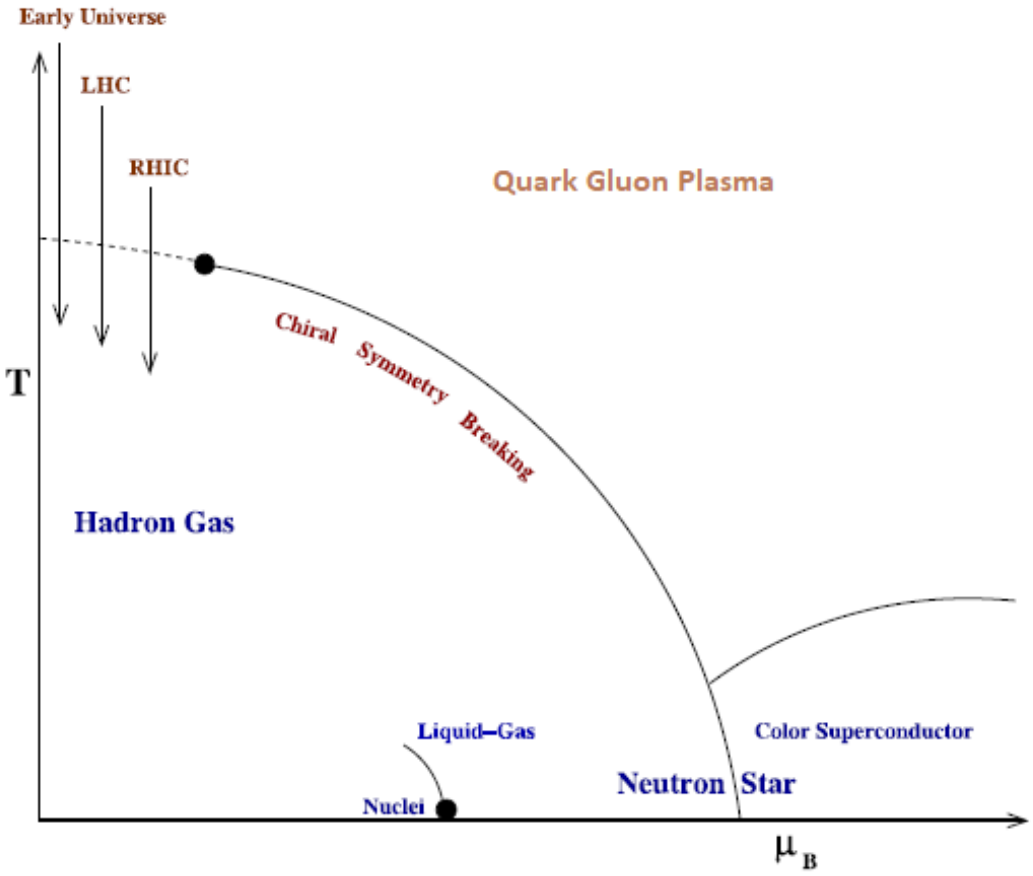

Figure 1.1: The QCD Phase Diagram [12]

The QCD phase diagram gives an idea about the different phases of QCD and the corresponding phase transitions. Fig. 1.1 [12] shows the QCD phase diagram as a function of temperature T and baryon chemical potential μ_B.

The available lattice simulations predict that, there are no phase transitions and hence no phase boundaries at zero chemical potential and finite temperature. Calculations also show a phase transition from hadronic phase to QGP for realistic values of light quark masses (u, d, and s) at a temperature in the range 150-180

MeV. The early universe was in this region of small μ_B. RHIC and LHC also explore this region.

As μ_B is increased at zero temperature, there occurs a first-order phase transition from the hadronic phase to the nuclear matter at about $\mu_B \approx 940MeV$. As μ_B is increased further, neutron fluidity is occurred as in neutron stars. At higher μ_B, high-density QGP is formed. Here there are different phases such as color superconductor, which is formed due to the condensation of quark cooper pairs. Many other phases are proposed in the high μ_B region such as Color Flavor Locked (CFL) phase and crystalline color superconductor.

In the region of small T and finite μ_B, the first-order transition line ends at the point with $T = T_c$ and $\mu_B = \mu_c$ and at which the phase transition is second order. This point is called the critical point.

At high temperature and/or high baryon density, because of asymptotic freedom, the phase of QCD is described in terms of quarks and gluons degrees of freedom. At sufficiently high temperature ($T > \Lambda_{QCD}$, where Λ_{QCD} is the QCD scaling parameter), the quarks and gluons are weakly interacting. Such a system can be described using perturbation theory. In the transition region, where the hadronic description is not valid and perturbation theory is not feasible, then the non-perturbative nature of QCD should be taken into account. The term strongly coupled quark-gluon plasma is used to represent the QCD state near the transition temperature.

At extremely high temperatures, QGP can be considered as an ideal gas of quarks and gluons. Around the phase transition temperature, the coupling constant is not weak and QGP can be considered as a non-ideal gas of quarks and gluons.

1.4 The quark-gluon plasma (QGP)

With the point that the quarks and gluons are confined within the hadrons, the important prediction of QCD is that at very high temperature and/or density, the hadrons dissolve into quarks and gluons. Such a state of deconfined quarks and gluons is called the quark-gluon plasma (QGP). The properties of QGP are expected to be extremely different from the hadronic matter at corresponding energy densities.

The hadronic matter is strongly interacting but according to the asymptotic freedom of non-abelian QCD, at very short distances and/or high momentum transfer the constituent quarks and gluons are weakly interacting. Thus the equation of state should be the same as that of a free system. The number of degrees of freedom in the hadronic phase consisting of pions is three, but the number of degrees of freedom in QGP is $(16 + \frac{21}{2}n_f)$, with n_f the number of flavors.

The characteristic values of temperature and density at which the transition from hadronic phase to QGP occurs correspond to $T_c = 10^{12}K$ and $\rho_c = 10^{15}g/cm^3$. Studies on QGP in laboratory give a clear picture of the early universe. During the first 10 μs after the big bang, the universe was filled with the QGP phase which was in the form of a dilute gas of weakly coupled quarks and gluons. Because of the expansion of the universe, the temperature decreased, neutrons and protons were formed from QGP, and atomic nuclei were formed further. Fig. 1.2 shows the evolution of the universe from Big-Bang up to toay [13]. QGP can occur naturally at very high baryon number densities and low temperatures in astrophysical compact objects (neutron stars). Many research projects are going on to produce QGP in laboratory conditions (RHIC, LHC).

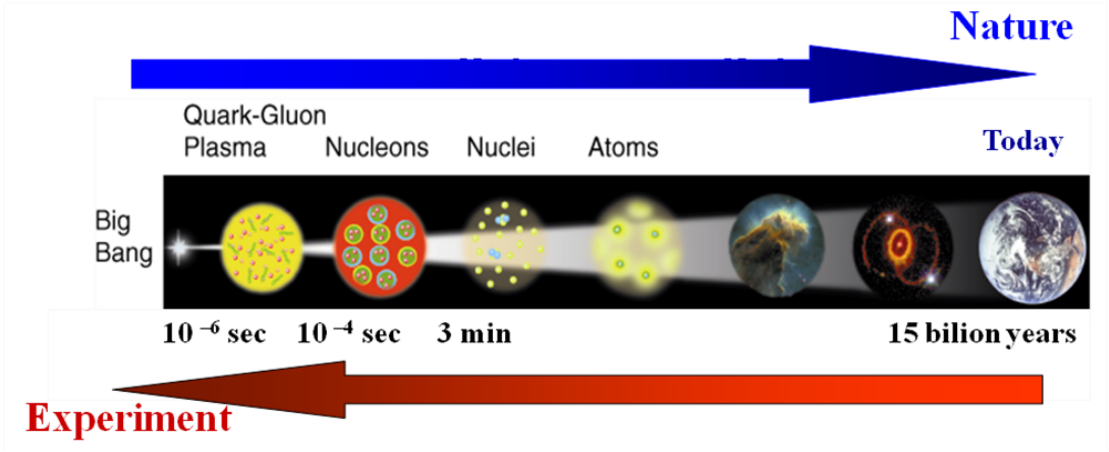

Figure 1.2: Evolution of the universe from Big-Bang up to today [13]

1.5 The search for QGP

QGP is studied experimentally in heavy-ion collisions at Relativistic Heavy Ion Collider (RHIC) and Large Hadron Collider (LHC) to provide critical data to the quest of QGP. Powerful accelerators in the heavy-ion colliders make head-on collisions between massive ions (Little bangs) to recreate the situation similar to the early universe just after the Big Bang. Such heavy-ion collisions were performed for more than 20 years at sufficiently high energies to produce the deconfined phase. In 1986, the first attempt to create QGP was done using light nuclei at Alternating Gradient Synchrotron (AGS) at Brookhaven National Laboratory (BNL), USA with Silicon (Si) and Super Proton Synchrotron (SPS) at CERN, the European Organization for Nuclear Research, Switzerland with Sulfur (S). Later in the early 1990s, collision with Gold ions (Au) was done at AGS and with Lead ions (Pb) at SPS. The centre of mass energy per colliding nucleon-nucleon pair at AGS and at SPS was 4.6 GeV and 17.2 GeV, respectively. In 2000, the evidence of a new state was announced by CERN SPS. In the same year, RHIC at BNL started

operation with four detectors PHENIX, STAR, PHOBOS, and BRAHMS with ten times larger the centre of mass energy than previously available. In 2010, LHC at CERN started Pb-Pb collisions at 14 times larger centre of mass energies than RHIC. The analysis of Au-Au collision at $\sqrt{S_{NN}} = 200GeV$ at RHIC and Pb-Pb collision at $\sqrt{S_{NN}} = 2.76TeV$ at LHC provided evidence for QGP [14]. The first results from RHIC showed that the QGP is a strongly coupled system which is a nearly perfect liquid [15]. The LHC results also gave clear evidence for the ideal liquid nature of QGP seen at RHIC [16, 17]. Fig. 1.3 schematically illustrates the nuclear collision time evolution.

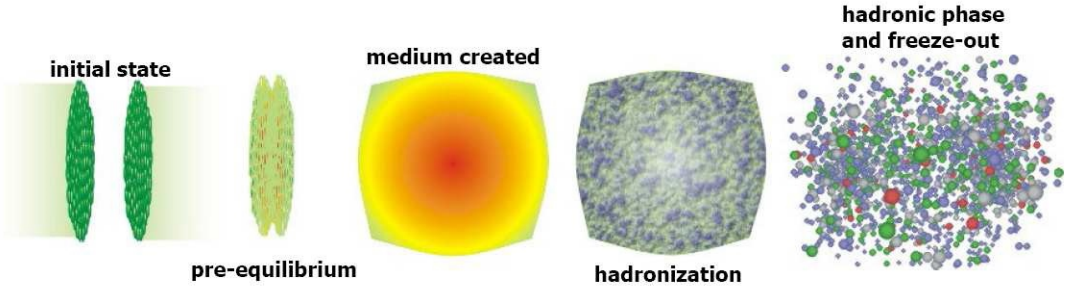

Figure 1.3: Schematic representation of Relativistic Nuclear Collisions (Courtesy to Prof. Steffan Bass)

1.6 The QGP signatures

The identification of QGP generation in relativistic heavy-ion collisions has appeared to be difficult [18]. The quarks and gluons in the deconfined plasma could not be measured directly. The signals of QGP can be extracted from the analysis of the particles produced at the final state. Some of the techniques for signaling QGP are discussed next.

1.6.1 Direct photon production

QGP can be observed directly through the electromagnetic radiation emitted by the quarks in the early stage. Since photons can escape the medium without much interaction, they seem to be a direct signal of QGP and they can provide information on the properties of QGP. In [19, 20], it is explained how photons become evidence for the production of QGP in high-energy heavy-ion collisions. Photons are produced in the QGP medium by processes like annihilation ($q+\overline{q} \rightarrow \gamma+g$) and Compton scattering ($q+g \rightarrow \gamma+q$, $\overline{q}+g \rightarrow \gamma+\overline{q}$). Fig. 1.4 shows the diagrams for the production of direct photons via the QCD Compton scattering process and annihilation process [21]. Since the photons are produced during the decay of pions and muons in heavy-ion collisions, it is not easy to measure the direct photons from the electromagnetic interaction of the constituents of the QGP.

There are many meaningful works for the subtraction of the photons from the π^0 and μ^0 background to obtain direct photons. In [22], a measurement of direct photon production in Pb+Pb collisions at 158 $AGeV$ has been carried out in the CERN WA98 experiment. A significant direct photon excess is observed at $p_T > 1.5 GeV/c$. To minimize the contribution of photon from the hadron phase, photon transverse momentum p_T must be greater than 2 GeV/c. In the hot QGP, photons have transverse momentum in the range 2 - 3 GeV/c [23]. Photons at this p_T are also produced by the collision of constituents of the projectile nucleons with that of target nucleons. In order to get the net photons from the QGP, the contributions from the other sources must be subtracted.

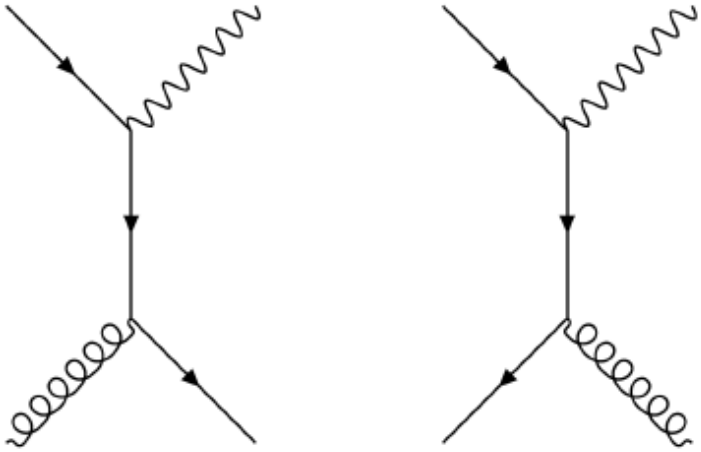

Figure 1.4: Feynman diagrams for direct photon production at leading order via the QCD Compton scattering process (left) and annihilation (right) [21]

1.6.2 Dilepton production

In QGP, the virtual photons that are produced by the annihilation of quark and antiquark decay into lepton pairs L^+L^- (e^+e^- and $\mu^+\mu^-$) which are termed as dileptons. These dileptons pass through the medium towards particle detectors without any further collisions. Thus they provide critical information about the interior of the fireball. Due to the effects of the medium, the quark dispersion relation in QGP changes in such a way that sharp gaps arise in the production rate of low mass dileptons. This is an important signature for the presence of deconfinement. Fig. 1.5 illustrates different elementary processes contributing to the dilepton production [24].

The dilepton mass can be written as,

$$M^2 = \left(P_L^+ + P_L^-\right)^2 \tag{1.2}$$

Where P_L^+ and P_L^- are the four-momenta of the dilepton. The dilepton's transverse

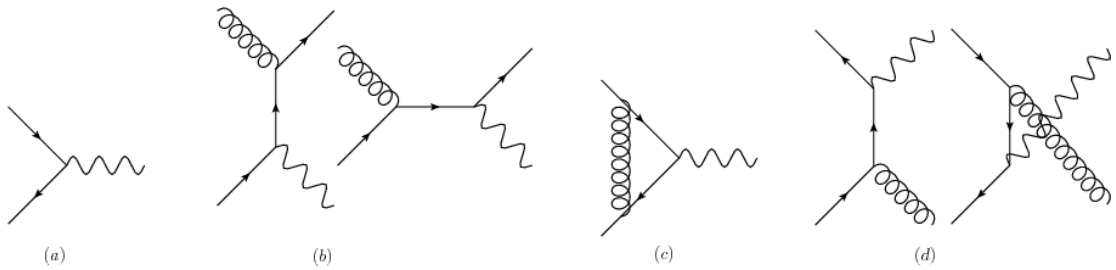

Figure 1.5: Diagrams contributing to the dilepton production from a QGP: (a) Born mechanism, (b) gluon-Compton scattering (GCS), (c) vertex correction, (d) gluon Bremsstrahlung (NLODY), where virtual photons (wavy lines) split into lepton pairs [23]

momenta can be written as,

$$P_T = (P_L^+)_T + (P_L^-)_T \tag{1.3}$$

where $(P_L^+)_T$ and $(P_L^-)_T$ are the transverse momenta of the dilepton.

1.6.3 Quarkonia suppression

Bound states of heavy quarks and their antiquarks are called quarkonia. The bound state of a charm quark and anti-charm quark ($c\bar{c}$) is called charmonium, and the corresponding bottom and anti-bottom quark pair ($b\bar{b}$) is known as bottomonium. They are formed during the initial hard collision and carry information about the initial stages of the QGP. Their binding energies are large so that they can survive in the QGP medium. The binding energy of the heavy quarkonium states is studied in [25,26]. Quarkonium suppression means the decrease in the production of quarkonia in the region where QGP is formed compared to the case where no QGP is formed in heavy-ion collision experiments. The main reason for this is the interaction of quarkonium with the QGP medium.

Thus the QGP formation affects the quarkonium suppression. The experimental evidence of the NA50 collaboration shows the anomalous J/ψ suppression in Pb+Pb collisions [27]. In [28] the phenomenon of anomalous J/ψ suppression has been studied in detail. In this thesis, we try to explain the quarkonium suppression in connection with the screening potential between quarks in strongly coupled quark-gluon plasma (SCQGP).

1.6.4 Strangeness enhancement

It is one of the most important probes for the detection of QGP. It is the observation of the abundance of strange particles (hadrons) in the detector. The strange quarks and antiquarks are easy to be created in a hot and dense QGP which combine with the other quarks to form a large number of strange hadrons. Fig. 1.6 shows the strange hadron production from QGP [29]. The strangeness evolution in QGP [30] can be described by the processes $u\overline{u} \rightarrow s\overline{s}$, $d\overline{d} \rightarrow s\overline{s}$ and $gg \rightarrow s\overline{s}$. The gluonic process provides a faster production rate. Thus the yield of strange and multi strange mesons and baryons has been strongly enhanced in the presence of QGP [31]. The WA97 collaboration [32] experimentally proved the enhancement in the production of multistrange hyperons in particular $\overline{\Omega}^{+}$ and $\overline{\Omega}^{-}$ in Pb+Pb collisions at $158AGeV$.

1.6.5 Jet quenching

Jet quenching means the modification of the energy of the hadron jet by the QGP. During nuclei collision, the partons produced with very high transverse momenta fly off to all possible directions and finally form narrow cones of hadrons

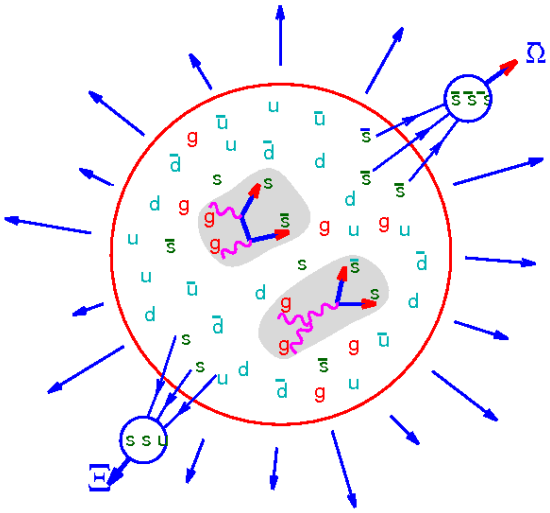

Figure 1.6: Strange hadron production from QGP [29]

called jets. The energies of these jets are modified by the QGP medium. The comparative study of jet energies with the same in the proton-proton collision may lead to the identification of QGP. Thus the study of jet quenching is an important tool for understanding the QGP. Fig. 1.7 explains the jet quenching in a head-on nucleus-nucleus collision [33]. The energy loss can be observed through the nuclear modification factor R_{AA}.

$$R_{AA}(p_T, b) = \frac{1}{T_{AA}(b)} \left[\frac{\frac{dN_{AA}}{d^2 p_T dy}}{\frac{d\sigma_{pp}}{d^2 p_T dy}} \right] \tag{1.4}$$

Here the numerator is a single particle momentum distribution of a jet in the nucleus-nucleus collision and traveling through the thermal medium and the denominator is the same in the proton-proton collision. $T_{AA}(b)$ is the nuclear thickness function and b is the impact parameter. If this ratio is less than unity, it is a measure of jet quenching in the medium [34, 35, 36, 37].

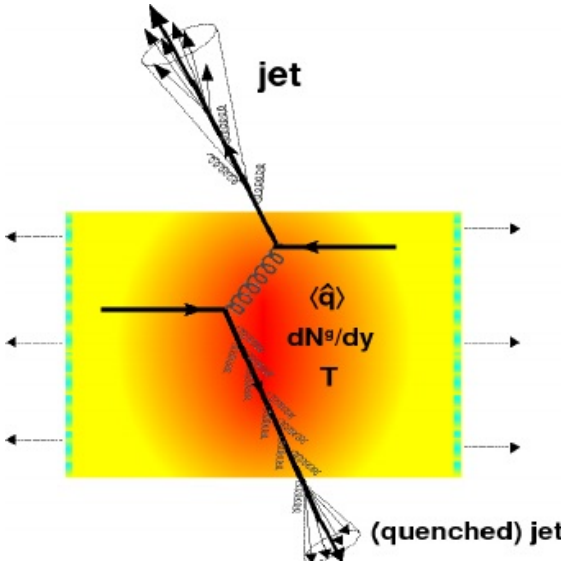

Figure 1.7: Jet quenching in a head-on nucleus-nucleus collision [33]

1.6.6 Anisotropic flow

Anisotropic flow provides information about the thermodynamics and collective flow of the hot and dense medium. In non-central collisions, the pressure and energy profile are not symmetric in the plane perpendicular to the beam axis. The large pressure gradient will lead to a larger expansion velocity and asymmetrical particle emission. This distribution can be explained by Fourier expansion. The first Fourier coefficient gives the strength of the direct flow and the second Fourier coefficient is called the elliptic flow. The higher coefficients are for studying the initial state fluctuations and to obtain the ratio of shear viscosity to energy density $(\eta/s\ )$ of the hot medium. The azimuthal momentum anisotropy is represented as,

$$E\frac{d^3N}{d^3p} = \frac{1}{2\pi p_T}\frac{d^2N}{dp_T dy}\left[1 + \sum_{n=1}^{\infty} 2\nu_n \cos\left[n\Big(\phi - \psi\Big)\right]\right] \tag{1.5}$$

where ϕ is the azimuthal angle of the particle and ψ is that of the reaction plane in the laboratory frame. 1.8 shows the magnitude of ellipti flow for different

particle species [38].

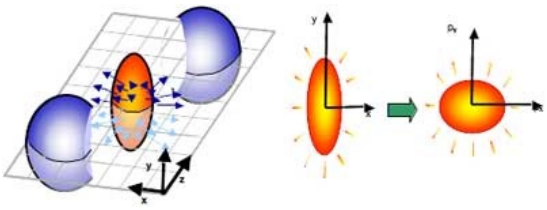

Figure 1.8: Elliptic flow in heavy ion collision [38]

1.7 Phenomenological models

A phenomenological model means a group of predictions about a system according to a theory. Using a phenomenological model, the properties of a system can be predicted. These predictions are experimentally verified. There are many phenomenological models about QGP. Some of them are explained below.

1.7.1 MIT Bag Model

It is a very simple phenomenological model. It was developed by Chodos et al. [39] in 1974 at the Masachusetts Institute of Technology in Cambridge (USA). According to this model, quarks are confined to move in a given spatial region forced by external pressure. The quark confinement can be visualized as an elastic bag (usually spherical in shape but can be deformable) in which the quarks move freely around as long as we don't try to pull them apart. If we try to pull a quark, then the bag stretches and resists the pulling, B is the pressure exerted by the vacuum on quarks and gluons. In this model, quarks are considered massless. Here quark confinement occurs due to the balance of the pressure B exerted on the bag from outside and the kinetic energy of quarks. B is called the bag pressure

which incorporates the non-perturbative effects of QCD ($B \approx 200MeV$). By compressing the bags against each other phase transition can be occurred. The pressure and energy in terms of Bag constant are,

$$P = \frac{37\pi^2}{90}T^4 - B(T) \tag{1.6}$$

$$\epsilon = \frac{37\pi^2}{90}T^4 + B(T) \tag{1.7}$$

The bag model gives an estimation of the critical temperature of the phase transition. It is very simple and easy to apply. This model could easily explain the properties of low-lying hadrons. It has some drawbacks too. The physics at the boundary of the bag is too complicated because of the sharpness of the boundary of the bag. The size of the bag is too large so that the bags would touch each other at normal nuclear density. Also, the chiral symmetry breaks at the boundary of the bag (bag surface).

1.7.2 The quasi particle QGP model (qQGP)

Within the approach of this model, the interacting plasma is considered as a system of massive quasi-particles. This model was independently proposed by Satz et al. and Peshier et al. [40, 41]. According to Peshier et al. in gluon plasma, all thermodynamic quantities can be derived from the partition function.

$$\frac{PV}{T} = -\sum_{k=0}^{\infty} \ln(1 - e^{-\beta\epsilon_k}) \tag{1.8}$$

Where $\beta = \frac{1}{T}$, ϵ_k is the single particle energy of the quasi-gluon,

$$\epsilon_k = \sqrt{k^2 + m^2(T)} \tag{1.9}$$

Where k is the momentum and $m(T)$ is the temperature-dependent mass. The pressure is similar to ideal gas with temperature dependent mass and can be denoted as P_i.

Later the thermodynamic inconsistency of the quasi-particle model was remedied by introducing the temperature-dependent bag pressure term in the expression of pressure and energy density [42, 43].

$$P = P_i - B(T) \tag{1.10}$$

$$\epsilon = \epsilon_i + B(T) \tag{1.11}$$

In [44] the authors proposed the self-consistent quasi particle model without the external terms like B(T). In this model, all the thermodynamic quantities can be derived in a self-consistent manner. Such models obtained good results in agreement with the lattice data.

1.7.3 Cornell Potential Model

The effective potential between quark and antiquark which has the form Coulomb + linear potential is termed as Cornell potential. Cornell potential was successful in studying non-relativistic systems such as mesons. The Cornell potential can be read as,

$$V(r) = -\frac{a}{r} + br \tag{1.12}$$

where a and b are constants.

At short distances, the Cornell potential becomes $V(r) \approx \frac{1}{r}$, which is known as the Coulomb like term and arises from the gluon exchange between quark and

antiquark and at large distances $V(r) \approx r$, which is the linear term which arises from the higher-order effects.

In [45], EOS of QGP was derived using the Cornell potential model based on Mayer's theory of plasma and the results were compared with the lattice QCD results of the gluon plasma. EOS for quark-antiquark plasma was derived in [46] and the results were in agreement with the 2-flavor and 3-flavor lattice QCD results. Also, the Cornell potential succeeded in explaining the spectra of both charmonium and bottomonium [47]. In [48], using Cornell potential EOS was obtained and the dissociation temperatures of quarkonia were found out.

1.7.4 Relativistic Harmonic Oscillator (RHO) Potential Model

RHO potential model was initially proposed by S. B. Khadkikar and S. K. Gupta [49]. It has been proved successful in explaining many properties of hadrons. Later a confinement model was formulated by S. B. Khadkikar and V. Kumar [50]. These two models are collectively called the RHO model. Energy eigenvalues for quarks and gluons are given as,

$$E_n = \sqrt{M_q^2 + (2n+1)\Omega_q} \tag{1.13}$$

$$E_n = \sqrt{C_g(2n+1)} \tag{1.14}$$

with n=1,2,3,...

where M_q is the mass of a quark, Ω_q is the size parameter which is energy dependent, and C_g is 'frequency' of gluon fields.

This model was used to find out the hadronic and mesonic masses and the results were found in agreement with the experimental results. The leptonic width also agrees with the experimental result. The confinement behavior of this model has been found smooth compared to the bag model. This model was helpful in describing many features of hadron spectroscopy, baryon magnetic moments and properties of glueballs, nucleon antinucleon annihilation, etc.

In [51], the authors found out the EOS of infinite gluon system with classical and quantum energy eigenvalues and both EOS show T^4 dependence of pressure and energy density at high pressure.

1.7.5 The Strongly Interacting Quark-Gluon Plasma Model (sQGP)

Heavy ion experiments and lattice calculations show that the QGP displays strong interaction between the constituents in the regime $T = T_c$ to $T = 3T_c$. In [52], the properties of bound states like colorless and colored pairs of gq, qq, and gg at $T > T_c$ were studied using the sQGP model. Also, their binding energies were calculated and zero binding endpoints were located. In the limit of the high coupling constant ($\Gamma >> 1$), the one component plasma shows liquid state properties [53]. In [53], the transport coefficients – self-diffusion, shear viscosity, and thermal conductivity were studied. Two types of collective modes (longitudinal and transverse modes) have been understood in OCP and transverse mode arises because of strong correlations.

1.7.6 Strongly Coupled Quark-Gluon Plasma Model (SCQGP)

In this model, QGP near T_c is proposed as a strongly coupled plasma called the strongly coupled quark-gluon plasma (SCQGP). At sufficiently high temperatures, QGP is a quasi-color-neutral gas of colored particles (like quarks and gluons) which exhibit collective behavior. In this model QGP near T_c can be treated as strongly coupled QED plasma with appropriate modifications due to the color and flavor degrees of freedom and quantum effects. In [54], the author derived a modified equation for energy density as,

$$\epsilon = \Big(2.7 + U_{ex}(\Gamma)\Big) nT \tag{1.15}$$

with $n = 1.1 a_f T^3$.

The coupling constant is defined as the ratio of the average potential energy to the average kinetic energy of the particles of SCQGP.

$$\Gamma = \frac{\langle P.E. \rangle}{\langle K.E. \rangle} \tag{1.16}$$

$$\Gamma = \left(\frac{4.4\pi a_f}{3}\right)^{\frac{1}{3}} g_c \alpha_s(T) \tag{1.17}$$

With $a_f = (16 + \frac{21}{2} n_f)\frac{\pi^2}{90}$.

In SCP, $g_c = 1$ but in SCQGP, it is different for gluon and flavored plasma. in SCP $\alpha_s = \frac{1}{137}$ and in SCQGP,

$$\alpha_s(T) = \frac{6\pi}{(33 - 2n_f)\ln(T/\Lambda_T)}\left(1 - \frac{3(153 - 19n_f)}{(33 - 2n_f)^2}\frac{\ln\Big(2\ln(T/\Lambda_T)\Big)}{\ln(T/\Lambda_T)}\right)$$

After this introduction, in the next chapter (chapter 2), a new screening potential between quarks in SCQGP has been proposed. Also, the temperature dependence of this potential has been explained. The binding energy of the bound states of quarks is calculated by solving the N-dimensional radial Schrödinger equation using this potential in three different methods. i.e., analytical exact iteration method (AEIM), power series method (PSM), and Nikiforov-Uvarov (NU) method in chapter 3. Using the results, effective masses of diquarks and the heavy quarkonium properties such as binding energies, mass spectra, and dissociation temperatures are discussed in chapter 4 and chapter 5. Finally, we study the properties of $b\overline{c}$ and $c\overline{s}$ mesons in chapter 6. Chapter 7 summarizes the work presented in this thesis.

Bibliography

[1] M. Gell-Mann, *A schematic model of baryons and mesons*, Phys. Lett. 8, 214 (1964).

[2] G. Zweig, *An SU3 model for strong interaction symmetry and its breaking*, CERN-Th 401 and 412 (1964).

[3] C. N. Yang and R. L. Mills, *Conservation of isotopic spin and isotopic gauge invariance*, Phys. Rev. 96, 191 (1954).

[4] D. J. Gross and F. Wilczek, *Ultraviolet behavior of non-abelian gauge theories*, Phys. Rev. Lett. 30, 1343 (1973).

[5] H. D. Politzer, *Reliable perturbative results for strong interactions?*, Phys. Rev. Lett. 30, 1346 (1973).

[6] R. K. Ellis, W. J. Stirling, and B. R. Webber, *QCD and collider physics*, Cambridge University Press (1996).

[7] E. D. Bloom, D. H. Coward, H. C. DeStaebler, J. Drees, G. Miller et al., *High-energy inelastic e-p scattering at* 6^0 *and* 10^0, Phys. Rev. Lett. 23, 930 (1969).

[8] R.P. Feynman, *Very high-energy collisions of hadrons*, Phys. Rev. Lett. 23, 1415 (1969).

[9] D. J. Gross and F. Wilczek, *Asymptotically free gauge theories. I*, Phys. Rev. D 8, 3633 (1973).

[10] D. J. Gross and F. Wilczek, *Asymptotically free gauge theories. II*, Phys. Rev. D 9, 980 (1974).

[11] W. Greiner, S. Schramm, and E. Stein, *Quantum chromodynamics*, Springer (2007).

[12] J. C. Collins and M. J. Perry, *Superdense matter: Neutrons or asymptotically free quarks?*, Phys. Rev. Lett. 34, 1353 (1975).

[13] *https://twiki.cern.ch/twiki/bin/view/ReteQuarkonii/ReteQuarkonii*,

[14] A. K. Chaudhuri, *Temperature dependence of the QGP viscosity over entropy ratio from hydrodynamical analysis of ALICE data in* $\sqrt{s_{NN}}$ *= 2.76 TeV Pb + Pb collisions*, J. Phys. G: Nucl. Part. Phys. 39, 125102 (2012).

[15] U. Heinz, *The strongly coupled quark–gluon plasma created at RHIC*, J. Phys. A: Math. Theor. 42, 214003 (2009).

[16] K. Aamodt et al. (ALICE Collaboration), *Elliptic flow of charged particles in Pb-Pb collisions at* $\sqrt{s_{NN}}$ *= 2.76 TeV*, Phys. Rev. Lett. 105, 252302 (2010).

[17] G. Aad et al. (ATLAS Collaboration), *Observation of a centrality-dependent Dijet asymmetry in lead-lead collisions at* $\sqrt{s_{NN}}$ *= 2.76 TeV with the ATLAS detector at the LHC*, Phys. Rev. Lett. 105, 252303 (2010).

[18] S. Mrowczynski, *Quark-gluon plasma*, Acta Phys. Polon. B, 29, 3711 (1998).

[19] E. L. Feinberg, *Direct production of photons and dileptons in thermodynamical models of multiple hadron production*, Nuovo. Cim. 34, 391 (1976).

[20] E. V. Shuryak, *Quark-gluon plasma and hadronic production of leptons, photons and psions*, Phys. Lett. B 78, 150 (1978).

[21] J. M. Campbell, J. Rojo, E. Slade, et al., *Direct photon production and PDF fits reloaded*, Eur. Phys. J. C 78 (6), 470 (2018).

[22] M. M. Aggarwal et al. (WA98 Collaboration), *Direct photon production in 158 A GeV 208Pb + 208Pb collisions*, nucl-ex/0006007 (2000).

[23] J. Kapusta, P. Lichard, and D. Seibert, *High-energy photons from quark - gluon plasma versus hot hadronic gas*, Phys. Rev. D 44, 2774 (1991).

[24] O. Linnyk, E. L. Bratkovskaya, J. Manninen, and W. Cassing, *Dilepton production from parton interactions in the early stage of relativistic heavy-ion collisions*, J. Phys.: Conf. Ser. 312, 012010 (2011).

[25] L. Thakur and B. K. Patra, *Quarkonium dissociation in an anisotropic QGP*, J. Phys.: Conf. Se. 668, 012085 (2016).

[26] V. Agotiya, V. Chandra, M. Y. Jamal, and I. Nilima, *Dissociation of heavy quarkonium in hot QCD medium in a quasiparticle model*, Phys. Rev. D 94, 094006 (2016).

[27] M. C. Abreu et al., *Evidence for deconfinement of quarks and gluons from the J / psi suppression pattern measured in Pb + Pb collisions at the CERN SPS*, Phys. Lett. B 477, 28 (2000).

[28] M. Nardi and H. Satz, *String clustering and J / psi suppression in nuclear collisions*, Phys. Lett. B 442, 14 (1998).

[29] J. Rafelski and J. Letessier, *Strangeness and statistical hadronization: How to study quark-gluon plasma*, Acta Phys. Polon. B 34, 5791 (2003).

[30] P. Koch, B. Muller, and J. Rafelski, *Strangeness in relativistic heavy ion collisions*, Phys. Rept. 142, 167 (1986).

[31] J. Rafelski, *Formation and observables of the quark-gluon plasma*, Phys. Rept. 88, 331 (1982).

[32] E. Andersen et al. (WA97 Collaboration), *Strangeness enhancement at mid-rapidity in Pb–Pb collisions at 158 A GeV/c*, Phys. Lett. B 449, 401 (1999).

[33] D. d'Enterria and B. Betz, *High-pT hadron suppression and jet quenching*, The Physics of the quark-gluon plasma, Springer (2009).

[34] J. D. Bjorken, *Energy loss of energetic partons in quark-gluon plasma : possible extinction of high p_T jets in hadron-hadron collisions*, Fermilab-Pub-82/59-THY, Batavia (1982).

[35] R. Karabowicz (BRAHMS Collaboration), *Nuclear modification factor for identified hadrons at forward rapidity in Au+ Au reactions at 200 GeV*, Nucl. Phys. A 774, 477 (2006).

[36] A. Grelli (ALICE Collaboration), *D meson nuclear modification factors in Pb–Pb collisions at $\sqrt{S_{NN}}$= 2.76 TeV with the ALICE detector*, Nucl. Phys. A 904, 635c (2013).

[37] M. B. Tonjes (CMS Collaboration), *Inclusive jet and charged hadron nuclear modification factors in PbPb collisions at 2.76 TeV with CMS*, Nucl. Phys. A 904, 713c (2013).

[38] A. Saini and S. Bhardwaj, *Elliptic flow in heavy ion collisions*, J. of Nucl. Part. Phys. 4 (6), 164 (2014).

[39] A. Chodos, R. L. Jaffe, K. Johnson, C. B. Thorn, and V. F. Weisskopf, *New extended model of hadrons*, Phys. Rev. D 9, 3471 (1974).

[40] V. Goloviznin and H. Satz, *The refractive properties of the gluon plasma in SU (2) gauge theory*, Z. Phys. C 57, 671(1993) .

[41] A. Peshier, B. Kampfer, O. P. Pavlenko, and G. Soff, *An effective model of the quark-gluon plasma with thermal parton masses*, Phys. Lett. B 337, 235 (1994).

[42] M. I. Gorenstein and S.N. Yang, *Gluon plasma with a medium-dependent dispersion relation*, Phys. Rev. D 52, 5206 (1995).

[43] A. Peshier, B. Kampfer, and G. Soff, *From QCD lattice calculations to the equation of state of quark matter*, Phys. Rev. D 66, 094003 (2002).

[44] V. M. Bannur, *Comments on quasiparticle models of quark–gluon plasma*, Phys. Lett. B 647, 271 (2007).

[45] V. M. Bannur, *Equation of state for a non-ideal quark gluon plasma*, Phys. Lett B 362, 7 (1995).

[46] K. M. Udayanandan, P. Sethumadhavan, and V. M. Bannur, *Equation of state of a quark-gluon plasma using the Cornell potential*, Phys. Rev.C 76, 044908 (2007).

[47] G. S. Bali, *QCD forces and heavy quark bound states*, Phys. Rept. 343, 1 (2001).

[48] B. S. Sabzevari, *Equation of state for hot quark-gluon plasma transitions to hadrons with full QCD potential*, Phys. Rev. C 65, 054904 (2002).

[49] S. B. Khadkikar and S. K. Gupta, *Magnetic moments of light baryons in harmonic model*, Phys. Lett. B 6, 124, 523 (1983).

[50] S. B. Khadkikar and P. C. Vinodkumar, *Confinement models for gluons*, Pramana - J. Phys. 29, 39 (1987).

[51] V. M. Bannur and K. M. Udayanandan, *Statistical mechanics of confined quantum particles*, Mod. Phys. Lett. A 22 (30), 2297 (2007).

[52] E. V. Shuryak and I. Zahed, *Toward a theory of binary bound states in the quark-gluon plasma*, Phys. Rev. D 70, 054507 (2004).

[53] Z. Donko, P. Hartmann, and G. J. Kalman, *Strongly coupled plasma liquids*, arXiv:0710.5229 [nucl-th] (2007).

[54] V. M. Bannur, *Strongly coupled quark gluon plasma (SCQGP)*, J. Phys. G: Nucl. Part. Phys. 32, 993 (2006).

Chapter 2

Screening of a Test Quark in the Strongly Coupled Quark Gluon Plasma

2.1 Introduction

As discussed in chapter 1, quark-gluon plasma (QGP) is a special kind of plasma where electric charges in plasma are replaced by the color charges of quarks and gluons mediating the strong interaction between them. Such a state of matter can be expected to occur at sufficiently high temperature ($\geq$ 150 MeV) and/or densities (>10 times nuclear density) [1]. These conditions could be fulfilled in the early universe after a few microseconds or in the interior of neutron stars and these conditions are recreated in the laboratory by heating nuclear matter to temperatures above the quark-gluon confinement temperature with high energy nuclear collisions at the RHIC at Brookhaven National Laboratory or the LHC at

CERN [2]. During these collisions, the hot and dense fireballs are created and they undergo thermalization, cooling, hadronization, chemical, and thermal freeze-out into hadrons. The search for QGP can be done by the detection and analysis of these hadrons, photons, etc. It has been proposed that the QGP near and above Tc is a strongly coupled coulombic plasma of color charges (SCQGP) [3]. The strongly coupled quark-gluon plasma is in several ways similar to some kinds of electromagnetic plasmas containing electrically charged particles that show some liquid-like or even solid-like behavior [4].

In plasma physics, the screening of charges is considered as one of the important collective effects. The Debye screening potential can be derived from the Linearized Poisson's equation within a homogeneous, isotropic plasma. The Coulomb potential of a charge Q at rest, in the plasma, is modified into Debye Huckel or Yukawa potential [5],

$$\phi(r) = \frac{Q}{r} exp\left(-\frac{r}{\lambda_D}\right) \tag{2.1}$$

where λ_D is the shielding radius of the sphere.

Bound states of heavy quarks, in particular J/ψ mesons, are produced in the initial hard scattering processes of the collision and will be dissociated in the QGP due to the screening of the quark potential and break up by the energetic gluons [6]. Hence the J/ψ suppression has been considered as one of the important signatures for the QGP formation [7]. A J/ψ meson suppression was observed experimentally [8] and it was interpreted as a major indication of the QGP formation in RHIC [9].

Experimental data suggest that QGP near to the confinement phase could be in liquid phase and for a transition from the liquid phase to the solid phase, a

Lennard Jones type interaction may be required [10]. In [11] a new attractive potential between the ions that are shielded by degenerate electrons in quantum plasmas was reported. A similar screening potential was found for a color charge at rest by using a polarization tensor beyond the high-temperature limit in [12]. The screening potential of a parton moving through QGP was calculated in [1] using semi-classical transport theory.

In this chapter, we try to find out the screening potential between quarks in SCQGP, through generalized quantum hydrodynamic (G-QHD) approach. We shall use the generalized QHD equations [13] for the quarks in SCQGP, supplemented by Poisson's equation. In G-QHD model, pressure and Bohm's potential are included [14]. Here the plasma is of high density, so exchange and correlation functions are neglected. Pressure is derived from the ground state energy equation of quarks in SCQGP. Here we demonstrate that the potential around a quark in strongly coupled quark-gluon plasma resembles the Lennard Jones type potential which may be responsible for the phase transition of SCQGP. We also try to explain the expected J/ψ suppression in connection with the screening potential.

2.2 Strongly coupled quark-gluon plasma

Strongly coupled plasma means the plasma where the plasma parameter, which may be defined as the ratio of average potential energy to average kinetic energy of the particles is equal to or greater than 1. In strongly coupled quark-gluon plasma, the interparticle potential energy dominates over the thermal energy of particles. Thus the coupling parameter for strongly coupled quark-gluon plasma is expected to be of the order of one [15]. So the theory of SCQGP can be explained using the

traditional mathematical descriptions of SCP.

Consider the quark-gluon plasma as a deconfined, quasi-color-neutral system of quarks, antiquarks, and gluons with color coulombic interactions. It can be treated in a similar way as the quantum electrodynamic plasma with a few modifications due to color degrees of freedom. The plasma parameter can be written as,

$$\Gamma = \frac{\langle P.E. \rangle}{\langle K.E. \rangle} = \frac{\frac{4}{3}\frac{\alpha_s}{a}}{T} \tag{2.2}$$

where α_s is the coupling constant, a is usually referred to as the ion-sphere radius or the Wigner-Seitz radius and can be estimated as $a = (\frac{3g_c}{4\pi n_f})^{\frac{1}{3}}$ Where g_c incorporates the color degrees of freedom, n_f stands for the number density corresponding to the particular flavor and T is the absolute temperature.

Taking the typical value of $\alpha_s \approx 0.5$, $a \approx 1fm$ and near the critical temperature $T_c \approx 200MeV$, $\Gamma \approx \frac{2}{3}$ which is of the order of 1. Thus QGP near T_c is strongly coupled plasma. For a degenerate electron system with number density n, we can use the Fermi energy, $E_F = \frac{h^2}{2m}(3\pi^2 n)^{\frac{2}{3}}$ instead of T. Since SCQGP is like the strongly coupled quantum electrodynamic plasma, we can write

$$\Gamma = \frac{\frac{4}{3}\frac{\alpha_s}{a}}{E_F} = 0.543 r_s \tag{2.3}$$

with

$$r_s = \left(\frac{3g_c}{4\pi n_f}\right)^{\frac{1}{3}} \frac{4M_q\alpha_s}{3}$$

where M_q is the quark mass, g_c incorporates the color degrees of freedom and n_f stands for the number density corresponding to the particular flavor [16]. For a quark system consisting of u and d quarks, the quark mass can be considered as $M_q \approx \frac{m_p}{3}$ and $\alpha_s \approx 0.5$. Also we can take $\left[\frac{4M_q\alpha_s}{3}\right]^{-1} \approx 1fm$, the hadron radius

[16]. For SCQGP,

$$P = \sum_{f=1}^{2} \frac{-n_f r_{sf}}{3} \frac{\partial E_G}{\partial r_s} - B \tag{2.4}$$

Here B is the confinement parameter in the form of MIT Bag constant. The general formula for the ground state energy per quark is known [16] using the method of Pade approximants [17]. By integrating this equation we get

$$\begin{aligned}\frac{dE_G}{dr} = \frac{8M_q\alpha_s^2}{9}\Bigg[&- 0.0614r_s^{1/2} + 0.0791r_s + 0.0158r_s^{3/2} - 0.2741r_s^2 + 0.6609r_s^{5/2} \\ &-4.3951r_s^3 - 44250\log\left(r_s^{1/2} - 4.1005\right) - 2944300\log\left(r_s^{1/2} + 5.0194\right) \\ &+505797\log\left(2(r_s^{1/2} + 1.50483)\right)\Bigg]\end{aligned} \tag{2.5}$$

Eq.(2.5) is obtained from the equation of state of degenerate electron system with a few modifications. It could be applicable at finite temperature since SCQGP can be treated in a similar way as the strongly coupled QED plasma. Using the above-mentioned EOS of QGP, the mass-radius relation of compact stars was estimated [16], which confirms the experimental result [18].

2.3 Screening potential in SCQGP through G-QHD approach

For Strongly Coupled QGP, $r_s \leq 1$ and Γ is of the order of 1 and it can be considered as collisionless. Thus the interaction energy between the partons will be greater than the kinetic energy. Here no magnetic effects are considered. Within the hydrodynamic limit, plasma can be treated as liquid and can be described in

terms of macroscopic variables that obey the equations of motion. Various color components of plasma have the same temperature and hydrodynamic velocities when local equilibrium is attained.

The G-QHD equations are

$$\frac{\partial n_f}{\partial t} + \nabla.(n_f u) = 0 \tag{2.6}$$

$$M_q \left(\frac{\partial u}{\partial t} + u.\nabla u \right) = \left(\frac{4\alpha_s}{3} \right)^{\frac{1}{2}} \nabla\phi - g_c n_f^{-1} \frac{\partial P}{\partial n_f} \nabla n_f + \nabla V_B \tag{2.7}$$

$$\nabla^2 \phi = \left(\frac{4\alpha_s}{3} \right)^{\frac{1}{2}} (n_f - n_{f0}) - Q\delta(r) \tag{2.8}$$

Where V_B is the Quantum Bohm potential, $V_B = -\frac{1}{2M_q} \frac{1}{\sqrt{n_f}} \nabla^2 \sqrt{n_f}$. Let $n_f = n_{f0} + n_{f1}$, where $n_{f1} << n_{f0}$.

Linearize the resultant equations to obtain perturbation density, n_{f1} and insert in to Eq.(2.8). The Fourier transformation in space leads to the electric potential around an isolated quark. Thus we have

$$\phi(r) = \frac{Q}{8\pi^3} \int \frac{e^{ik.r}}{k^2 D} d^3k \tag{2.9}$$

Where D is the dielectric constant, r denotes the position relative to the instantaneous position of the test quark and Q is the charge of the test quark. The inverse dielectric constant can be written as

$$\frac{1}{D} = \frac{\frac{k^2}{k_s^2} + \alpha \frac{k^4}{k_s^4}}{1 + \frac{k^2}{k_s^2} + \alpha \frac{k^4}{k_s^4}} \tag{2.10}$$

Where $k_s^2 = \frac{M_q \omega_p^2}{g_c \left(\frac{\partial P}{\partial n_f} \right)}$ is the inverse Thomas Fermi screening length and $\alpha =$

$\frac{\omega_p^2}{2g_c\left(\frac{\partial P}{\partial n_f}\right)^2}$ measures the importance of quantum recoil effect.

$\frac{\partial P}{\partial n_f}$ can be calculated by using Eq.(2.4) and (2.5).

$$\frac{\partial P}{\partial n_f} = 2\Big(-70315.3n_f^{-1/3} + 0.0023n_f^{-2/3} - 0.0002n_f^{-5/6} - 0.1044n_f^{-4/3} \\ -0.0083n_f^{-7/6} + 17240.6n_f^{-1/2} + 365329n_f^{-1}\Big) \tag{2.11}$$

Inserting Eq.(2.10) in Eq.(2.9),

$$\phi(r) = \frac{Q}{16\pi^3}\int\left(\frac{1+b}{k^2+k_+^2} + \frac{1-b}{k^2+k_-^2}\right)e^{ik.r}d^3k \tag{2.12}$$

Where $b = \frac{1}{\sqrt{1-4\alpha}}$ and $k_\pm^2 = k_s^2\frac{(1\mp\sqrt{1-4\alpha})}{2\alpha}$.

The above integral was evaluated for different values of α. The boundary condition is $\phi \to 0$ at $r \to \infty$. Eq.(2.12) becomes

$$\phi(r) = \frac{Q}{8\pi r}\Big[(1+b)e^{-k_+r} + (1-b)e^{-k_-r}\Big] \tag{2.13}$$

For $\alpha \to 0$, the modified Thomas-Fermi screened Coulomb potential can be recovered.

$$\phi(r) = \frac{Q}{4\pi r}e^{-k_sr} \tag{2.14}$$

For $\alpha \to \frac{1}{4}$, we have $k_+ = k_- = \sqrt{2}k_s$ and

$$\phi(r) = \frac{Q}{4\pi r}\left(1 + \frac{k_s}{\sqrt{2}}r\right)e^{-\sqrt{2}k_sr} \tag{2.15}$$

For $\alpha = 1$,

$$\phi(r) = \frac{Q}{4\pi r}\left(\cos(k_ir) + \frac{1}{\sqrt{3}}\sin(k_ir)\right)e^{-k_rr} \tag{2.16}$$

Where

$$k_i = \frac{k_s}{2}$$

,

$$k_r = \frac{\sqrt{3}}{2} k_s$$

With $\alpha >> 1$ the exponential cosine-screened Coulomb potential is recovered.

$$\phi(r) = \frac{Q}{4\pi r}\Big(\cos(k_s r_*)\Big)e^{-k_s r_*} \tag{2.17}$$

Where $r_* = \frac{r}{(4\alpha)^{\frac{1}{4}}}$

2.4 Suppression of J/ψ meson

The two-body potential associated with the dipole created by two test charges q_1 and q_2 at positions r_1 and r_2 respectively can be represented as,

$$\phi(r_1 - r_2) = \frac{q_1 q_2}{16\pi^3}\int\left(\frac{e^{ik.(r_1-r_2)}}{k^2 D} + \frac{e^{-ik.(r_1-r_2)}}{k^2 D}\right)d^3k \tag{2.18}$$

This two-body potential is equal to the one-body potential given by Eq.(2.9). For two quarks, the potential shows attraction and thus bound state of quarks is formed. The existence of colored bound states (eg. diquarks) of partons at rest has been claimed by analyzing lattice data [19]. For a quark-antiquark system, $q_1 q_2 < 0$. Thus the two-body potential is inverted, showing a maximum. This may lead to short living mesonic resonances and an enhancement of the attraction between quarks and antiquarks of mesonic states moving through SCQGP [1] which results in the expected suppression.

2.5 Temperature dependence of screening potential

For deriving Eq.(2.16), the value of α_s has been fixed ($\alpha_s \approx 0.5$) but by considering the temperature dependence of α_s from [20] we get,

$$\alpha_s(T) = \frac{6\pi}{(33-2n_f)\ln(T/\Lambda_T)}\left(1 - \frac{3(153-19n_f)}{(33-2n_f)^2}\frac{\ln\left(2\ln(T/\Lambda_T)\right)}{\ln(T/\Lambda_T)}\right) \quad (2.19)$$

The screening potential between quarks at finite temperature plays an important role in the study of various bound states in Quark Gluon Plasma. Theoretically many forms of screening potential have been proposed [21]. The study of static quark potential is significant for several reasons. Phenomenologically the properties of bound states of quarks can be derived from potential models [22]. So it is necessary to find out the temperature dependence of the potential [23]. Substituting Eq.(2.19) in Eq.(2.13), we get the temperature-dependent quark potential as $\phi(r,T)$.

2.6 Results

In Fig. 2.1, the profiles of the potential given by the Eq.(2.14), (2.16), and (2.17) for different values of α are displayed. It can be seen that the new short-range attractive electric potential that resembles the LJ type potential for $\alpha = 1$ while for the smaller values of α the attractive potential vanishes. In high density strongly coupled plasma, with Bohm's potential, the attractive potential exists only for $\alpha \geq 1$. We have investigated the temperature dependence of screening potential

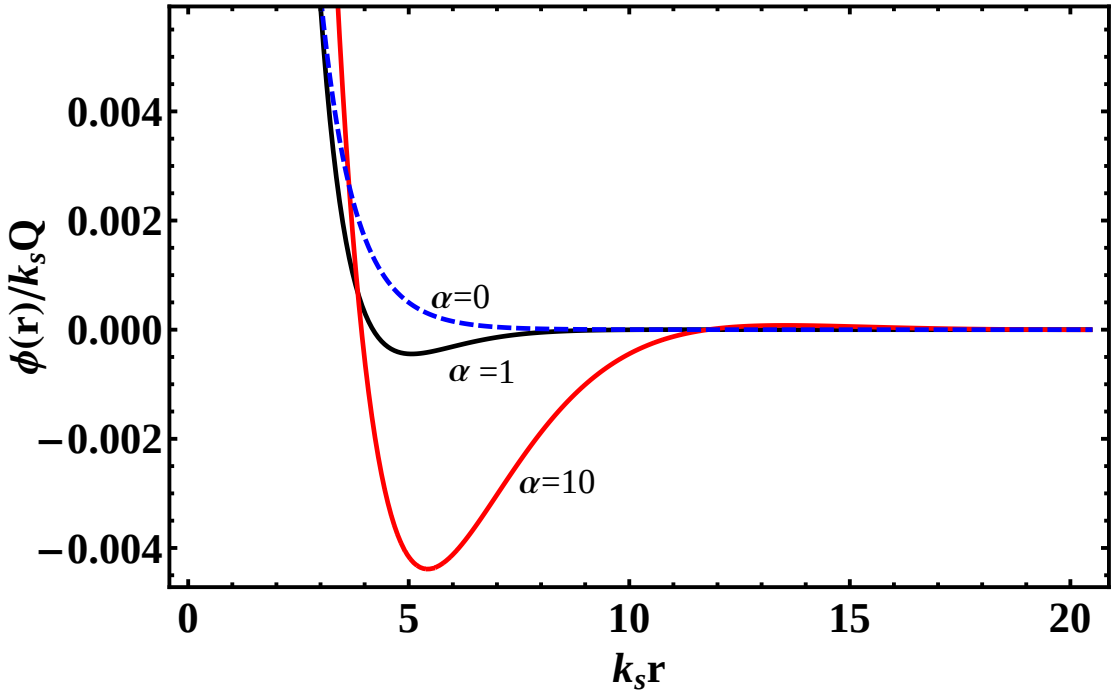

Figure 2.1: Variation of electric potential with r for different values of α

in strongly coupled quark-gluon plasma. The result is displayed in Figures 2.2 and 2.3. The attractive potential for $\alpha \geq 1$ is plotted against temperature. For plotting the graphs, we have taken the density n=0.589, $M_q = 1$, Q=1 and $\hbar = 1$ (in the case of QGP, Lorentz Heaviside units are used). The potential shows a minimum near to the critical temperature T_c. The minimum potential near T_c will give rise to bound states (diquarks). This potential satisfies both the screening and the confinement type forces just like the Cornell potential.

In strongly coupled systems with high density, quantum effects are important [24]. Here the results have been obtained in the non-relativistic domain, but QGP composes an ultra-relativistic system. Since Coulomb interaction is common in both cases, it may be concluded that the screening effect is present in SCQGP. The minimum potential can give rise to bound states (diquarks) if thermal fluctuations

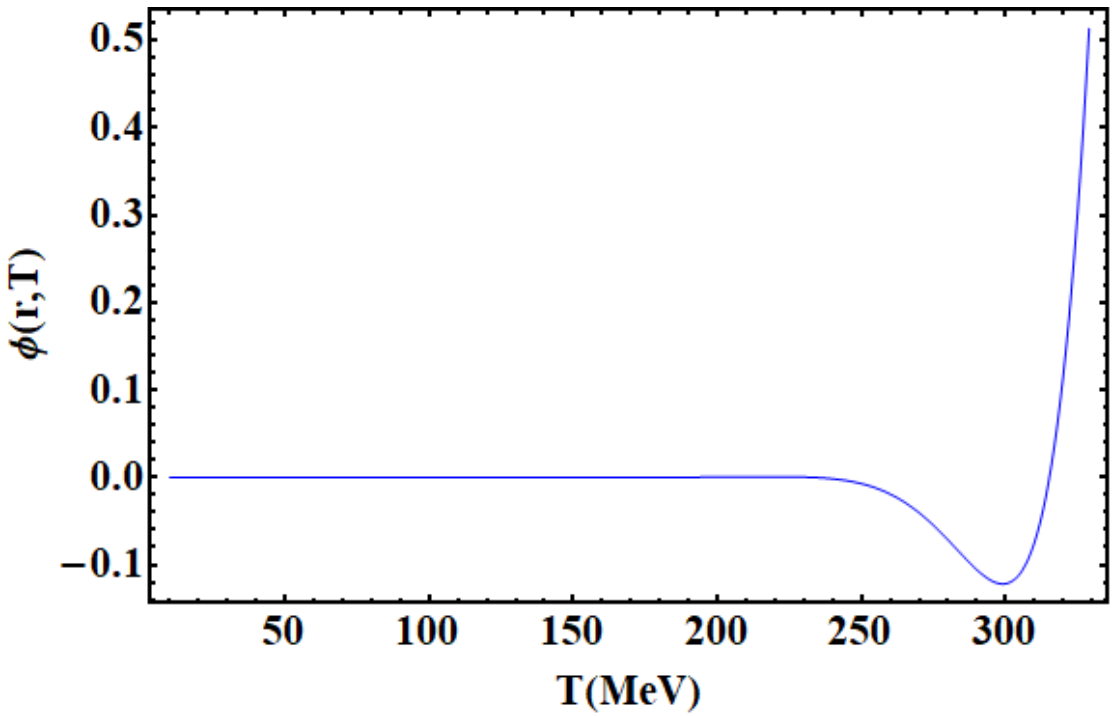

Figure 2.2: Variation of screening potential $\phi(r, T)$ with temperature T

do not destroy them. Here nonabelian effects are included in the expression for pressure. They cannot be treated separately in this method. Since there is an attraction even in complex plasmas and in QGP, close to the critical temperature [15], this seems to be a general feature of weakly as well as strongly coupled plasmas. Therefore, there will not be any qualitative change of the screening potential due to nonperturbative or nonabelian effects [1]. For a J/ψ meson, the binding may become weaker and of shorter range due to screening in QGP [7]. When the screening radius falls below the binding radius, the quark and antiquark can no longer be bound and the bound state becomes dissociated. The quarkonium dissociation points therefore determine the temperature and energy density of the QGP [22].

From direct finite temperature lattice studies, both in quenched and in full

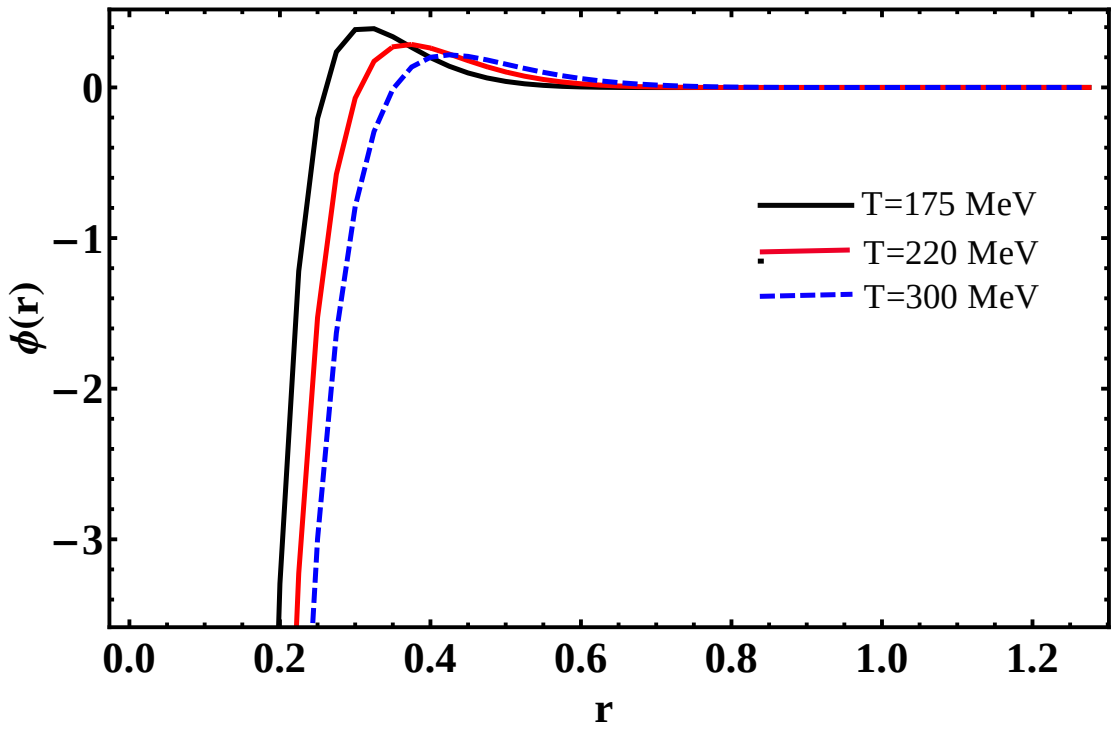

Figure 2.3: The potential $\phi(r)$ between the quark and antiquark as a function of r for different temperature

QCD as well as in lattice-based potential work, it can be shown that the J/ψ meson can survive up to $T \geq 2T_c$ [25]. At temperature above the critical temperature, QGP is strongly coupled quark-gluon plasma (SCQGP) and the screening potential explains the expected J/ψ suppression.

Bibliography

[1] M. G. Mustafa, M. H. Thoma, and P. Chakraborty, *Screening of a moving parton in the quark-gluon plasma*, Phys. Rev. C 71, 017901 (2005).

[2] U. Heinz, *The strongly coupled plasma created at RHIC*, J. Phys. A 42, 214003 (2009).

[3] V. M. Bannur, *Quark gluon plasma as a strongly coupled color Coulombic plasma*, Eur. Phys. J. C 11, 169 (1999).

[4] Z. Donko, P. Hartmann, and G. J. Kalman, *Strongly coupled plasma liquids*, EPJ manuscripts (2007).

[5] L. P. Pitaevskii and E. M. Lifshitz, *Physical kinetics*, Pergamon, Newyork (1981).

[6] B. K. Patra and D. K. Srivastava, *J/ψ suppression gluonic dissociation vs colour screening*, Phys. Lett. B 505, 113 (2001).

[7] T. Matsui and H. Satz, *J/ψ suppression by quark-gluon plasma formation*, Phys. Lett. B 178, 416 (1986).

[8] M. Gonin (NA50 Collaboration), *Anomalous J/ψ suppression in Pb+ Pb collisions at 158-A-GeV/c*, Nucl. Phys. A 610, 404C (1996).

[9] J. P. Blaizot and J. Y. Ollitrault, *J/ψ suppression in Pb–Pb Collisions: A hint of quark–gluon plasma production?*, Phys. Rev. Lett. 77, 1703 (1996).

[10] M.H. Thoma, *Complex plasmas as a model for the quark-gluon-plasma liquid*, Nucl. Phys. A 774, 307 (2006).

[11] P. K. Shukla and B. Eliasson, *Novel attractive force between ions in quantum plasmas*, Phys. Rev. Lett. 108, 1650070 (2012) .

[12] C. Gale and J. Kapusta, *Modification of Debye screening in gluon plasma*, Phys. Lett. B 198, 89 (1987).

[13] N. Crouseilles, P. A. Hervieux, and G. Manfredi, *Quantum hydrodynamic model for the nonlinear electron dynamics in thin metal films*, Phys. Rev. B 78, 155412 (2008).

[14] F. D. (Tony) Smith, Jr., *Bohm confirmed by non relativistic quark model*, quant-ph TS-TH-98-1 (1998).

[15] M.H Thoma, *The quark gluon plasma liquid*, J. Phys. G: Nucl. Part. Phys. 31, 539 (2005).

[16] S. Ramadas and V.M. Bannur, *SCQGP in compact stars*, Eur. Phys. J. C 72, 1975 (2012).

[17] A. Isihara and E.W. Montroll, *A note on the ground state energy of an assembly of interacting electrons*, Proc. Natl. Acad. Sci. USA 68, 12, 3111 (1971).

[18] P.B. Demorest, T. Pennucci, S. M. Ransom et al, *A two-solar-mass neutron star measured using Shapiro delay*, Nature 467, 1081 (2010).

[19] E.V. Shuryak and I. Zahed, *Towards a theory of binary bound states in the quark-gluon plasma*, Phys. Rev. D 70, 054507 (2004).

[20] V. M. Bannur, *Strongly coupled quark gluon plasma (SCQGP)*, J. Phys. G: Nucl. Part. Phys. 32 993 (2006).

[21] D. Bala and S. Datta, *Nonperturbative potential for the study of quarkonia in QGP*, Phys. Rev. D 101, 034507 (2020).

[22] F. Karsch, M. T. Mehr, and H. Satz, *Color screening and deconfinement for bound states of heavy quarks*, Z. Phys. C 37, 617 (1988).

[23] O. Kaczmarek , F. Karsch , E. Laermann, and M. Lutgemeier, *Heavy quark potentials in quenched QCD at high temperature*, Phys. Rev. D 62, 034021 (2000).

[24] R. Car and M. Parrinello, *Unified approach for molecular dynamics and density-functional theory*, Phys. Rev. Lett. 55, 2471 (1985).

[25] H. Satz, *Quarkonium binding and dissociation: the spectral analysis of the QGP*, Nuclear Physics A 783, 249 (2007).

Chapter 3

Calculation of Binding Energy of Bound States of Quarks in Strongly Coupled Quark Gluon Plasma

3.1 Introduction

There occurs a phase transition from a confined hadronic phase to a deconfined partonic phase at critical temperature (T_c), as discussed in section 1.3. This phase of deconfined quarks and gluons is called quark-gluon plasma (QGP) [1]. At extremely high temperatures QGP can be considered as an ideal gas of quarks and gluons because of the very weak interaction. At temperature near T_c, QGP can be considered as strongly coupled and termed as strongly coupled quark-gluon plasma (SCQGP) [2].

The existence of bound states above the critical temperature can be studied by using the effective temperature-dependent potential in the QGP. In fact, no strictly stationary bound state can exist in QGP as the interaction with the particles in the medium will lead to a definite lifetime for all bound states [3]. The bound state properties in quark-gluon plasma can be studied using two different approaches. The first one is a direct calculation using QCD [4] and the other one is the use of a potential model [5,6,7]. The nonrelativistic interaction potential model can reproduce the experimentally observed mass spectra of bound states [8,9]. This approach uses the potential as a function of the relative separation between the particles and the binding energy can be calculated mathematically by solving the Schrödinger equation.

N-dimensional non-relativistic radial Schrödinger equation can be solved for the interaction potential for different bound states in SCQGP. For solving the SE, the interaction potential should be known. A confining potential is a mathematical representation of a force that governs the dynamics of the particles in a particular system. Depending on the nature of interaction among the particles, a large number of confining potentials have been used. Some of them are Harmonic [10], Cornell [11], Coulomb [12], Coulomb perturbed [13], Ring-shaped [14], Double-ring shaped [15], Gaussian, modified Gaussian [16] Energy-dependent harmonic [17] etc.

There exist a number of exact, approximate, and numerical methods to solve the SE. In the last chapter, the existence of bound states has been discussed in the context of new attractive potential between the quarks in SCQGP. In this chapter we try to find out the binding energy of bound state of quarks in strongly coupled quark-gluon plasma by solving the N-dimensional Schrödinger equation for two

particles interacting via the two-body potential in three different methods i.e., analytical exact iteration method (AEIM) [18], power series method via a suitable ansatz to the wave function (PSM) [13] and the Nikiforov- Uvarov (NU) method [19].

3.2 Exact solution of the N-dimensional Schrödinger equation with the two body potential in SCQGP at finite temperature

3.2.1 Analytical exact iteration method (AEIM)

The N-dimensional non-relativistic radial Schrödinger equation for two particles [18, 20] interacting via the two-body potential is given by

$$\left[\frac{d^2}{dr^2}+\frac{N-1}{r}\frac{d}{dr}-\frac{l(l+N-2)}{r^2}+2\mu\Big(E_{nl}-\Phi(r)\Big)\right]\Psi(r)=0 \qquad (3.1)$$

where n , l and N are the principal quantum number, angular quantum number and the dimensional number respectively. μ is the reduced mass of two particles,

$$\mu=\frac{M_{q_1}M_{q_2}}{M_{q_1}+M_{q_2}}$$

Substituting $\Psi(r)=\frac{R(r)}{r^{\frac{N-1}{2}}}$ in Eq.(3.1)

$$\left[\frac{d^2}{dr^2}+\frac{N-1}{r}\frac{d}{dr}-\frac{l(l+N-2)}{r^2}+2\mu\Big(E_{nl}-\Phi(r)\Big)\right]\frac{R(r)}{r^{\frac{N-1}{2}}}=0 \qquad (3.2)$$

$$\left[\frac{d^2}{dr^2} - \frac{l(l+N-2) + \frac{N^2-4N+3}{4}}{r^2} + 2\mu\Big(E_{nl} - \Phi(r)\Big)\right] R(r) = 0 \tag{3.3}$$

where $\phi(r)$ is the two-body potential represented by the following equation [21]

$$\phi(r) = \frac{Q}{4\pi r}\left(\cos(k_i r) + \frac{1}{\sqrt{3}}\sin(k_i r)\right) e^{-k_r r} \tag{3.4}$$

where

$$k_i = \frac{k_s}{2}$$

$$k_r = \frac{\sqrt{3}}{2}k_s$$

with $Q = q_1 q_2$

Substituting Eq.(3.4) in Eq.(3.3) and rearranging,

$$\begin{aligned}\frac{d^2R(r)}{dr^2} = \Bigg[&- 2\mu E_{nl} + \frac{2\mu Q}{4\pi r}\left[\left(\cos(k_i r) + \frac{1}{\sqrt{3}}\sin(k_i r)\right) e^{-k_r r}\right] \\ &+ \frac{l(l+N-2) + \frac{N^2-4N+3}{4}}{r^2}\Bigg] R(r)\end{aligned} \tag{3.5}$$

The analytical exact iteration method (AEIM) assumes the wave function as [18],

$$R(r) = f_n(r)\exp\Big(g_l(r)\Big) \tag{3.6}$$

with,

$$f_n(r) = 1, n = 0 \tag{3.7}$$

$$f_n(r) = \Pi\left(r - \alpha_i^{(n)}\right), n = 1, 2, 3, ... \tag{3.8}$$

$$g_l(r) = -\frac{1}{2}\alpha r^2 - \beta r + \delta \ln r, \alpha > 0, \beta > 0 \tag{3.9}$$

From Eq.(3.6),

$$\frac{d^2R_{nl}}{d^2r} = \left[g_l"(r) + g_l(r)^2 + \frac{f_n"(r) + 2g_l'(r)f_n'(r)}{f_n(r)}\right] R_{nl}(r) \tag{3.10}$$

At n=0, substituting Eq.(3.7) and Eq.(3.9) in Eq.(3.10) , equating with Eq.(3.5) and comparing the powers of r on both sides, we get

$$\alpha = \sqrt{\left[\frac{2\mu Q}{4\pi}\left[-\frac{k_i^2k_r}{2} + \frac{k_ik_r^2}{2\sqrt{3}} - \frac{k_r^3}{6} - \frac{k_i^3}{6\sqrt{3}}\right]\right]} \tag{3.11}$$

$$\beta = \frac{\frac{2\mu Q}{4\pi}\left[-\frac{k_i^2}{2} - \frac{k_ik_r}{\sqrt{3}} + \frac{k_r^2}{2}\right]}{2\sqrt{\left[\frac{2\mu Q}{4\pi}\left[-\frac{k_i^2k_r}{2} + \frac{k_ik_r^2}{2\sqrt{3}} - \frac{k_r^3}{6} - \frac{k_i^3}{6\sqrt{3}}\right]\right]}} \tag{3.12}$$

$$\delta = \frac{1}{2} \pm \sqrt{\frac{1}{4} + l(l+N-2) + \frac{N^2-4N+3}{4}} \tag{3.13}$$

$$E_{0l}^N = \frac{Q}{4\pi}\left(-k_r + \frac{k_i}{\sqrt{3}}\right) - \frac{\beta^2}{2\mu} + \frac{\alpha}{2\mu}(1+2\delta) \tag{3.14}$$

$$E_{0l}^N = \frac{Q}{4\pi}\left(-k_r + \frac{k_i}{\sqrt{3}}\right) - \frac{\left[\frac{Q}{4\pi}\left[-\frac{k_i^2}{2} - \frac{k_ik_r}{\sqrt{3}} + \frac{k_r^2}{2}\right]\right]^2}{\left[\frac{Q}{\pi}\left[-\frac{k_i^2k_r}{2} + \frac{k_ik_r^2}{2\sqrt{3}} - \frac{k_r^3}{6} - \frac{k_i^3}{6\sqrt{3}}\right]\right]} + \frac{\sqrt{\left[\frac{2\mu Q}{4\pi}\left[-\frac{k_i^2k_r}{2} + \frac{k_ik_r^2}{2\sqrt{3}} - \frac{k_r^3}{6} - \frac{k_i^3}{6\sqrt{3}}\right]\right]}}{2\mu}\left(1 \pm \sqrt{1 + 4l(l+N-2) + N^2 - 4N + 3} + 1\right) \tag{3.15}$$

At n=1, substituting Eq.(3.8) and Eq.(3.9) in Eq.(3.10), equating with Eq.(3.5) and comparing the powers of r, we get

$$E_{1l}^{N}=\frac{Q}{4\pi}\left(-k_r+\frac{k_i}{\sqrt{3}}\right)-\frac{\beta^2}{2\mu}+\frac{\alpha}{2\mu}\Big(1+2(\delta+1)\Big) \tag{3.16}$$

$$E_{1l}^{N}=\frac{Q}{4\pi}\left(-k_r+\frac{k_i}{\sqrt{3}}\right)-\frac{\left[\frac{Q}{4\pi}\left[-\frac{k_i^2}{2}-\frac{k_ik_r}{\sqrt{3}}+\frac{k_r^2}{2}\right]\right]^2}{\left[Q\pi\left[-\frac{k_i^2k_r}{2}+\frac{k_ik_r^2}{2\sqrt{3}}-\frac{k_r^3}{6}-\frac{k_i^3}{6\sqrt{3}}\right]\right]}$$
$$+\frac{\sqrt{\left[\frac{2\mu Q}{4\pi}\left[-\frac{k_i^2k_r}{2}+\frac{k_ik_r^2}{2\sqrt{3}}-\frac{k_r^3}{6}-\frac{k_i^3}{6\sqrt{3}}\right]\right]}}{2\mu}\Big(3\pm\sqrt{1+4l(l+N-2)+N^2-4N+3}+1\Big) \tag{3.17}$$

Similarly at n=2,

$$E_{2l}^{N}=\frac{Q}{4\pi}\left(-k_r+\frac{k_i}{\sqrt{3}}\right)-\frac{\beta^2}{2\mu}+\frac{\alpha}{2\mu}\Big(1+2(\delta+2)\Big) \tag{3.18}$$

$$E_{2l}^{N}=\frac{Q}{4\pi}\left(-k_r+\frac{k_i}{\sqrt{3}}\right)-\frac{\left[\frac{Q}{4\pi}\left[-\frac{k_i^2}{2}-\frac{k_ik_r}{\sqrt{3}}+\frac{k_r^2}{2}\right]\right]^2}{\left[\frac{Q}{\pi}\left[-\frac{k_i^2k_r}{2}+\frac{k_ik_r^2}{2\sqrt{3}}-\frac{k_r^3}{6}-\frac{k_i^3}{6\sqrt{3}}\right]\right]}$$
$$+\frac{\sqrt{\left[\frac{2\mu Q}{4\pi}\left[-\frac{k_i^2k_r}{2}+\frac{k_ik_r^2}{2\sqrt{3}}-\frac{k_r^3}{6}-\frac{k_i^3}{6\sqrt{3}}\right]\right]}}{2\mu}\Big(5\pm\sqrt{1+4l(l+N-2)+N^2-4N+3}+1\Big) \tag{3.19}$$

The iteration can be repeated many times and the exact energy formula at finite temperature can be written as,

$$E_{nl}^{N}=\frac{Q}{4\pi}\left(-k_r+\frac{k_i}{\sqrt{3}}\right)-\frac{\beta^2}{2\mu}+\frac{\alpha}{2\mu}\Big(1+2(\delta+n)\Big) \tag{3.20}$$

$$E_{nl}^{N} = \frac{Q}{4\pi}\left(-k_r + \frac{k_i}{\sqrt{3}}\right) - \frac{\left[\frac{Q}{4\pi}\left[-\frac{k_i^2}{2} - \frac{k_i k_r}{\sqrt{3}} + \frac{k_r^2}{2}\right]\right]^2}{\left[\frac{Q}{\pi}\left[-\frac{k_i^2 k_r}{2} + \frac{k_i k_r^2}{2\sqrt{3}} - \frac{k_r^3}{6} - \frac{k_i^3}{6\sqrt{3}}\right]\right]}$$
$$+ \frac{\sqrt{\left[\frac{2\mu Q}{4\pi}\left[-\frac{k_i^2 k_r}{2} + \frac{k_i k_r^2}{2\sqrt{3}} - \frac{k_r^3}{6} - \frac{k_i^3}{6\sqrt{3}}\right]\right]}}{2\mu}\left(2(n+1) + \sqrt{1 + 4l(l+N-2) + N^2 - 4N + 3}\right) \tag{3.21}$$

where

$$k_i = \frac{k_s}{2}$$

$$k_r = \frac{\sqrt{3}}{2}k_s$$

$$k_s^2 = \frac{M_q \omega_p^2}{g_c \frac{\partial P}{\partial n_f}}$$

By considering the temperature dependence of α_s from the literature [2] we get,

$$\alpha_s(T) = \frac{6\pi}{(33-2n_f)\ln\left(T/\Lambda_T\right)}\left(1 - \frac{3(153-19n_f)}{(33-2n_f)^2}\frac{\ln\left(2\ln\left(T/\Lambda_T\right)\right)}{\ln\left(T/\Lambda_T\right)}\right)$$

Eq.(3.21) gives the expression for the binding energy of the bound state of quarks.

3.2.2 Power series method (PSM)

In N-dimensional space, the Schrödinger equation can be written as Eq.(3.1). In order to find out the solution to Eq.(3.1) ansatz for the wave function is taken as,

$$\Psi(r) = \exp(-\eta r^2 - \delta r)G(r) \tag{3.22}$$

Here η and δ are positive parameters that are to be determined in terms of potential parameters. $G(r)$ is assumed in series form as,

$$G(r) = \sum_{n=0}^{\infty} a_n r^{n+l} \tag{3.23}$$

Where a_0 and a_1 are non zero expansion coefficients. Now substituting Eqs.(3.22) and (3.23) in Eq.(3.1) and collecting the coefficients of like powers of r, we get

$$\begin{aligned}\sum_{n=0}^{\infty} a_n \Bigg[&\Bigg((n+l)(n+l-1) + (N-1)(n+l) - l(l+N-2)\Bigg) r^{n+l-2} \\ &+\Bigg(-\delta - \delta(n+l) - \delta(N-1) - \frac{2\mu Q}{4\pi}\Bigg) r^{n+l-1} \\ &+\Bigg(\delta^2 - 2\eta(n+l) - 2\eta(N-1) + 2\mu E - \frac{2\mu Q}{4\pi}\Big(-k_r + \frac{k_i}{\sqrt{3}}\Big)\Bigg) r^{n+l} \\ &+\Bigg(4\eta\delta - 2\eta - \frac{2\mu Q}{4\pi}\Big(\frac{k_r^2}{2} - \frac{k_i k_r}{\sqrt{3}} - \frac{k_i^2}{2}\Big)\Bigg) r^{n+l+1} \\ &+\Bigg(4\eta^2 - \frac{2\mu Q}{4\pi}\Big(-\frac{k_r^3}{6} + \frac{k_i k_r^2}{2\sqrt{3}} - \frac{k_i^2 k_r}{2} - \frac{k_i^3}{6\sqrt{3}}\Big)\Bigg) r^{n+l+2}\Bigg] = 0\end{aligned} \tag{3.24}$$

Equating each coefficient of r to zero, we get the following set of relation

$$(n+l)(n+l+N-2) - l(l+N-2) = 0 \tag{3.25}$$

$$-\delta(n+l+N)-\frac{2\mu Q}{4\pi}=0 \tag{3.26}$$

$$4\eta\delta-2\eta-\frac{2\mu Q}{4\pi}\left(\frac{k_r^2}{2}-\frac{k_ik_r}{\sqrt{3}}-\frac{k_i^2}{2}\right)=0 \tag{3.27}$$

$$4\eta^2-\frac{2\mu Q}{4\pi}\left(-\frac{k_r^3}{6}+\frac{k_ik_r^2}{2\sqrt{3}}-\frac{k_i^2k_r}{2}-\frac{k_i^3}{6\sqrt{3}}\right)=0 \tag{3.28}$$

$$2\mu E=-\delta^2+\frac{2\mu Q}{4\pi}\left(-k_r+\frac{k_i}{\sqrt{3}}\right)+2\eta(n+l+N-1) \tag{3.29}$$

In order to find out the eigenvalues from Eq.(3.29), the ansatz parameters η and δ should be known which can be obtained from Eq.(3.28) and (3.26) respectively.

$$\eta=\sqrt{\frac{2\mu Q}{16\pi}\left(-\frac{k_r^3}{6}+\frac{k_ik_r^2}{2\sqrt{3}}-\frac{k_i^2k_r}{2}-\frac{k_i^3}{6\sqrt{3}}\right)} \tag{3.30}$$

$$\delta=-\frac{2\mu Q}{4\pi(n+l+N)} \tag{3.31}$$

After substituting the values of η and δ the energy eigenvalue can be written as,

$$\begin{aligned}E_{nl}^N=&-\frac{2\mu Q^2}{\Big(4\pi(n+l+N)\Big)^2}+\frac{Q}{4\pi}\left(-k_r+\frac{k_i}{\sqrt{3}}\right)\\&+2\sqrt{\frac{Q}{32\pi\mu}\left(-\frac{k_r^3}{6}+\frac{k_ik_r^2}{2\sqrt{3}}-\frac{k_i^2k_r}{2}-\frac{k_i^3}{6\sqrt{3}}\right)}(n+l+N-1)\end{aligned} \tag{3.32}$$

Eq.(3.32) gives the expression for the binding energy of the bound state of quarks.

3.2.3 Nikiforov-Uvarov (NU) Method

a) A brief description of NU method

Consider a second-order differential equation of the form

$$\Psi''(s) + \frac{\tilde{\tau}(s)}{\sigma(s)}\Psi'(s) + \frac{\tilde{\sigma}(s)}{\sigma^2(s)}\Psi(s) = 0 \tag{3.33}$$

where $\sigma(s)$ and $\tilde{\sigma}(s)$ are polynomials of maximum second degree and $\tilde{\tau}(s)$ is a polynomial of maximum first degree with an appropriate $s = s(r)$ coordinate transformation.

If

$$\Psi(s) = \Phi(s)\chi(s) \tag{3.34}$$

Substituting Eq.(3.34) in Eq.(3.33)

$$2\Phi'(s)\chi'(s)+\Phi(s)\chi''(s)+\Phi''(s)\chi(s)+\frac{\tilde{\tau}(s)}{\sigma(s)}\Big(\Phi(s)\chi'(s)+\Phi'(s)\chi(s)\Big)+\frac{\tilde{\sigma}(s)}{\sigma^2(s)}\Phi(s)\chi(s) = 0$$

Rearranging the terms we get,

$$\phi(s)\chi''(s)+\Big(2\Phi'(s)+\frac{\tilde{\tau}(s)}{\sigma(s)}\Phi'(s)\Big)\chi'(s)+\Big(\Phi''(s)+\frac{\tilde{\tau}(s)}{\sigma(s)}\Phi'(s)+\frac{\tilde{\sigma}(s)}{\sigma^2(s)}\Phi(s)\Big)\chi(s) = 0$$

Dividing throgh out by $\Phi(s)$

$$\chi''(s) + \Big(\frac{2\Phi'(s)}{\Phi(s)} + \frac{\tilde{\tau}(s)}{\sigma(s)}\Big)\chi'(s) + \Big(\frac{\Phi''(s)}{\Phi(s)} + \frac{\tilde{\tau}(s)}{\sigma(s)}\frac{\Phi'(s)}{\Phi(s)} + \frac{\tilde{\sigma}(s)}{\sigma^2(s)}\Big)\chi(s) = 0$$

The coefficient of $\chi'(s)$ is taken in the form $\tau(s)/\sigma(s)$, where $\tau(s)$ is a polynomial

of degree atmost one. Then

$$\frac{2\Phi'(s)}{\Phi(s)} + \frac{\tilde{\tau}(s)}{\sigma(s)} = \frac{\tau(s)}{\sigma(s)} \tag{3.35}$$

This happens only if

$$\frac{\Phi'(s)}{\Phi(s)} = \frac{\pi(s)}{\sigma(s)} \tag{3.36}$$

Therefore

$$\frac{2\pi(s)}{\sigma(s)} + \frac{\tilde{\tau}(s)}{\sigma(s)} = \frac{\tau(s)}{\sigma(s)}$$

That is

$$2\pi(s) + \tilde{\tau}(s) = \tau(s)$$

Thus

$$\pi(s) = \frac{1}{2}\Big(\tau(s) - \tilde{\tau}(s)\Big)$$

and

$$\tau(s) = \tilde{\tau}(s) + 2\pi(s); \tau'(s) < 0 \tag{3.37}$$

The term $\Phi''(s)/\Phi(s)$ in the coefficient of $\chi(s)$ can be written as

$$\frac{\Phi''(s)}{\Phi(s)} = \Big(\frac{\Phi'(s)}{\Phi(s)}\Big)' + \Big(\frac{\Phi'(s)}{\Phi(s)}\Big)^2$$

Using Eq.(3.36),

$$\frac{\Phi''(s)}{\Phi(s)} = \Big(\frac{\pi(s)}{\sigma(s)}\Big)' + \Big(\frac{\pi(s)}{\sigma(s)}\Big)^2 \tag{3.38}$$

Now the coefficient of $\chi(s)$ is transformed in to a more suitable form,

$$\frac{\Phi''(s)}{\Phi(s)} + \frac{\tilde{\tau}(s)}{\sigma(S)}\frac{\Phi'(s)}{\Phi(s)} + \frac{\tilde{\sigma}(s)}{\sigma^2(s)} = \frac{\overline{\sigma}(s)}{\sigma^2(s)} \tag{3.39}$$

Substituting Eq.(3.38) in Eq.(3.39),

$$-\frac{\pi(s)\sigma'(s)}{\sigma^2(s)}+\frac{\pi'(s)}{\sigma(s)}+\frac{\pi^2(s)}{\sigma^2(s)}+\frac{\pi(s)\tilde{\tau}(s)}{\sigma^2(s)}+\frac{\tilde{\sigma}(s)}{\sigma^2(s)}=\frac{\overline{\sigma}(s)}{\sigma^2(s)}$$

Therefore

$$\overline{\sigma}(s)=\tilde{\sigma}(s)+\pi^2(s)+\pi(s)\Big(\tilde{\tau}(s)-\sigma(s)\Big)+\pi'(s)\sigma(s)$$

Substituting the right hand sides of Eq.(3.35), Eq.(3.38) and Eq.(3.39), Eq.(3.33) reduces to an equation of hypergeometric type as

$$\chi''(s)+\frac{\tau(s)}{\sigma(s)}\chi'(s)+\frac{\overline{\sigma}(s)}{\sigma^2(s)}\chi(s)=0 \tag{3.40}$$

with

$$\sigma(s)=\pi(s)\frac{\Phi(s)}{\Phi'(s)} \tag{3.41}$$

As a consequence of the algebraic transformations above, the functional form of Eq.(3.33) is protected in a systematic way. If the polynomial $\overline{\sigma}(s)$ in Eq.(3.40) is divisible by $\sigma(s)$, we can write

$$\overline{\sigma}(s)=\lambda\sigma(s)$$

Where λ is a constant. Then Eq.(3.40) is reduced to,

$$\sigma(s)\chi''(s)+\tau(s)\chi'(s)+\lambda\chi(s)=0 \tag{3.42}$$

To determine the polynomial $\pi(s)$,

$$\overline{\sigma}(s) = \tilde{\sigma}(s) + \pi^2(s) + \pi(s)\Big(\tilde{\tau}(s) - \sigma(s)\Big) + \pi'(s)\sigma(s) = \lambda\sigma(s)$$

That is

$$\tilde{\sigma}(s) + \pi^2(s) + \pi(s)\Big(\tilde{\tau}(s) - \sigma(s)\Big) - K\sigma(s) = 0$$

with

$$K = \lambda - \pi'(s) \tag{3.43}$$

The solution of this quadratic equation for $\Pi(s)$ gives

$$\pi(s) = \frac{\sigma'(s) - \overline{\tau}(s)}{2} \pm \sqrt{\left(\frac{\sigma'(s) - \overline{\tau}(s)}{2}\right)^2 - \overline{\sigma}(s) + K\sigma(s)} \tag{3.44}$$

where $\pi(s)$ is a polynomial of first degree. The values of K in the square root of Eq.(3.44) can be calculated if the expressions under the square root are square of expressions. This is possible if its discriminant is zero. $\chi(s) = \chi_n(s)$ is a polynomial of n^{th} degree which satisfies the hypergeometric equation, in order to obtain an eigen value solution through the NU method, a relation between λ and λ_n must be set up which is given by,

$$\lambda = \lambda_n = -n\tau'(s) - \frac{n(n-1)}{2}\sigma''(s), n = 0, 1, 2.... \tag{3.45}$$

$\chi_n(s)$ is a hypergeometric type function whose polynomial solutions are given by the Rodrigue's relation

$$\chi_n(s) = \frac{B_n}{\rho_n}\frac{d^n}{ds^n}(\sigma''(s)\rho(s)) \tag{3.46}$$

where B_n is a normalization constant and $\rho(s)$ is the weight function that satisfies the equation

$$\frac{d}{ds}\omega(s) = \frac{\tau(s)}{\sigma(s)}\omega(s); \omega(s) = \sigma(s)\rho(s) \tag{3.47}$$

b) Solution of N-dimensional Schrödinger equation at finite temperature

The Schrödinger equation for two particles interacting via a spherically symmetric potential $\phi(r)$ in N- dimensional space is given by Eq.(3.1), where $\phi(r)$ is given by Eq.(3.4). Now the N-dimensional Schrödinger equation can be written as,

$$\begin{aligned}\Bigg[\frac{d^2}{dr^2} + 2\mu\Bigg[E - \frac{Q}{4\pi r}\Bigg[\Big(\cos(k_i r) + \frac{1}{\sqrt{3}}\sin(k_i r)\Big)e^{-k_r r}\Bigg] \\ - \frac{l(l+N-2) + \frac{N^2-4N+3}{4}}{2\mu r^2}\Bigg]\Bigg]R(r) = 0\end{aligned} \tag{3.48}$$

or

$$\begin{aligned}\Bigg[\frac{d^2}{dr^2} + 2\mu\Bigg(E - \frac{Q}{4\pi}\Bigg[\frac{1}{r} + \Big(-k_r + \frac{k_i}{\sqrt{3}}\Big) + \Big(\frac{k_r^2}{2} - \frac{k_i k_r}{\sqrt{3}} - \frac{k_i^2}{2}\Big)r \\ + \Big(-\frac{k_r^3}{6} + \frac{k_i k_r^2}{2\sqrt{3}} - \frac{k_i^2 k_r}{2} - \frac{k_i^3}{6\sqrt{3}}\Big)r^2\Bigg] - \frac{l(l+N-2) + \frac{N^2-4N+3}{4}}{2\mu r^2}\Bigg)\Bigg]R(r) = 0\end{aligned} \tag{3.49}$$

Putting $r = \frac{1}{x}$, equation becomes

$$\left[\frac{d^2}{dx^2}+\frac{2x}{x^2}\frac{d}{dx}+\frac{2\mu}{x^4}\left(E-\frac{Q}{4\pi}\left[x+\left(-k_r+\frac{k_i}{\sqrt{3}}\right)\right.\right.\right.$$
$$+\left(\frac{k_r^2}{2}-\frac{k_ik_r}{\sqrt{3}}-\frac{k_i^2}{2}\right)\frac{1}{x}+\left(-\frac{k_r^3}{6}+\frac{k_ik_r^2}{2\sqrt{3}}-\frac{k_i^2k_r}{2}-\frac{k_i^3}{6\sqrt{3}}\right)\frac{1}{x^2}\Bigg] \tag{3.50}$$
$$\left.\left.\left.-\frac{l(l+N-2)+\frac{N^2-4N+3}{4}}{2\mu}x^2\right)\right]R(x)=0$$

or

$$\left[\frac{d^2}{dx^2}+\frac{2x}{x^2}\frac{d}{dx}+\frac{2\mu}{x^4}\left[E-Ax-B-\frac{C}{x}-\frac{D}{x^2}\right.\right.$$
$$\left.\left.-\frac{l(l+N-2)+\frac{N^2-4N+3}{4}}{2\mu}x^2\right]\right]R(x)=0 \tag{3.51}$$

where

$$A=\frac{Q}{4\pi}$$

$$B=\frac{Q}{4\pi}\left(-k_r+\frac{k_i}{\sqrt{3}}\right)$$

$$C=\frac{Q}{4\pi}\left(\frac{k_r^2}{2}-\frac{k_ik_r}{\sqrt{3}}-\frac{k_i^2}{2}\right)$$

$$D=\frac{Q}{4\pi}\left(-\frac{k_r^3}{6}+\frac{k_ik_r^2}{2\sqrt{3}}-\frac{k_i^2k_r}{2}-\frac{k_i^3}{6\sqrt{3}}\right)$$

Now expand $\frac{C}{x}$ and $\frac{D}{x^2}$ in a power series around the characteristic radius r_0 of the meson up to the second-order, Setting $y=x-\delta$, where $\delta=\frac{1}{r_0}$. Now we expand $\frac{C}{x}$ and $\frac{D}{x^2}$ in a power series around $y=0$ [19] as,

$$\frac{C}{x}=C\left(\frac{3}{\delta}-\frac{3x}{\delta^2}+\frac{x^2}{\delta^3}\right) \tag{3.52}$$

and

$$\frac{D}{x^2}=D\left(\frac{6}{\delta^2}-\frac{8x}{\delta^3}+\frac{3x^2}{\delta^4}\right) \tag{3.53}$$

Substituting Eq.(3.52) and (3.53) in Eq.(3.51),

$$\left[\frac{d^2}{dx^2}+\frac{2x}{x^2}\frac{d}{dx}+\frac{2\mu}{x^4}\left[E-Ax-B-C\left(\frac{3}{\delta}-\frac{3x}{\delta^2}+\frac{x^2}{\delta^3}\right)\right.\right.$$
$$\left.\left.-D\left(\frac{6}{\delta^2}-\frac{8x}{\delta^3}+\frac{3x^2}{\delta^4}\right)-\frac{l(l+N-2)+\frac{N^2-4N+3}{4}}{2\mu}x^2\right]\right]R(x)=0 \tag{3.54}$$

or we can write

$$\left[\frac{d^2}{dx^2}+\frac{2x}{x^2}\frac{d}{dx}+\frac{2\mu}{x^4}\left[-D_1+D_2x-D_3x^2\right]\right]R(x)=0 \tag{3.55}$$

where

$$D_1=-\left[E-B-\frac{3C}{\delta}-\frac{6D}{\delta^2}\right]$$

$$D_2=-A+\frac{3C}{\delta^2}+\frac{8D}{\delta^3}$$

$$D_3=\frac{C}{\delta^3}+\frac{3D}{\delta^4}+\frac{l(l+N-2)+\frac{N^2-4N+3}{4}}{2\mu}$$

Comparing Eq.(3.33) and Eq.(3.55) we get,

$$\overline{\tau}(s)=2x$$

$$\sigma(s)=x^2$$

$$\overline{\sigma}(s)=2\mu\left(-D_1+D_2x-D_3x^2\right)$$

By following NU method,

$$\pi=\sqrt{2a-2bx+(K+2c_1)x^2} \tag{3.56}$$

where

$$a = 2\mu D_1$$

$$b = 2\mu D_2$$

$$c_1 = 2\mu D_3$$

The constant K is chosen such as the discriminant of the function under the square root is zero i.e

$$\Delta = 4b^2 - 8a(K + 2c_1) = 0$$

$$b^2 = 2a(K + 2c_1)$$

$$K = \frac{b^2}{2a} - 2c_1$$

$$\pi = \frac{2a - bx}{\sqrt{2a}} \tag{3.57}$$

Thus

$$\tau = 2x \pm \frac{2(2a - bx)}{\sqrt{2a}} \tag{3.58}$$

We choose the positive sign in the above equation for bound state solutions.

$$\tau' = 2 - \frac{2b}{\sqrt{2a}} \tag{3.59}$$

By using Eq.(3.43), we obtain

$$\lambda = \frac{b^2}{a} - 2c_1 - \frac{b}{\sqrt{2a}} \tag{3.60}$$

$$\lambda_n = -n\left(2 - \frac{2b}{\sqrt{2a}}\right) - n(n-1) \tag{3.61}$$

From Eq.(3.45),

$$\lambda = \lambda_n$$

$$\frac{b^2}{a} - 2c_1 - \frac{b}{\sqrt{2a}} = -n\left(2 - \frac{2b}{\sqrt{2a}}\right) - n(n-1)$$

$$\frac{b^2}{2a} - \frac{b}{\sqrt{2a}}(1+2n) = -n^2 - n + 2c_1$$

$$\left(\frac{b}{\sqrt{2a}} - \frac{(2n+1)}{2}\right)^2 = \frac{1}{4} + 2c_1$$

$$\frac{b}{\sqrt{2a}} - \frac{(2n+1)}{2} = \sqrt{\frac{1}{4} + 2c_1}$$

$$\frac{b}{\sqrt{2a}} = \frac{(2n+1)}{2} \pm \sqrt{\frac{1}{4} + 2c_1}$$

$$\frac{b^2}{2a} = \left(\frac{(2n+1)}{2} \pm \sqrt{\frac{1}{4} + 2c_1}\right)^2$$

$$a = \frac{b^2}{2\left(\frac{(2n+1)}{2} \pm \sqrt{\frac{1}{4} + 2c_1}\right)^2}$$

$$D_1 = \frac{2\mu D_2^2}{\left((2n+1) \pm \sqrt{1 + 8\mu D_3}\right)^2}$$

$$-E + B + \frac{3C}{\delta} + \frac{6D}{\delta^2} = \frac{2\mu\left(-A + \frac{3C}{\delta^2} + \frac{8D}{\delta^3}\right)^2}{\left((2n+1) \pm \sqrt{1 + 8\mu\left(\frac{C}{\delta^3} + \frac{3D}{\delta^4} + \frac{l(l+N-2) + \frac{N^2-4N+3}{4}}{2\mu}\right)}\right)^2}$$

The energy eigen values at finite temperature in N-dimensional space can be writ-

ten as

$$E_{nl}^{N} = B+\frac{3C}{\delta}+\frac{6D}{\delta^2}-\frac{2\mu\left(-A+\frac{3C}{\delta^2}+\frac{8D}{\delta^3}\right)^2}{\left((2n+1)\pm\sqrt{1+\frac{8\mu C}{\delta^3}+\frac{24\mu D}{\delta^4}+4\left(l(l+N-2)+\frac{N^2-4N+3}{4}\right)}\right)^2} \tag{3.62}$$

Eq.(3.62) gives the expression for the binding energy of the bound state of quarks.

3.3 Conclusion

In this work, we have used the screening attractive potential to study the formation of bound states of quarks in a simple manner. Using this attractive potential, Schrodinger's equation is solved for getting the binding energy of the bound state of quarks in strongly coupled quark-gluon plasma in three different methods. These three methods incorporate no different Physics. But they are three ways for obtaining the results by solving SE. These are done in order to compare the numerical results such as binding energy, mass spectra and dissociation temperatures.

Bibliography

[1] R. Pasechnik and M. Šumbera, *Phenomenological review on quark–gluon plasma: Concepts vs. observations*, Universe 3 (1), 7 (2017).

[2] V. M. Bannur, *Strongly coupled quark gluon plasma (SCQGP)*, J. Phys. G: Nucl. Part. Phys. 32, 993 (2006).

[3] M. Escobedo, J. Soto, and M. Mannarelli, *Non-relativistic bound states in a moving thermal bath*, Phys. Rev. D 84, 016008 (2011).

[4] H. Mutuk, *Mass spectra and decay constants of heavy-light mesons: A case study of QCD sum rules and quark model*, Advances in High Energy Physics, Vol. 2018, Article ID 8095653 (2018).

[5] K. K. Pathak and D. K. Choudhury, *Open flavour charmed mesons in a quantum chromodynamics potential model*, Pramana-J. Phys. 79 (6), 1385 (2012).

[6] K. K. Pathak, D. K. Choudhury, and N. S. Bordoloi., *Leptonic decay of heavy–light mesons in a QCD potential model*, Int. J. Mod. Phys. A 28 (2), 1350010 (2013).

[7] H. Hassanabadi, M. Ghafourian, and S. Rahmani, *Study of heavy-light mesons properties via the variational method for Cornell interaction*, Few-Body Syst. 57, 249 (2016).

[8] S. M. Ikhdair and R. Sever, *B_c meson spectrum and hyperfine splittings in the shifted large-N-expansion technique*, Int. J. Mod. Phys. A 18 (23), 4215 (2003).

[9] P. Gupta and I. Mehrotra, *Heavy quark spectroscopy*, Ind. J. Phys. 85 (1), 111 (2011).

[10] A. Jahanshir, *Di-mesonic molecules mass spectra* Indian Journal of Science and Technology, Vol 10 (22) (2017).

[11] S. N. Gupta, S. F. Radford, and W. W. Repko, *Quarkonium spectra and quantum chromodynamics*, Phys. Rev. D 26, 3305 (1982).

[12] S. Rahmani and H. Hassanabadi, *Mass spectra of meson molecular states for heavy and light sectors*, Chin. Phys. C 41, 093105 (2017).

[13] R. Kumar and F. Chand, *Energy spectra of the coulomb perturbed potential in N-dimensional Hilbert space*, Chin. Phys. Lett. 29, 060306 (2012).

[14] B. J. Falaye, *The Klein-Gordon equation with ring-shaped potentials: Asymptotic iteration method*, J. Math. Phys. 53, 082107 (2012).

[15] F. Yasuk and A. Durmus, *Relativistic solutions for double ring-shaped oscillator potential via asymptotic iteration method*, Phys. Scr. 77, 015005 (2007).

[16] S. Bednarek, B. Szafran, K. Lis, and J. Adamowski, *Modeling of electronic properties of electrostatic quantum dots*, Phys. Rev. B 68, 155333 (2003).

[17] P. Gupta and I. Mehrotra, *Study of heavy quarkonium with energy dependent Potential*, J. Mod. Phys. 3 (10), 1530 (2012).

[18] M. Abu-Shady, T. A. Abdel-Karim, and E. M. Khokha, *Binding energies and dissociation temperatures of heavy quarkonia at finite temperature and chemical potential in the N-dimensional space*, Advances in High Energy Physics, Volume 2018, Article ID 7356843 (2018).

[19] M. Abu-Shady, T.A. Abdel-Karim, and S.Y. Ezz-Alarab, *Masses and thermodynamic properties of heavy mesons in the non-relativistic quark model using the Nikiforov–Uvarov method*, J. Egypt. Math. Soc. 27, 14 (2019).

[20] T. Das and A. Arda, *Exact analytical solution of the N-dimensional radial Schrödinger equation with pseudoharmonic potential via Laplace transform approach*, Advances in High Energy Physics, Vol. 2015, Article ID 137038 (2015).

[21] K. T. Rethika and V. M. Bannur, *Screening of a test quark in the strongly coupled quark gluon plasma*, Few-Body Syst 60, 38 (2019).

Chapter 4

Binding Energies and Effective Masses of Diquarks in SCQGP

4.1 Introduction

In [1], it is proposed that near and above T_c there are multiple bound states of quasi-particles which are very important for the thermodynamics of the QGP. At $T \geq T_c$, it has been argued that there is no color confinement and there is Coulomb-like interaction at small distances with a Debye type screening at large distances [2].

The deconfined quarks and gluons pair up non-perturbatively in order to lower the energy of the system. This may lead to the formation of a system of two quarks called diquark [3] or multi quark system consisting of more number of quarks. These multi-quark systems can be studied using different models such as the MIT bag model [4] and the Potential model [5]. Out of all possible multi-quark states, the study of diquarks is more important in the context of QGP

formed in RHIC experiments [6]. In 1964 GellMann first mentioned the possibility of diquarks. A diquark is any system of two quarks considered collectively. The idea of diquarks has been used in hadron physics for describing many properties of hadrons [3]. This study is also important in the context of astrophysical conditions [7], especially in cosmological contexts involving early phases of the evolution of the universe [8]. The question about the existence of diquarks as quasi-bound states in cold quark matter was emerged in [6], in which the authors have claimed that the quark-diquark matter was energetically more favorable than the free quark matter. The idea of the possible existence of quasi-bound states of quarks and gluons including diquarks with the temperature in the range $T_c \leq T \leq 4T_c$ was put forward by Shuryak et al. [1]. In [9] it was shown that the Λ_c/D^0 ratio could be enhanced by a factor of 4-8 than the case without diquarks in quark-qluon plasma. Diquark correlations play an important role inside baryons. Two quarks bound in a color anti triplet configuration can couple with a single quark to form a color singlet baryon. Recent studies of baryons as bound states of a quark and a confined diquark are done [10]. Some lattice simulations also indicate the existence of correlations in the diquark channel. A diquark in its ground state has positive poarity and may be a scalar (Spin 0) or an axial vector (Spin 1). It has been pointed out that the production of scalar diquarks is much larger than the vector diquarks. Evidence for scalar diquarks has been confirmed by lattice QCD simulation [11].

In chapter 2, a new screening potential is proposed and in chapter 3, the binding energy of the bound states of quarks is calculated by solving the Schrodinger's equation using this potential in three different methods i.e., analytical exact iteration method (AEIM), power series method (PSM) and Nikiforov - Uvarov (NU)

method. In this chapter, we calculate the binding energies of scalar diquarks in two methods i.e., analytical exact iteration method (AEIM) and power series method (PSM). The scalar diquark masses are calculated using the ground state binding energy of the bound states in strongly coupled quark-gluon plasma (SCQGP). Also, the relativistic correction is done to the light diquark mass.

4.2 Binding energy of diquarks

4.2.1 Analytical exact iteration method (AEIM)

Using Eq.(3.21), the binding energy of diquarks in the strongly coupled quark-gluon plasma at N=3 can be written as,

$$E_{nl} = \frac{Q}{4\pi}\left(-k_r + \frac{k_i}{\sqrt{3}}\right) - \frac{\left[Q4\pi\left[-\frac{k_i^2}{2} - \frac{k_i k_r}{\sqrt{3}} + \frac{k_r^2}{2}\right]\right]^2}{\left[\frac{Q}{\pi}\left[-\frac{k_i^2 k_r}{2} + \frac{k_i k_r^2}{2\sqrt{3}} - \frac{k_r^3}{6} - \frac{k_i^3}{6\sqrt{3}}\right]\right]} + \frac{\sqrt{\left[\frac{2\mu Q}{4\pi}\left[-\frac{k_i^2 k_r}{2} + \frac{k_i k_r^2}{2\sqrt{3}} - \frac{k_r^3}{6} - \frac{k_i^3}{6\sqrt{3}}\right]\right]}}{2\mu}\left(2(n+1) \pm \sqrt{1+4l(l+1)}\right) \tag{4.1}$$

4.2.2 Power series method (PSM)

Using Eq.(3.32), the binding energy of diquarks in the strongly coupled quark-gluon plasma at N=3 can be written as,

$$E_{nl} = -\frac{2\mu Q^2}{\left(4\pi(n+l+3)\right)^2} + \frac{Q}{4\pi}\left(-k_r + \frac{k_i}{\sqrt{3}}\right) + 2\sqrt{\frac{Q}{32\pi\mu}\left(-\frac{k_r^3}{6} + \frac{k_i k_r^2}{2\sqrt{3}} - \frac{k_i^2 k_r}{2} - \frac{k_i^3}{6\sqrt{3}}\right)}(n+l+2) \tag{4.2}$$

where $Q = q_1 q_2$

The ground state binding energies of different scalar diquarks in two methods were given in Fig. 4.1 as functions of temperature.

4.3 Effective mass of diquarks

Using the binding energy, the mass of diquark can be calculated as [12],

$$M_D^* = M_{q_1} + M_{q_2} + E_{nl} \tag{4.3}$$

where M_{q_1} and M_{q_2} are the masses of constituent quarks, M_D^* is the effective mass of the diquark and E_{nl} is the binding energy given by Eq.(4.1) and (4.2).

Effective masses of scalar diquarks were calculated using the ground state binding energy of the diquarks in two methods at temperature $1.05T_c$, where $T_c = 175MeV$ and the result is given in Table 3.1. Since the heavy diquark states are weakly bound, the nonrelativistic treatment could be completely justified. A similar conclusion would be reached for light qq pairs. Since the binding is weak, relativistic correction may be excluded. But here we try to do the relativistic correction in a simple manner.

4.4 Relativistic Correction

The potential used above was evaluated for static charges without spin and therefore it does not include the effects of particle velocities and spin. The relativistic

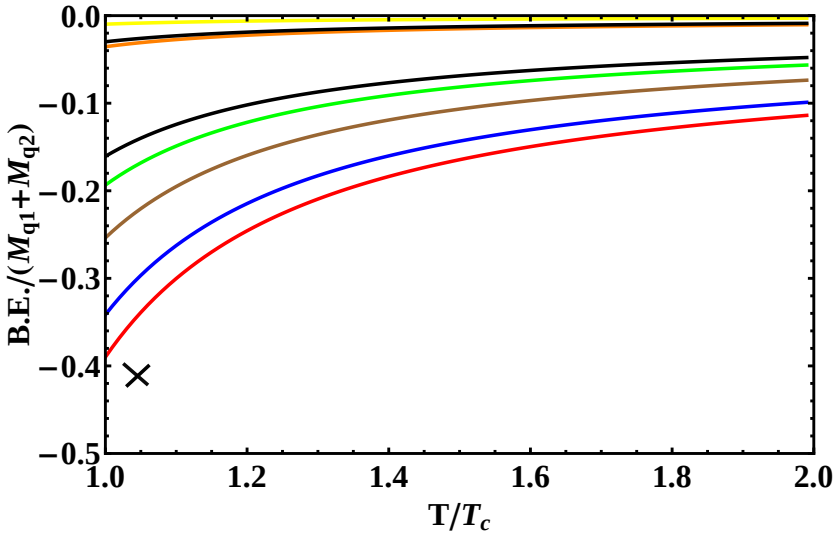

(a) Dependence of diquark binding energy in units of the constituent quark mass on temperature, from bottom to top,(i)$[qq]_0$ (ii) $[qs]_0$ (iii) $[ss]_0$ (iv) $[qc]_0$ (v) $[cc]_0$ (vi) $[qb]_0$ (vii) $[sb]_0$ (viii) $[bb]_0$. The single cross represents the relativistic correction to the binding energy of $[qq]_0$ diquark at temperature $1.05T_c$ (q=u,d) (AEIM)

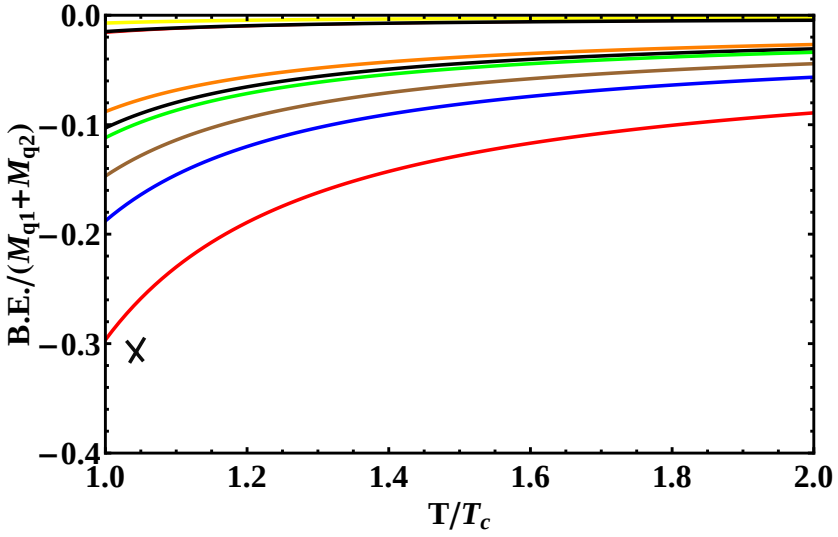

(b) Dependence of diquark binding energy in units of the constituent quark mass on temperature, from bottom to top,(i)$[qq]_0$ (ii) $[qs]_0$ (iii) $[ss]_0$ (iv) $[qc]_0$ (v) $[cc]_0$ (vi) $[qb]_0$ (vii) $[sb]_0$ (viii) $[bb]_0$. The single cross represents the relativistic correction to the binding energy of $[qq]_0$ diquark at temperature $1.05T_c$ (q=u,d) (PSM)

Figure 4.1: Dependence of diquark binding energy in units of the constituent quark mass on temperature

Table 4.1: Diquark Masses

Quark Content	AEIM	PSM
$[qq]_0$	0.5072 (0.4609)	0.5343 (0.4954)
$[qs]_0$	0.7023	0.8124
$[ss]_0$	0.8991	0.9972
$[qc]_0$	1.3711	1.7319
$[sc]_0$	2.5588	2.3914
$[sb]_0$	5.4453	5.5172
$[qb]_0$	5.2437	5.3313
$[cc]_0$	2.9431	3.1144
$[cb]_0$	6.9690	6.8582
$[bb]_0$	10.0144	10.0373

effect can be included by the substitution of the effective Coulomb coupling by [2]

$$\alpha_s \to \alpha_s(1 - \beta_1\beta_2) \tag{4.4}$$

where β_1 and β_2 are the velocities (in units of c) of both the particles. Since the velocities are always opposite in C.M., the coupling increases. Let $< v^2 >= 0.12$ for light quarks at $\frac{T}{T_c} = 1.05$ [2]. If we include this correction to the potential we get larger binding. By including this correction at $T \approx T_c$, the light quarks become relativistic. The relativistically corrected light diquark mass is written in brackets in Table 4.1. If the particle velocity becomes the speed of light this correction doubles the coupling.

4.5 Results and Discussion

In the current chapter, we have investigated the binding energies of some scalar diquarks. In Fig. 4.1, the light diquark binding energy looks considerable than the heavy diquark and light-heavy diquarks. This shows the relatively large possibility

for the existence of light diquarks near the transition temperature. The diquarks can be described as elementary excitations stimulating the many-body interactions and behave like scalar bosons [13]. Two quarks should be antisymmetric in color so that a total color singlet state is obtained. Recent lattice works have found that the bound states can persist to at least $T = 2T_c$ [2]. This new potential also supports this condition. In general, diquark masses have contributions from the constituent masses, the confining and spin-dependent part of the quark-quark interaction [14]. These contributions are additive in a simple potential model [15]. The spin-dependent contribution may include a contribution from flavor-spin and color-spin dependent interaction terms. The masses are expected to get the largest contribution from the constituent mass term and the confinement part [14], the spin-dependent part is related to the mass splitting of the S=0, S=1 diquarks and it is not considered here as we have reported only the scalar diquark masses.

Bibliography

[1] E. V. Shuryak and I. Zahed, *Rethinking the properties of the quark-gluon plasma at* $T_c < T < 4T_c$, Phys. Rev. C 70, 021901 (2004).

[2] E. V. Shuryak and I. Zahed, *Toward a theory of binary bound states in the quark-gluon plasma*, Phys. Rev. D 70, 054507 (2004).

[3] D.B. Lichtenberg, L.J. Tassie, and P. J. Keleman, *Quark-diquark model of baryons and SU(6)*, Phys. Rev. 167, 1535 (1968).

[4] R. L. Jaffe and F. E. Low, *Connection between quark-model eigenstates and low-energy scattering*, Phys. Rev. D 19, 2105 (1979).

[5] J. Weinstein and N. Isgur, $qq\overline{qq}$ *system in a potential model*, Phys. Rev D 27, 588 (1983).

[6] J. F. Donoghue and K.S .Sateesh, *Diquark clusters in the quark-gluon plasma*, Phys. Rev. D 38, 360 (1988).

[7] D. Blaschke, S. Fredriksson, H. Grigorian, and A.M. Oztas, *Diquark condensation effects on hot quark star configurations*, Nucl. Phys. A 736, 203 (2004).

[8] S. K. Karn, R. S. Kaushal, and Y. K. Mathur, *On diquark clusters in a quark-gluon plasma*, Z. Phys. C 72, 297 (1996).

[9] S. H. Lee, K. Ohnishi, S. Yasui, I.K. Yoo, and C. M. Ko, Λ_c *enhancement from strongly coupled quark-gluon plasma*, Phys. Rev. Lett. 100 (22), 222301 (2008).

[10] J. Liao and E. V. Shuryak, *Polymer chains and baryons in a strongly coupled quark-gluon plasma*, Nucl. Phys. A, 775, 224 (2006).

[11] C. Alexandrou, Ph. de Forcrand, and B. Lucini, *Evidence for diquarks in lattice QCD*, Phys. Rev. Lett. 97, 222002 (2006).

[12] M. Abu-Shady, T. A. Abdel-Karim, and E. M. Khokha, *Binding energies and dissociation temperatures of heavy quarkonia at finite temperature and chemical potential in the N-dimensional space*, Advances in High Energy Physics, Volume 2018, 7356843 (2018).

[13] A. Chandra, A. Bhattacharya, and B. Chakrabarti, *Temperature dependent diquark and baryon masses*, J. Mod. Phys. 4, 945 (2013).

[14] M. Hess, F. Karsch, E. Laermann, and I. Wetzorke, *Diquark masses from lattice QCD*, Phys. Rev. D 58, 111502(R) (1998) .

[15] L. Y. Glozman and D.O. Riska, *The spectrum of the nucleons and the strange hyperons and chiral dynamics*, Phys. Rep. 268, 264 (1996).

Chapter 5

Heavy Quarkonium Properties at Finite Temperature in Strongly Coupled Quark Gluon Plasma

5.1 Introduction

The bound states of a heavy quark and its antiquark are generally referred to as quarkonia. Other than the vector ground states J/ψ and Υ both the $c\bar{c}$ and $b\bar{b}$ systems give rise to many other stable states of different quantum numbers. The stable charmonium spectrum consists of 1S scalar η_c and vector J/ψ, three 1P states χ_c (scalar, vector, and tensor) and 2S vector state ψ'. The stable bottomonium spectrum contains Υ, χ_b, Υ', χ_b' and Υ" [1]. Heavy quarkonium has received more theoretical attention because heavy quark states are dominated by short-distance physics and can be treated using heavy quark effective theory [2]. Both experimental and theoretical studies suggest that the dissociation tempera-

tures of heavy quarkonia are slightly smaller than twice the critical temperature [3]. Because of the large mass, the velocity of heavy quarks is smaller and hence the spectrum of the quarkonia comprised of heavy quarks can be estimated using potential-based nonrelativistic treatments [4]. It has been argued that the screening above the critical temperature is strong enough to lead to the dissociation of the J/ψ state which may be considered as the signal of QGP formation [5]. Charmonium suppression and screening may be related as in [6].

Various potential models have been used to study the quarkonium properties at finite temperature, the first work in this field was done by Karsch, Mehr, and Satz [7]. Heavy quarkonium suppression has been an interesting subject after the theoretical work of Matzui and Satz [5]. Later Digal, Petreczky, and Satz reported the dissociation temperatures of quarkonia in hadron and QGP phases [8, 9]. Recent research successfully attempted to estimate the mass spectra of charmonium and bottomonium mesons and to determine the binding energy and dissociation temperature of heavy quarkonia [10, 11, 12]. In [4, 11, 12] the authors tried to solve the Schrödinger equation at finite temperature for the charmonium and bottomonium states using an effective temperature-dependent potential. The binding energy of the heavy quarkonium states is studied in [13, 14]. At finite chemical potential and in a small temperature region the dissociation of quarkonia states was studied in a deconfined medium of quarks and gluons [15]. In [8, 9, 16, 17], where the color singlet free energy was directly inserted into the Schrödinger equation, the dissociation temperature of J/ψ was found to be 1.10 T_c [8] and 0.99 T_c [16], and all other charmonium states were melting below the transition temperature,T_c. In [18], where a parameterization of the lattice color singlet potential was used, the dissociation temperature of T_c was calculated at 2 T_c and also the dissocia-

tion temperatures of different states of charmonium and bottomonium were also reported. In [19, 20, 21], dissociation temperatures were obtained using spectral analysis.

In this chapter, we use the solution of the N-dimensional radial Schrödinger equation with generalized two-body potential proposed in chapter 2 at finite temperature using the analytical exact iteration method (AEIM), Power Series Method (PSM), and Nikiforov-Uvarov (NU) method to determine the binding energy of heavy quarkonia. We try to find out the mass spectra and dissociation temperatures of heavy quarkonium states. Also, the influence of the dimensionality number has been investigated on the binding energy and mass spectra of heavy quarkonium at finite temperature.

5.2 Binding energy of quarkonium

5.2.1 Analytical exact iteration method (AEIM)

For quarkonium, $M_q = M_{\overline{q}} = m$ and $Q = -q^2$

Using Eq.(3.21),

$$E_{nl}^{N} = \frac{Q}{4\pi}\left(-k_r + \frac{k_i}{\sqrt{3}}\right) - \frac{\left[\frac{Q}{4\pi}\left[-\frac{k_i^2}{2} - \frac{k_i k_r}{\sqrt{3}} + \frac{k_r^2}{2}\right]\right]^2}{\left[\frac{Q}{\pi}\left[-\frac{k_i^2 k_r}{2} + \frac{k_i k_r^2}{2\sqrt{3}} - \frac{k_r^3}{6} - \frac{k_i^3}{6\sqrt{3}}\right]\right]} + \frac{\sqrt{\left[\frac{mQ}{4\pi}\left[-\frac{k_i^2 k_r}{2} + \frac{k_i k_r^2}{2\sqrt{3}} - \frac{k_r^3}{6} - \frac{k_i^3}{6\sqrt{3}}\right]\right]}}{m}\left(2(n+1) + \sqrt{1 + 4l(l+N-2) + N^2 - 4N + 3}\right) \tag{5.1}$$

where

$$k_i = \frac{k_s}{2}$$

$$k_r = \frac{\sqrt{3}}{2}k_s$$

$$k_s^2 = \frac{M_q\omega_p^2}{g_c\frac{\partial P}{\partial n_f}}$$

5.2.2 Power Series Method (PSM)

Using Eq.(3.32),

$$\begin{aligned} E_{nl}^N = &-\frac{mQ^2}{\left(4\pi(n+l+N)\right)^2} + \frac{Q}{4\pi}\left(-k_r + \frac{k_i}{\sqrt{3}}\right) \\ &+ 2\sqrt{\frac{Q}{16\pi m}\left(-\frac{k_r^3}{6} + \frac{k_i k_r^2}{2\sqrt{3}} - \frac{k_i^2 k_r}{2} - \frac{k_i^3}{6\sqrt{3}}\right)}(n+l+N-1) \end{aligned} \tag{5.2}$$

5.2.3 Nikiforov-Uvarov (NU) method

Using Eq.(3.62),

$$E_{n,l}^N = B + \frac{3C}{\delta} + \frac{6D}{\delta^2} - \frac{m\left(-A + \frac{3C}{\delta^2} + \frac{8D}{\delta^3}\right)^2}{\left((2n+1) \pm \sqrt{1 + \frac{4mC}{\delta^3} + \frac{12mD}{\delta^4} + 4\left(l(l+N-2) + \frac{N^2-4N+3}{4}\right)}\right)^2} \tag{5.3}$$

Eq.(5.1), Eq.(5.2), and Eq.(5.3) give the expressions for binding energy of quarkonium.

5.3 Variation of Binding energy of quarkonium with temperature

By considering the temperature dependence of α_s from the literature [22] we get,

$$\alpha_s(T) = \frac{6\pi}{(33-2n_f)\ln(T/\Lambda_T)}\left(1 - \frac{3(153-19n_f)}{(33-2n_f)^2}\frac{\ln\left(2\ln(T/\Lambda_T)\right)}{\ln(T/\Lambda_T)}\right)$$

The binding energy of quarkonia such as charmonium and bottomonium is calculated in the N-dimensional space for any state at finite temperature using Eq.(5.1), Eq.(5.2), and Eq.(5.3). Here $m = M_c$ for charmonium and $m = M_b$ for bottomonium mesons. The variation of binding energy with temperature for different states of quarkonia is shown in Figures 5.1 - 5.9.

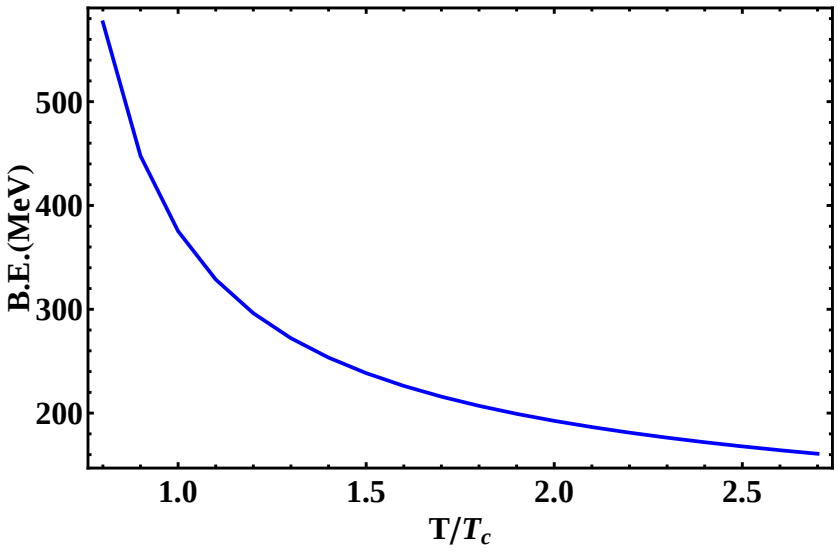

(a)

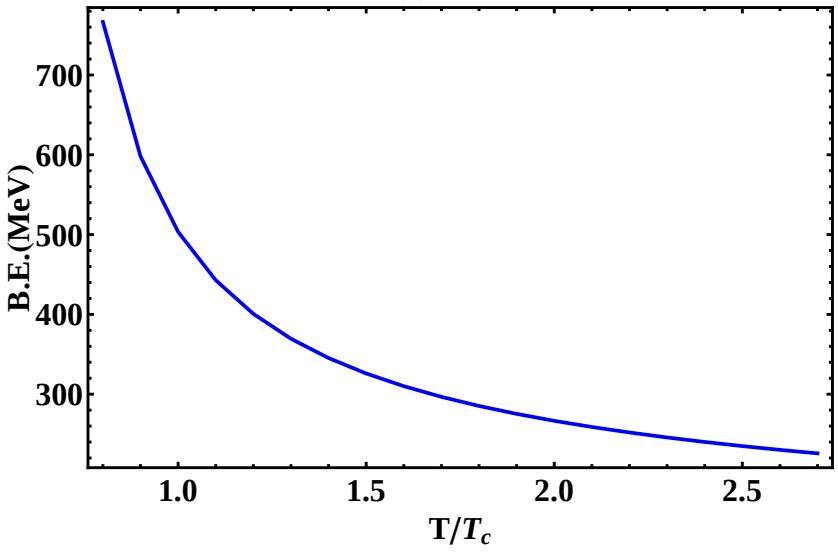

(b)

Figure 5.1: (a) Variation of J/ψ binding energy on temperature T and (b) Variation of χ_c binding energy on temperature T (AEIM)

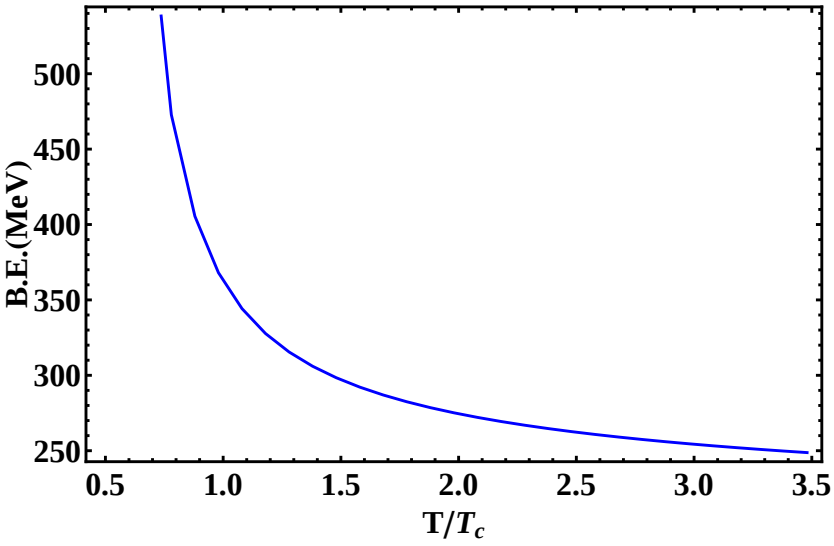

(a)

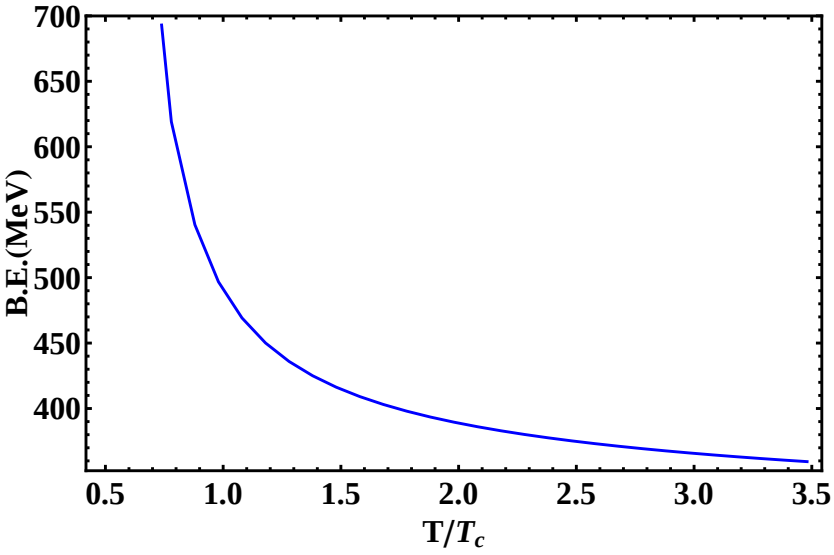

(b)

Figure 5.2: (a) Variation of J/ψ binding energy on temperature T and (b) Variation of χ_c binding energy on temperature T (PSM)

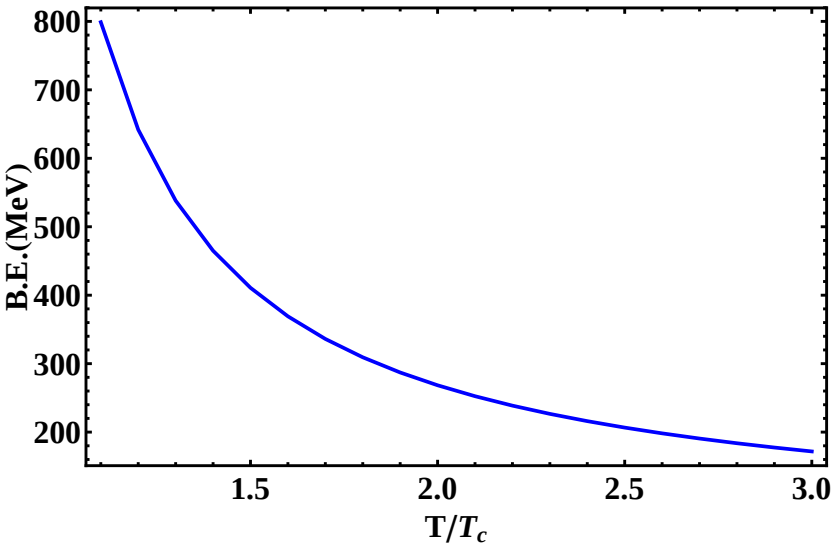

(a)

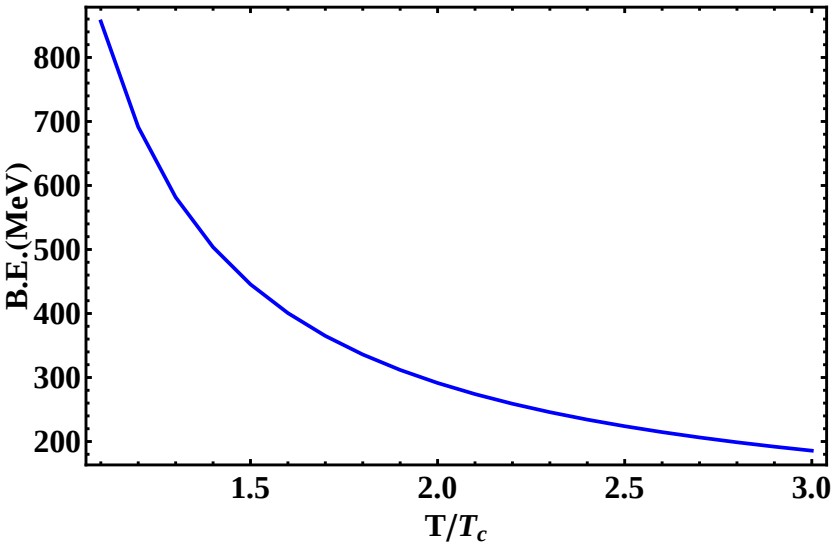

(b)

Figure 5.3: (a) Variation of J/ψ binding energy on temperature T and (b) Variation of χ_c binding energy on temperature T (NU Method)

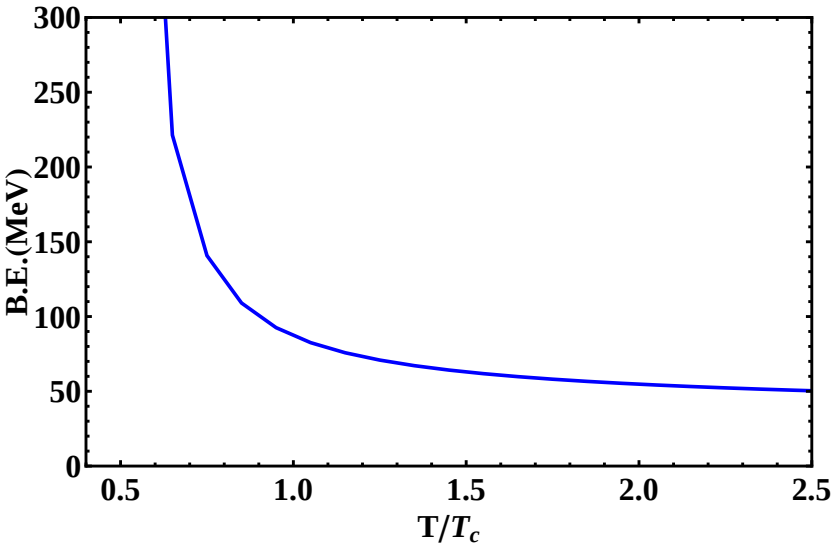

(a)

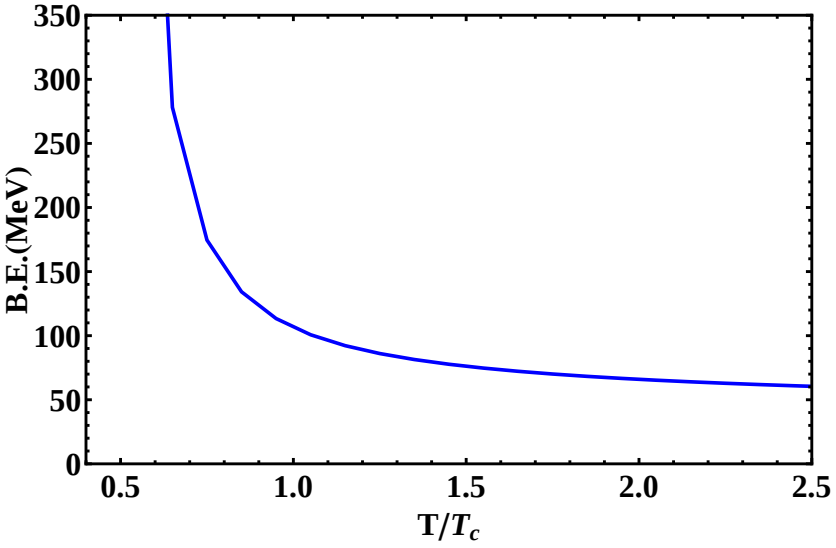

(b)

Figure 5.4: (a) Variation of Υ binding energy on temperature T and (b) Variation of χ_b binding energy on temperature T (AEIM)

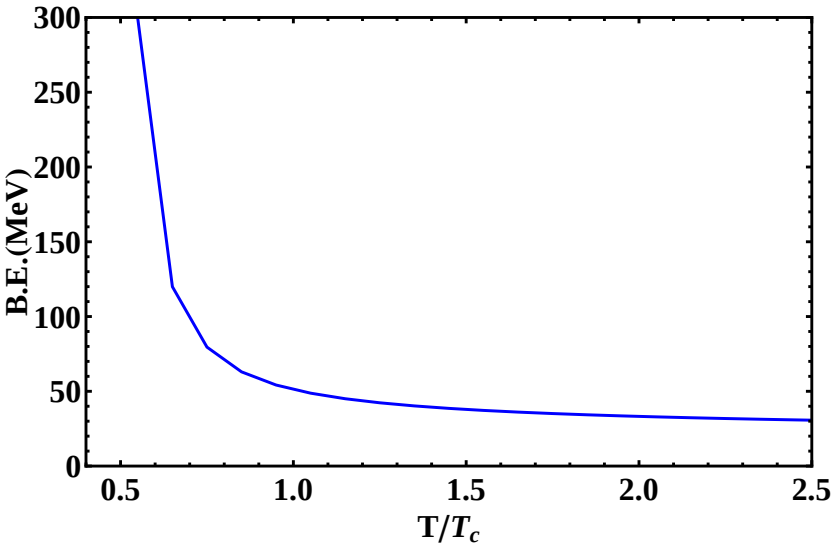

(a)

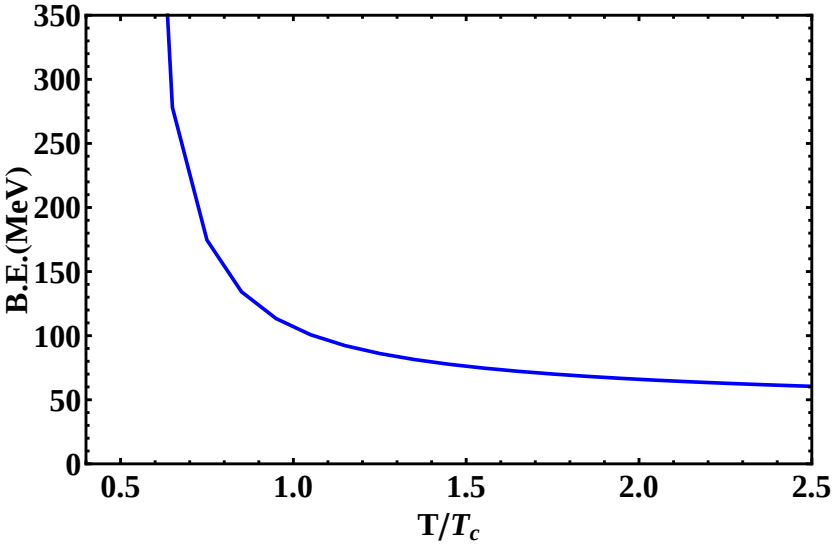

(b)

Figure 5.5: (a) Variation of Υ binding energy on temperature T and (b) Variation of χ_b binding energy on temperature T (PSM)

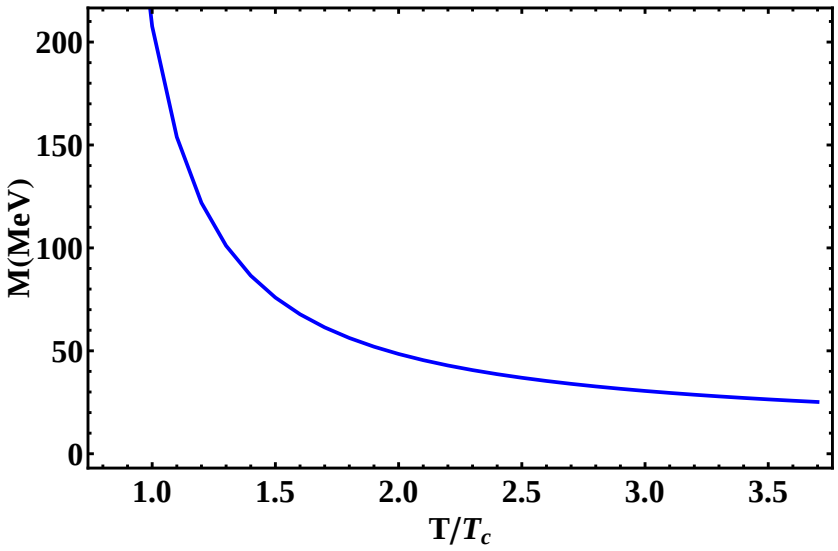

(a)

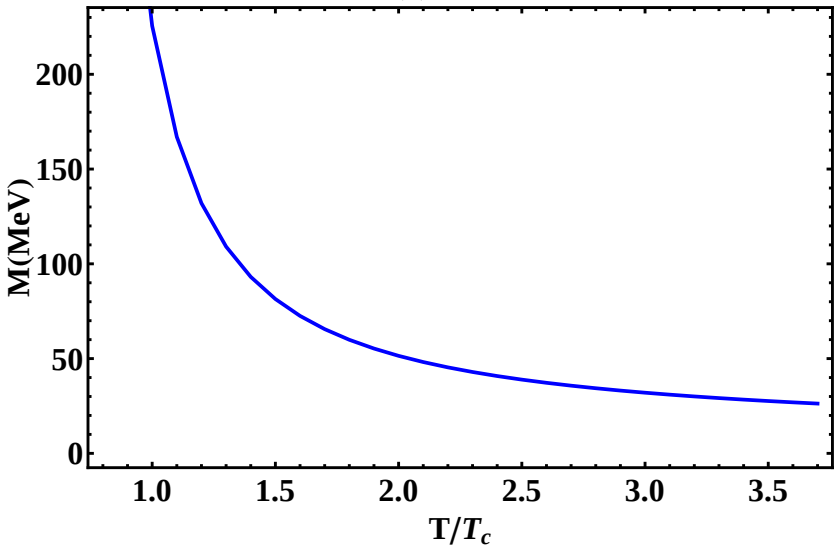

(b)

Figure 5.6: (a) Variation of Υ binding energy on temperature T and (b) Variation of χ_b binding energy on temperature T (NU method)

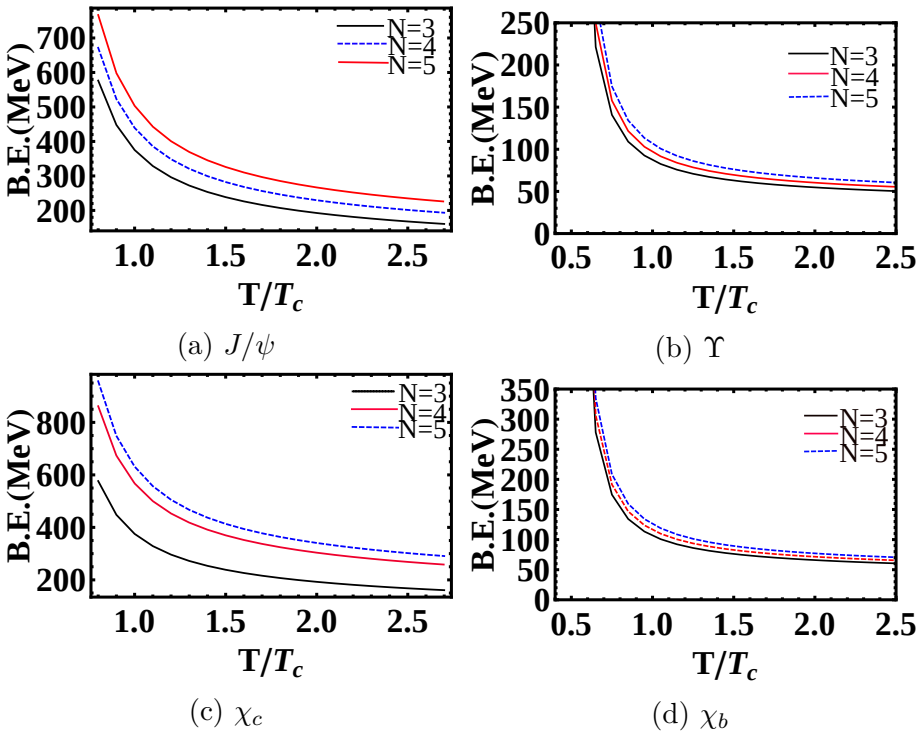

(a) J/ψ (b) Υ

(c) χ_c (d) χ_b

Figure 5.7: Variation of quarkonium binding energy on temperature T for different values of N (AEIM)

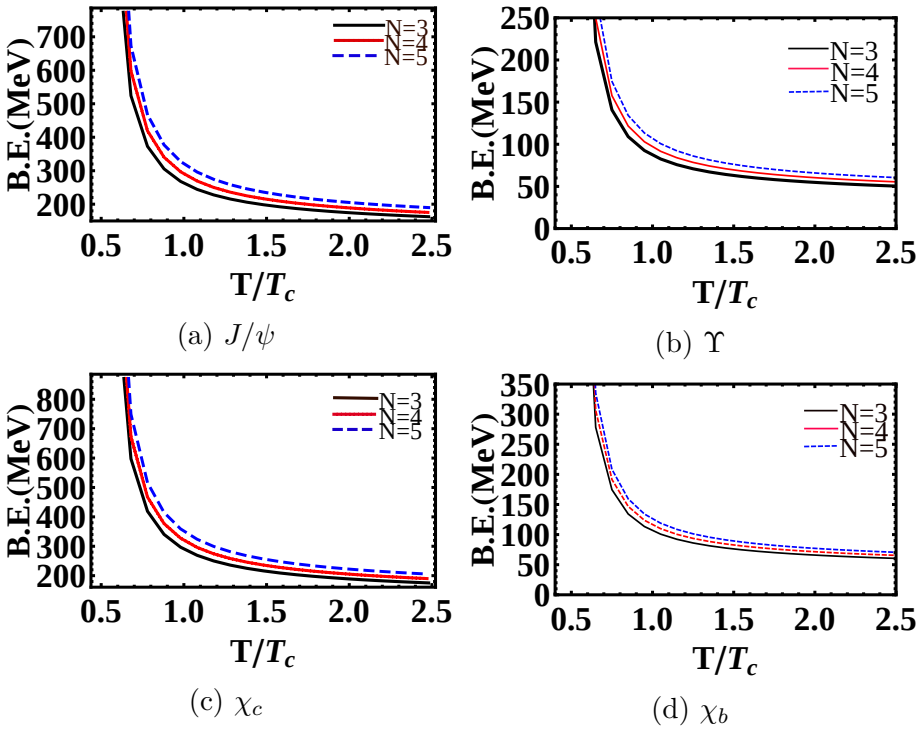

(a) J/ψ (b) Υ

(c) χ_c (d) χ_b

Figure 5.8: Variation of quarkonium binding energy on temperature T for different values of N (PSM)

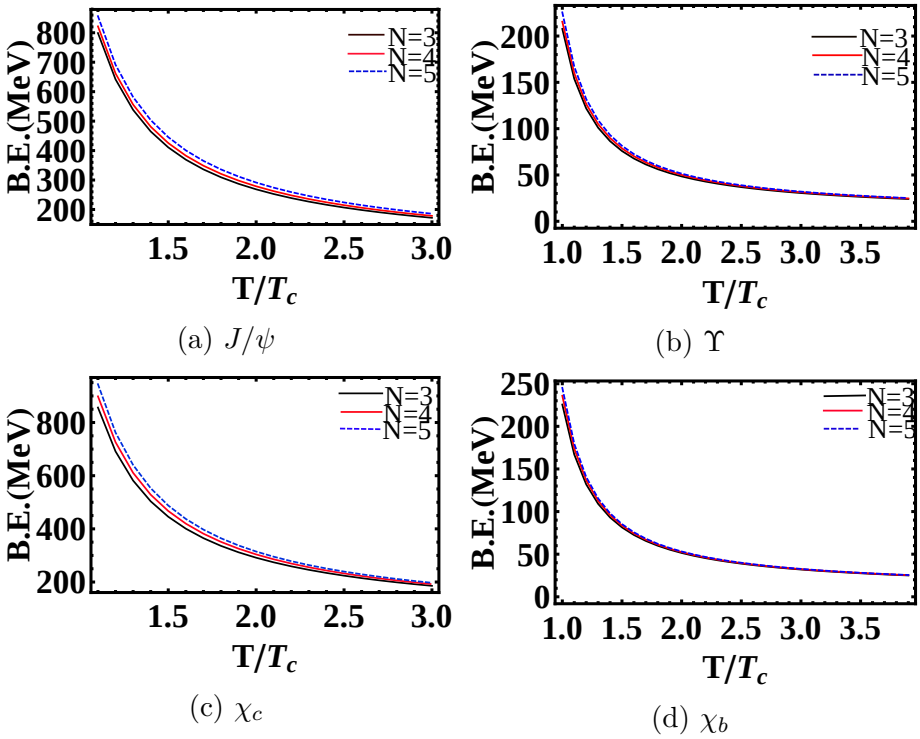

(a) J/ψ (b) Υ

(c) χ_c (d) χ_b

Figure 5.9: Variation of quarkonium binding energy on temperature T for different values of N (NU method)

5.4 Mass spectra of quarkonia

For calculating the mass of heavy quarkonium the following relation is used [23].

$$M = 2M_q + E_{nl}^N \tag{5.4}$$

5.4.1 Analytical exact iteration method (AEIM)

Substituting Eq.(5.1) into Eq.(5.4), the mass spectra for different states of heavy quarkonia as a function of temperature is given by,

$$M = 2m + \frac{Q}{4\pi}\Big(-k_r + \frac{k_i}{\sqrt{3}}\Big) - \frac{\left[\frac{Q}{4\pi}\left[-\frac{k_i^2}{2} - \frac{k_i k_r}{\sqrt{3}} + \frac{k_r^2}{2}\right]\right]^2}{\left[\frac{Q}{\pi}\left[-\frac{k_i^2 k_r}{2} + \frac{k_i k_r^2}{2\sqrt{3}} - \frac{k_r^3}{6} - \frac{k_i^3}{6\sqrt{3}}\right]\right]} + \frac{\sqrt{\left[\frac{mQ}{4\pi}\left[-\frac{k_i^2 k_r}{2} + \frac{k_i k_r^2}{2\sqrt{3}} - \frac{k_r^3}{6} - \frac{k_i^3}{6\sqrt{3}}\right]\right]}}{m}\Big(2(n+1) + \sqrt{1 + 4l(l+N-2) + N^2 - 4N + 3}\Big) \tag{5.5}$$

5.4.2 Power Series Method (PSM)

Substituting Eq.(5.2) into Eq.(5.4), the mass spectra for different states of heavy quarkonia as a function of temperature is given by,

$$\begin{aligned} M = 2m - \frac{mQ^2}{\Big(4\pi(n+l+N)\Big)^2} + \frac{Q}{4\pi}\left(-k_r + \frac{k_i}{\sqrt{3}}\right) \\ +2\sqrt{\frac{Q}{16\pi m}\left(-\frac{k_r^3}{6} + \frac{k_i k_r^2}{2\sqrt{3}} - \frac{k_i^2 k_r}{2} - \frac{k_i^3}{6\sqrt{3}}\right)}(n+l+N-1) \end{aligned} \tag{5.6}$$

5.4.3 Nikiforov-Uvarov (NU) method

Substituting Eq.(5.3) into Eq.(5.4), the mass spectra for different states of heavy quarkonia as a function of temperature is given by,

$$M = 2m+B+\frac{3C}{\delta}+\frac{6D}{\delta^2}-\frac{m\left(-A+\frac{3C}{\delta^2}+\frac{8D}{\delta^3}\right)^2}{\left((2n+1)\pm\sqrt{1+\frac{4mC}{\delta^3}+\frac{12mD}{\delta^4}+4\left(l(l+N-2)+\frac{N^2-4N+3}{4}\right)}\right)^2} \tag{5.7}$$

The mass spectra of different states of heavy quarkonia as function of temperature are plotted in Fig. 5.10 - 5.18.

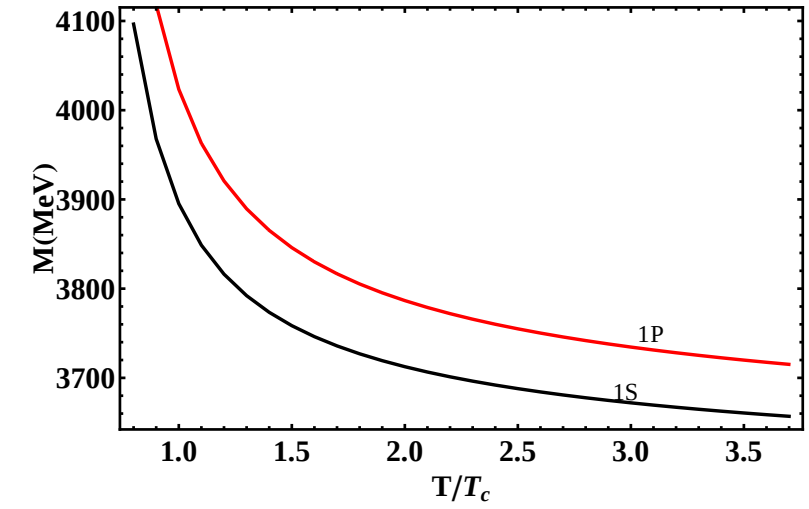

(a)

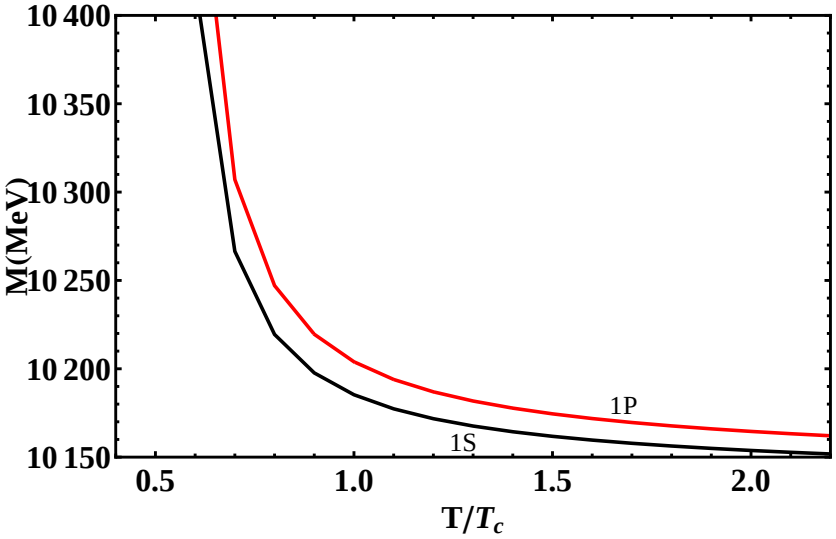

(b)

Figure 5.10: The mass spectra of charmonium and bottomonium as a function of temperature T for 1S and 1P states (AEIM)

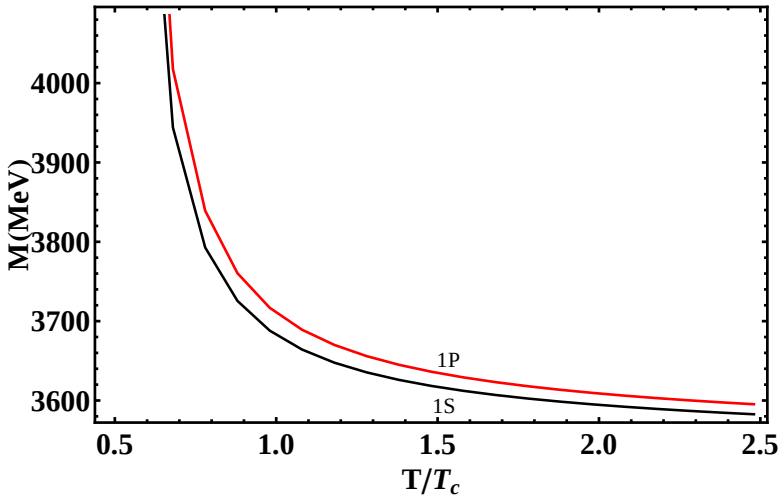

(a)

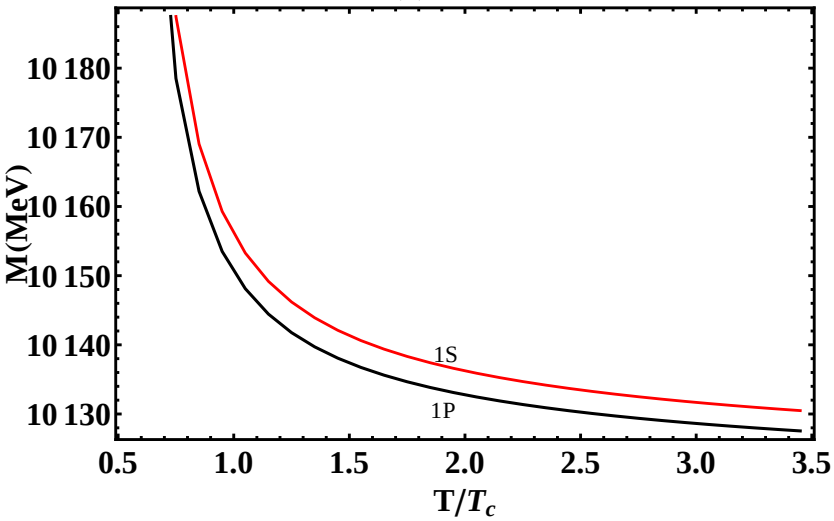

(b)

Figure 5.11: The mass spectra of charmonium and bottomonium as a function of temperature T for 1S and 1P states (PSM)

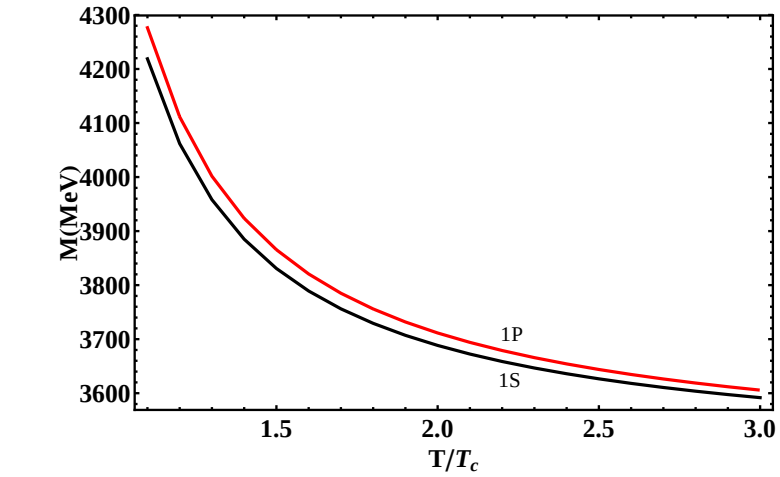

(a)

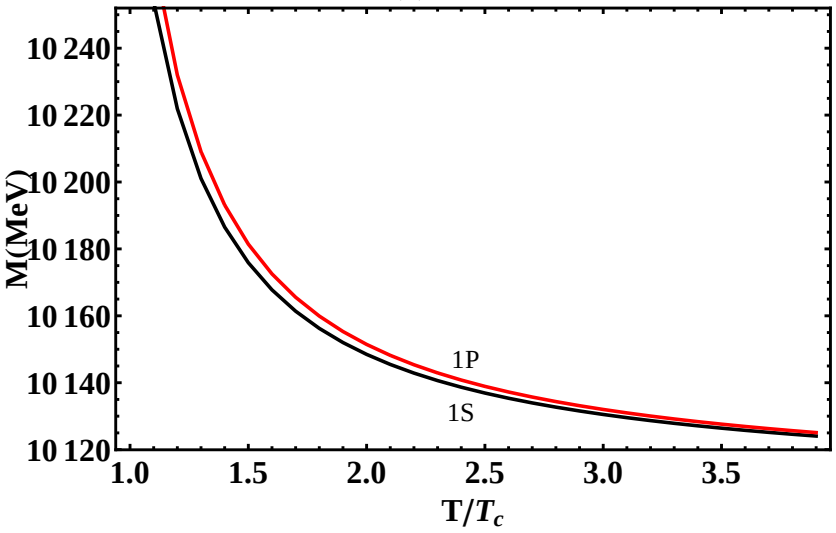

(b)

Figure 5.12: The mass spectra of charmonium and bottomonium as a function of temperature T for 1S and 1P states (NU method)

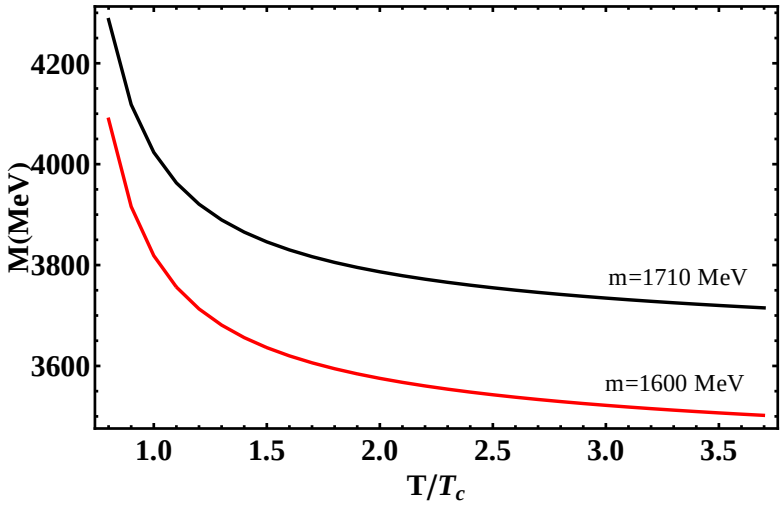

(a)

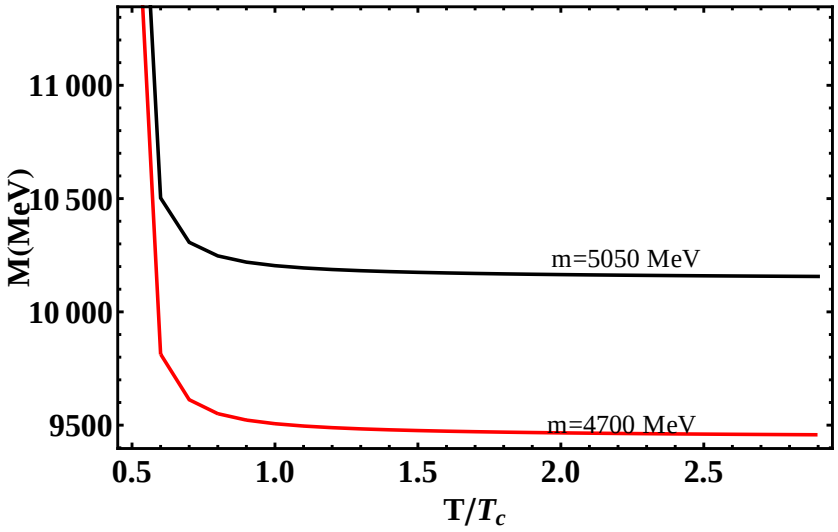

(b)

Figure 5.13: The mass spectra of charmonium as a function of temperature T for 1P state for different charm quark mass and (b) the mass spectra of bottomonium as a function of temperature T for 1P state for different bottom quark mass (AEIM)

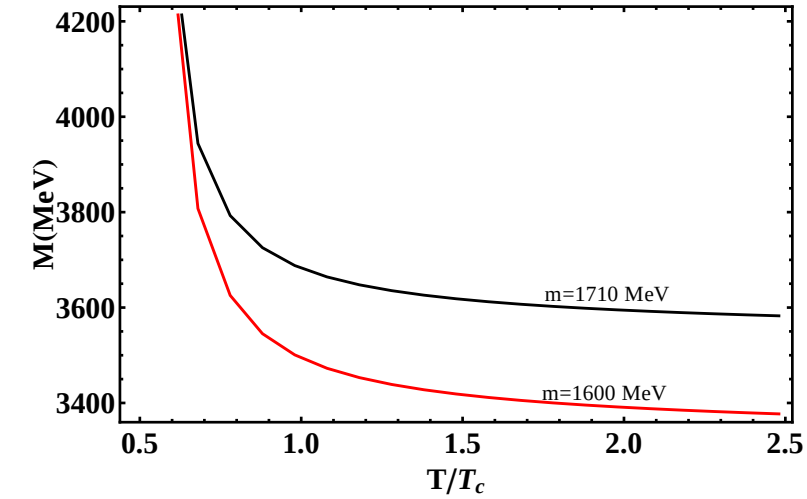

(a)

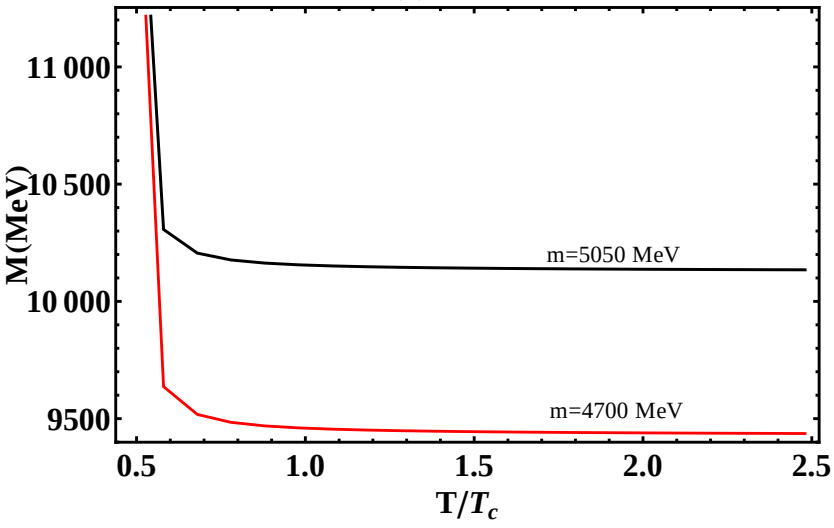

(b)

Figure 5.14: The mass spectra of charmonium as a function of temperature T for 1P state for different charm quark mass and (b) the mass spectra of bottomonium as a function of temperature T for 1P state for different bottom quark mass (PSM)

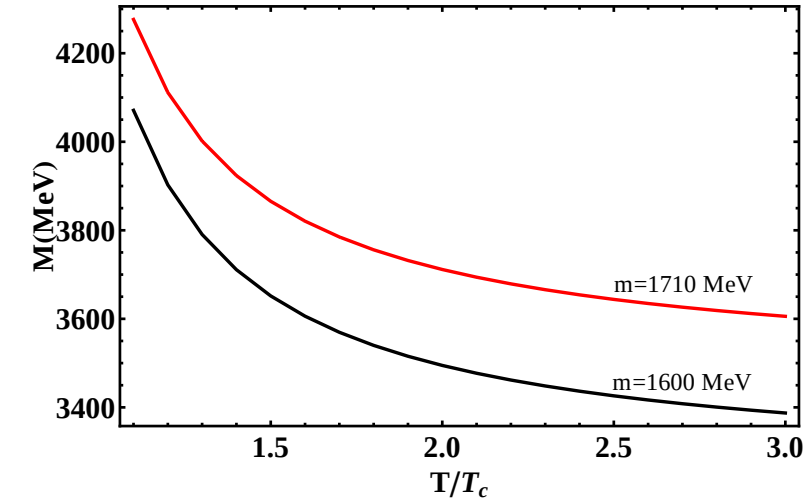

(a)

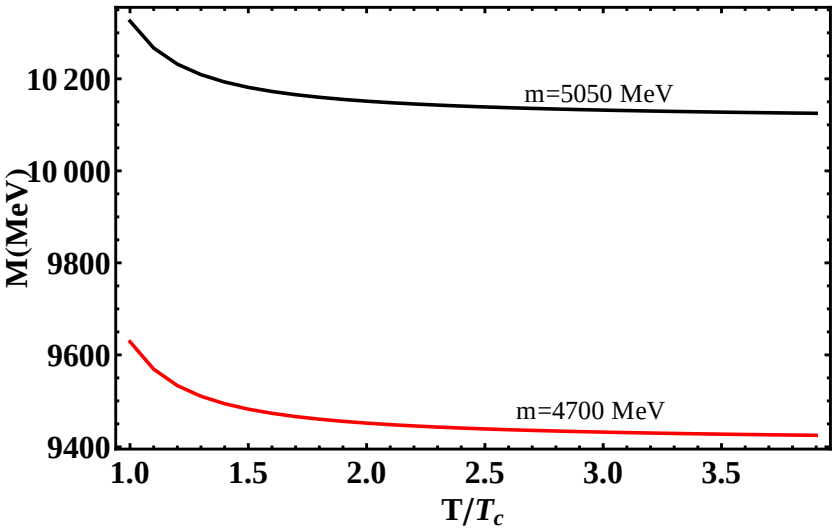

(b)

Figure 5.15: The mass spectra of charmonium as a function of temperature T for 1P state for different charm quark mass and (b) the mass spectra of bottomonium as a function of temperature T for 1P state for different bottom quark mass (NU method)

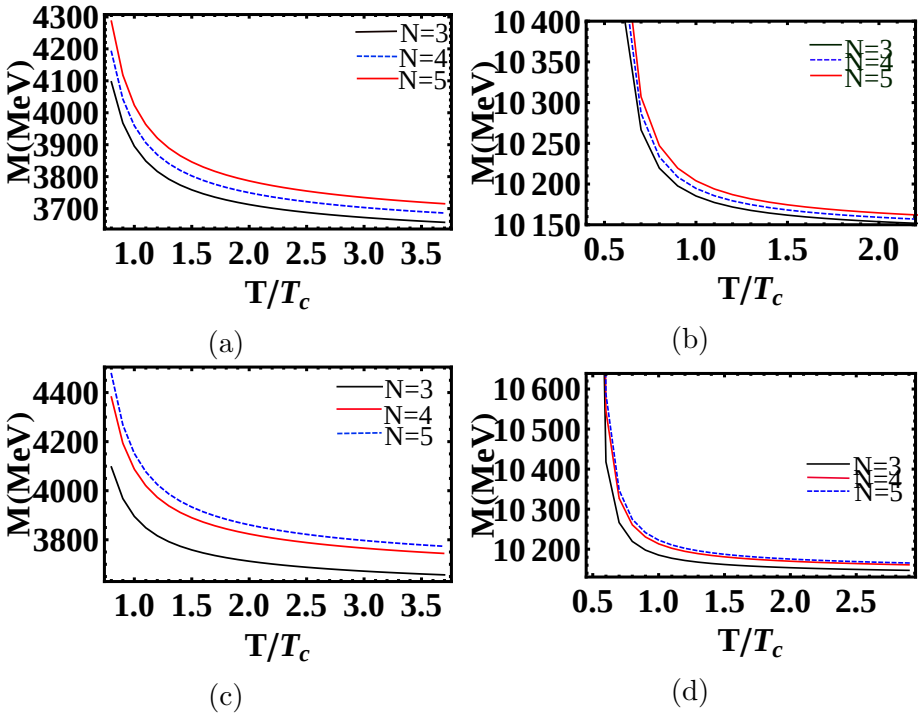

Figure 5.16: (a)The mass spectra of charmonium as a function of temperature T for 1S state for different values of N , (b) the mass spectra of bottomonium as a function of temperature T for 1S state for different values of N ,(c) the mass spectra of charmonium as a function of temperature T for 1P state for different values of N and (d) the mass spectra of bottomonium as a function of temperature T for 1P state for different values of N (AEIM)

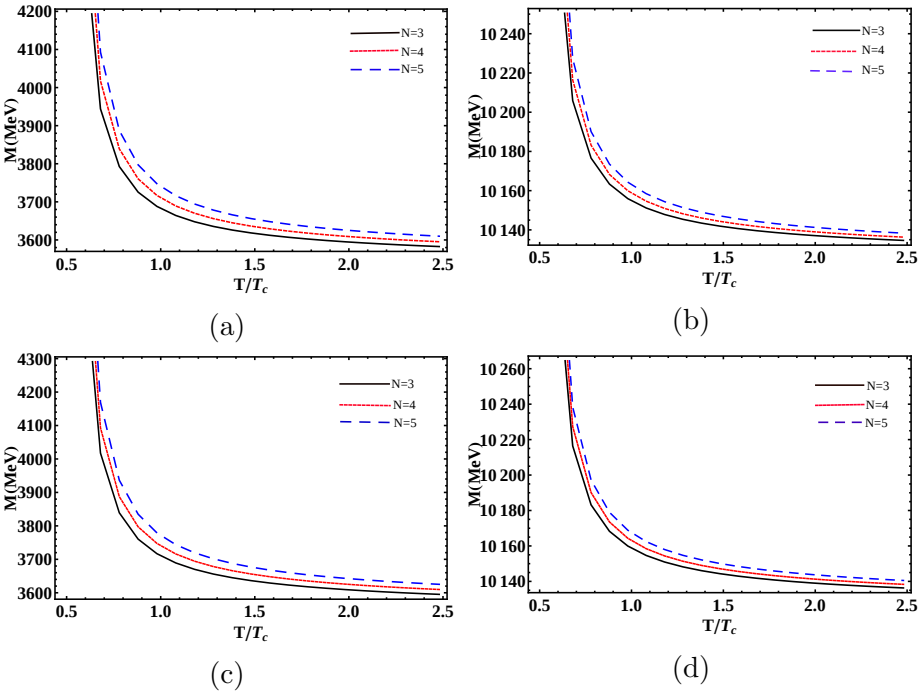

Figure 5.17: (a)The mass spectra of charmonium as a function of temperature T for 1S state for different values of N , (b) the mass spectra of bottomonium as a function of temperature T for 1S state for different values of N ,(c) the mass spectra of charmonium as a function of temperature T for 1P state for different values of N and (d) the mass spectra of bottomonium as a function of temperature T for 1P state for different values of N (PSM)

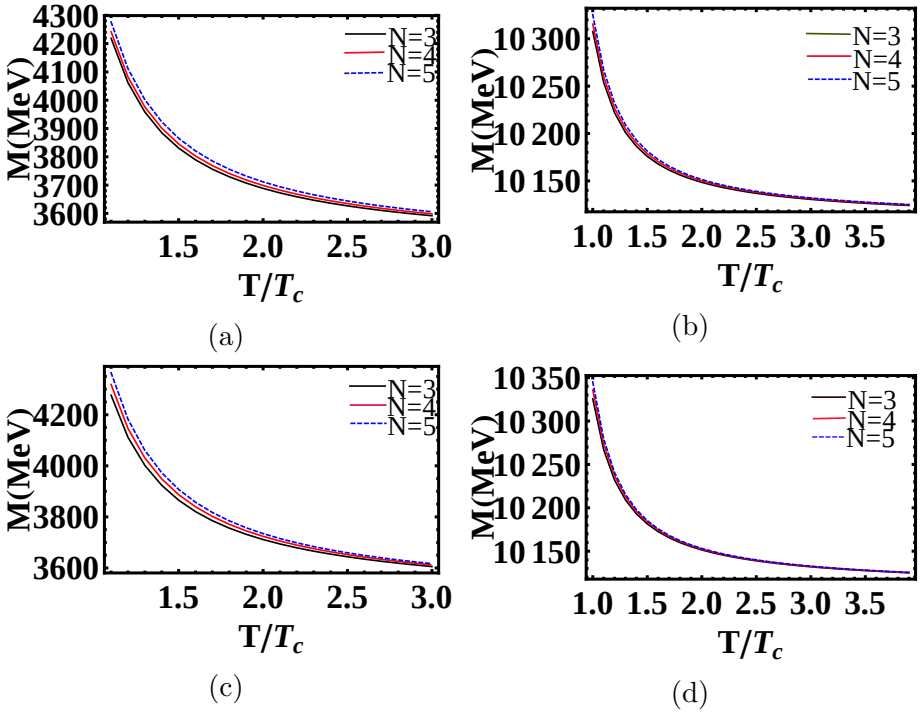

Figure 5.18: (a)The mass spectra of charmonium as a function of temperature T for 1S state for different values of N , (b) the mass spectra of bottomonium as a function of temperature T for 1S state for different values of N ,(c) the mass spectra of charmonium as a function of temperature T for 1P state for different values of N and (d) the mass spectra of bottomonium as a function of temperature T for 1P state for different values of N (NU method)

5.5 Dissociation temperature of heavy quarkonium in N-dimensional space

When the binding energy of a quarkonium falls below the temperature, that state is weakly bound and it can be destroyed by thermal fluctuations by transferring energy. The dissociation temperature is defined as the smallest temperature where no resonance structure can be observed in reality. The value of binding energy need not be reached zero for the dissociation of quarkonia. There are a lot of previous works which have determined the dissociation temperatures for different states of quarkonia. In [24] the dissociation temperatures were calculated from the thermal width. In Ref. [4] the upper bound for the dissociation temperature of quarkonium states was found by using the condition $\Gamma(T) \geq 2E_{bin}(T)$. In [12] the upper bound and lower bound for the dissociation temperatures have been calculated by the conditions $E_{bin} = T$ and $E_{bin} = 3T$ respectively. In [10, 25] the condition of vanishing binding energy have used for calculating the dissociation temperature for different states of heavy quarkonium. In this chapter, we use the condition $E_{bin} = T$ to find out the dissociation temperatures for the different states of quarkonium. We have obtained the dissociation temperatures for different states of quarkonium using AEIM and NU method and are summarized in Table 5.1, Table 5.2, and Table 5.3.

Table 5.1: The dissociation temperature (T_D) with $T_c = 175MeV$ for the quarkonium states using $M_c = 1710MeV$ and $M_b = 5050MeV$ at N=3

State	J/ψ	χ_c	ψ'	Υ	χ_b	Υ'
$T_D(AEIM)$	$1.47Tc$	$1.62Tc$	$1.62Tc$	$0.77Tc$	$0.82Tc$	$0.82Tc$
$T_D(PSM)$	$1.46Tc$	$1.61Tc$	$1.62Tc$	$0.79Tc$	$0.83Tc$	$0.83Tc$
$T_D(NU)$	$1.72T_c$	$1.81T_c$	$1.84T_c$	$1.04T_c$	$1.06T_c$	$1.07T_c$

Table 5.2: The dissociation temperature (T_D) with $T_c = 175MeV$ for the quarkonium states using $M_c = 1710MeV$ and $M_b = 5050MeV$ at N=4

State	J/ψ	χ_c	ψ'	Υ	χ_b	Υ'
$T_D(AEIM)$	$1.54Tc$	$1.71Tc$	$1.71Tc$	$0.8Tc$	$0.85Tc$	$0.85Tc$
$T_D(PSM)$	$1.55Tc$	$1.72Tc$	$1.73Tc$	$0.84Tc$	$0.85Tc$	$0.85Tc$
$T_D(NU)$	$1.77T_c$	$1.82T_c$	$1.86T_c$	$1.07T_c$	$1.08T_c$	$1.09T_c$

5.6 Results and Discussions

Fig. 5.1 and Fig. 5.4 show the variation of the binding energy of heavy quarkonia with temperature for 1S and 1P states respectively, where binding energy is calculated using the analytical exact iteration method. Fig. 5.2 and Fig. 5.5 show the variation of the binding energy of heavy quarkonia with temperature for 1S and 1P states respectively, where binding energy is calculated using the Power Series method. Fig. 5.3 and Fig. 5.6 show the variation of the binding energy of heavy quarkonia with temperature for 1S and 1P states respectively, where binding energy is calculated using the Nikiforov-Uvarov method. It has been observed that the binding energy becomes weaker with increasing temperature. This result

Table 5.3: The dissociation temperature (T_D) with $T_c = 175MeV$ for the quarkonium states using $M_c = 1710MeV$ and $M_b = 5050MeV$ at N=5

State	J/ψ	χ_c	ψ'	Υ	χ_b	Υ'
$T_D(AEIM)$	$1.63Tc$	$1.81Tc$	$1.81Tc$	$0.83Tc$	$0.88Tc$	$0.88Tc$
$T_D(PSM)$	$1.61T_c$	$1.83T_c$	$1.82T_c$	$0.83T_c$	$0.82T_c$	$0.88T_c$
$T_D(NU)$	$1.8T_c$	$1.85T_c$	$1.87T_c$	$1.08T_c$	$1.09T_c$	$1.1T_c$

agrees with the literature [4, 10]. Fig. 5.7, Fig. 5.8, and Fig. 5.9 show the dependence of binding energy on dimensionality number (N). It is clear from the figure that the binding energy increases with the dimensionality number. This result also agrees with [10].

Fig. 5.10, Fig. 5.11, and Fig. 5.12 show the mass spectra of heavy quarkonia with temperature for 1S and 1P states. It is clear from the figures that the mass spectra decrease with increasing temperature for 1S and 1P states. The values of the 1P state are larger than the values of the 1S state. This also agrees with [10].

Fig. 5.13, Fig. 5.14, and Fig. 5.15 show the behavior of mass spectra of J/ψ state and Υ state with temperature for two different values of constituent quark mass. The increase of constituent quark mass leads to increasing mass spectra of charmonium for 1S state. Thus the mass spectra of heavy quarkonia increase with increasing quark mass. This also agrees with the previous findings [11]. Fig. 5.16, Fig. 5.17, and Fig. 5.18 show the variation of mass spectra with dimensionality number. The increase in dimensionality number increases the mass spectra as in [10]. The values of binding energy and mass spectra of different quarkonium states agree with the previous reports for the lower dimension. Comparing these values with the experimental results [26], it can be concluded that out of the three methods, the Nikiforov-Uvarov method has the minimum error. As the dimensionality number increases, these values also increase.

In Table 5.1, we have summarized the dissociation temperatures for different states of $c\bar{c}$ and $b\bar{b}$ at N=3. Considering the results obtained via AEIM, we found that due to color screening the bottomonia states dissolve at temperatures near the critical temperature and the charmonia states exist up to higher temperatures. The dissociation temperature of J/ψ, χ_c, and ψ' states agree with [10]. The dis-

sociation temperature of Υ'' agrees with [8,9]. The dissociation temperature of χ_b agrees with [9, 17]. The value of dissociation temperature of Υ is slightly lesser than that reported in some literature [4, 10]. The results obtained through PSM are comparable with that obtained via AEIM. It is observed that the dissociation temperature becomes slightly higher when calculated through NU method. The dissociation temperature of J/ψ state agrees with [27]. The dissociation temperature of χ_b agrees with [3]. In Table 5.2 and Table 5.3, we have summarized the dissociation temperatures for different states of $c\bar{c}$ and $b\bar{b}$ at N=4 and N=5. The above three tables display the effect of dimensionality number on the dissociation temperature of different quarkonium states. It is clear from the tables that the increasing dimensionality number leads to increasing dissociation temperature for different quarkonium states.

Bibliography

[1] H. Satz, *Colour deconfinement and quarkonium binding*, J. Phys. G: Nucl. Part. Phys. 32, R25 (2006).

[2] M. Strickland and D. Bazow, *Thermal bottomonium suppression at RHIC and LHC*, Nuclear Physics A 879, 25 (2012).

[3] H. Satz, *Quarkonium binding and dissociation: The spectral analysis of the QGP*, Nucl. Phys. A 783, 249 (2007).

[4] Á. Mócsy and P. Petreczky, *Color screening melts quarkonium*, Phys. Rev. Lett. 99, 211602 (2007).

[5] T. Matsui and H. Satz, *J/ψ suppression by quark gluon plasma formation*, Phys. Lett. B 178, 416 (1986).

[6] K. T. Rethika and V. M. Bannur, *Screening of a test quark in the strongly coupled quark gluon plasma*, Few-Body Syst 60, 38 (2019).

[7] F. Karsch, M. T. Mehr, and H. Satz, *Color screening and deconfinement for bound states of heavy quarks*, Z. Phys. C 37, 617 (1988).

[8] S. Digal, P. Petreczky, and H. Satz, *String breaking and quarkonium dissociation at finite temperatures*, phys. Lett. B 514, 57 (2001).

[9] S. Digal, D. Petreczky, and H. Satz, *Quarkonium feed-down and sequential suppression*, Phys. Rev. D 64, 094015 (2001).

[10] M. Abu-Shady, T. A. Abdel-Karim, and E. M. Khokha, *Binding energies and dissociation temperatures of heavy quarkonia at finite temperature and chemical potential in the N-Dimensional space*, Advances in High Energy Physics, Volume 2018, Article ID 7356843 (2018).

[11] W. M. Alberico, A. Beraudo, A. De Pace, and A. Molinari, *Quarkonia in the deconfined phase: effective potentials and lattice correlators*, Phys. Rev. D 75, 074009 (2007).

[12] V. Agotiya, V. Chandra, and B. K. Patra, *Dissociation of quarkonium in a hot QCD medium: Modification of the inter quark potential*, Phys. Rev. C 80, 025210 (2009).

[13] L. Thakur and B. K. Patra, *Quarkonium dissociation in an anisotropic QGP*, J. Phys.: Conf. Se. 668, 012085 (2016).

[14] V. Agotiya, V. Chandra, M. Y. Jamal, and I. Nilima, *Dissociation of heavy quarkonium in hot QCD medium in a quasiparticle model*, Phys. Rev. D 94, 094006 (2016).

[15] U. Kakade and B. K. Patra, *Quarkonium dissociation at finite chemical potential*, Phys. Rev. C 92, 024901 (2015).

[16] C. Y. Wong, *Dissociation of a heavy quarkonium at high temperatures*, Phys. Rev. C 65, 034902 (2002).

[17] C. Y. Wong, *Dissociation of heavy quarkonia in the quark–gluon plasma*, J. Phys. G 28, 2349 (2002).

[18] C. Y. Wong, *Heavy quarkonia in quark-gluon plasma*, Phys. Rev. C 72, 034906 (2005).

[19] S. Datta, F. Karsch, P. Petreczy, and I. Wetzorke, *Behavior of charmonium systems after deconfinement*, Phys. Rev. D 69, 094507 (2004).

[20] M. Asakawa, T. Hatsuda, and Y. Nakahara, *Hadronic spectral functions above the QCD phase transition*, Nucl. Phys. A 715, 863 (2003).

[21] M. Asakawa and T. Hatsuda, *J/ψ and η_c in the deconfined plasma from lattice QCD*, Phys. Rev. Lett. 92, 012001 (2004).

[22] V. M. Bannur , *Strongly coupled quark gluon plasma*, J. Phys. G: Nucl. Part. Phys. 32, 993 (2006).

[23] R. Kumar and F. Chand, *Asymptotic study to the N-Dimensional radial Schrödinger equation for the quark-antiquark system*, Commun. Theor. Phys. 59, 528 (2013).

[24] D. Kharzeev L. McLerran, and H. Satz, *Non perturbative quarkonium dissociation in hadronic matter*, Phys. Lett. B 356, 349 (1995).

[25] H. Satz, *Charm and beauty in a hot environment*, hep-ph/0602245 [hep-ph] (2006)

[26] J. Beringer, *The review of particles physics, (particle data group)*, Phys. Rev. D 86 (2012)

[27] M. Hasan and B. K. Patra, *Dissociation of heavy quarkonia in a weak magnetic field*, Phys. Rev. D 102, 036020 (2020).

Chapter 6

Properties of b$\bar{c}$ and c$\bar{s}$ mesons at Finite Temperature in Strongly Coupled Quark Gluon Plasma

6.1 Introduction

In RHIC experiments the production and survival of heavy quarkonia have been considered as a tool to test the deconfinement for a long time [1]. Initially, these studies were focused on charmonia and bottomonia only. During the last few years, a rapid increase in the number of new mesonic states has been observed by various collider experiments leading to a new focus on hadron spectroscopy [2,3,4]. In p-p collisions, production of c$\bar{c}$ and b$\bar{b}$ appears to be more favorable whereas in A-A collisions production of B_c meson (b$\bar{c}$ or c$\bar{b}$) is more relevant [5]. The bottom-charmed meson family is the only quarkonium bound state consisting of two heavy quarks with different flavors (c$\bar{b}$ for positively charged channel and b$\bar{c}$ for

negatively charged channel) and due to this special feature, we can include these in the category of heavy-light mesons [6]. It is the heaviest and latest discovered double heavy meson predicted by the standard model [6]. Unlike the charmonium and bottomonium states the B_c mesons do not annihilate into gluons and thus these states are very stable [7]. Recently LHCb presented evidence for three new excited charm-strange mesons [8,9,10]. These states are important due to their narrow widths and low masses [11]. experimental information on the spectrum of the $c\overline{s}$ meson states is limited.

In this chapter, we try to find out the binding energies and mass spectra of $b\overline{c}$ and $c\overline{s}$ mesons at finite temperature. For studying the temperature dependence of binding energy and mass spectra of $b\overline{c}$ and $c\overline{s}$ mesons, we shall use a nonrelativistic treatment because of the large constituent quark masses. We also calculate the dissociation temperatures of these mesons in strongly coupled quark-gluon plasma for different dimensionality numbers.

6.2 Variation of binding energy of $b\overline{c}$ and $c\overline{s}$ mesons with temperature

The binding energy of bound state of quarks is calculated in the N-dimensional space for any state at finite temperature using the Nikiforov-Uvarov method [12] which is given by Eq.(3.62).

Here $M_{q_1} = M_b$ and $M_{q_2} = M_c$ for $b\overline{c}$ meson and $M_{q_1} = M_c$ and $M_{q_2} = M_s$ for $c\overline{s}$ meson.

The variation of binding energy with temperature for different states of $b\overline{c}$ and

$c\bar{s}$ mesons is shown in Figures 6.1 and 6.2.

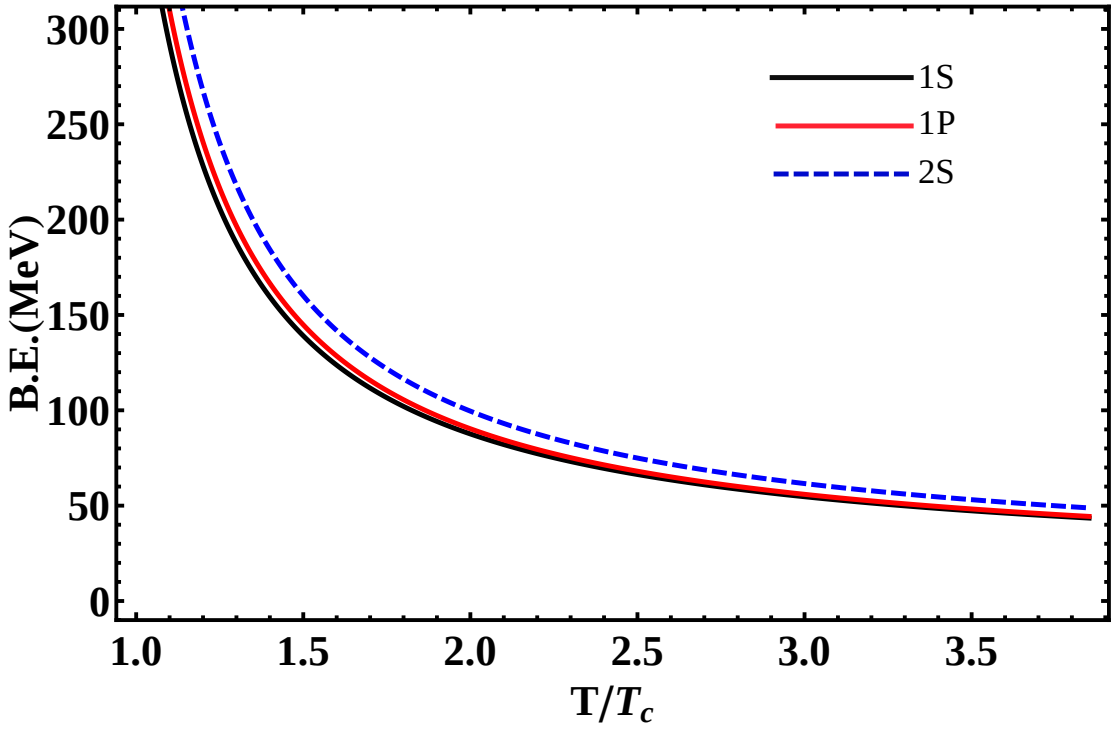

Figure 6.1: Variation of $b\bar{c}$ binding energy on temperature T

6.3 Mass spectra of quarkonia

For calculating the mass of $b\bar{c}$ meson the following relation is used [12].

$$M_{b\bar{c}} = M_b + M_c + E_{nl}^N \tag{6.1}$$

For calculating the mass of $c\bar{s}$ meson,

$$M_{c\bar{s}} = M_c + M_s + E_{nl}^N \tag{6.2}$$

Substituting from Eq.(3.62) in to Eq.(6.1) and (6.2), the mass spectra for dif-

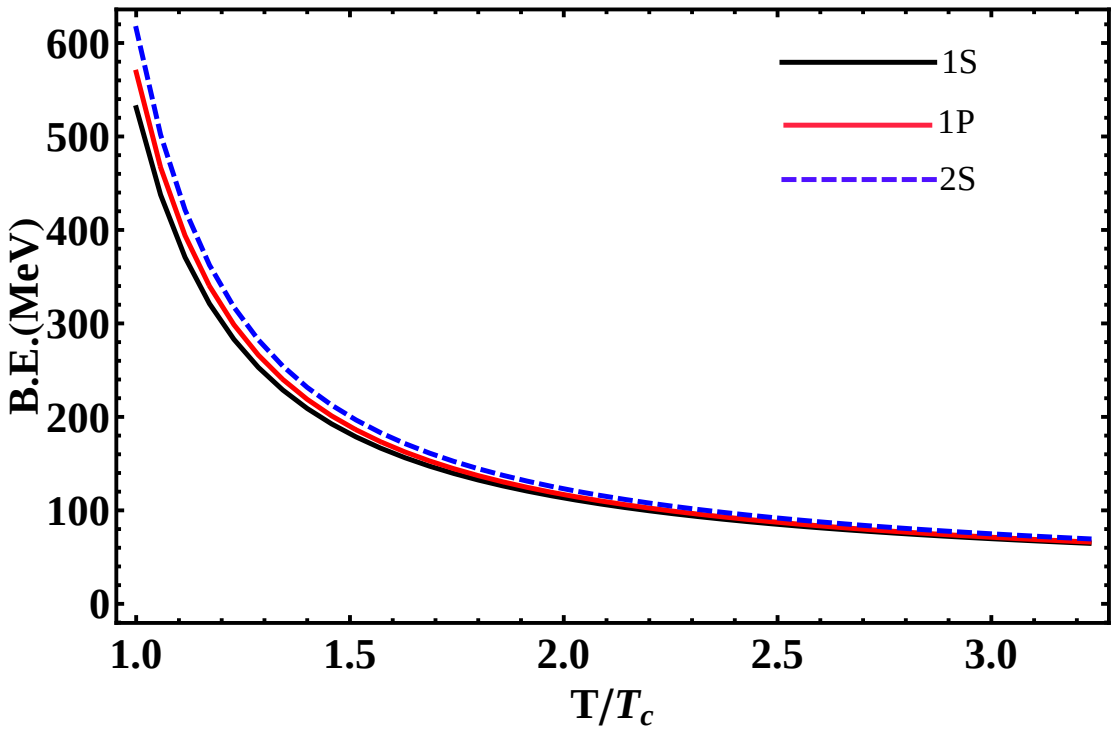

Figure 6.2: Variation of c$\bar{s}$ binding energy on temperature T

ferent states of b$\bar{c}$ meson as a function of temperature is given by,

$$M_{b\bar{c}} = M_b + M_c + B + \frac{3C}{\delta} + \frac{6D}{\delta^2} - \frac{2\mu\left(-A + \frac{3C}{\delta^2} + \frac{8D}{\delta^3}\right)^2}{\left((2n+1) \pm \sqrt{1 + \frac{8\mu C}{\delta^3} + \frac{24\mu D}{\delta^4} + 4(l(l+N-2) + \frac{N^2-4N+3}{4})}\right)^2} \tag{6.3}$$

and the mass spectra for different states of c$\bar{s}$ meson as a function of temperature is given by,

$$M_{c\bar{s}} = M_c + M_s + B + \frac{3C}{\delta} + \frac{6D}{\delta^2} - \frac{2\mu\left(-A + \frac{3C}{\delta^2} + \frac{8D}{\delta^3}\right)^2}{\left((2n+1) \pm \sqrt{1 + \frac{8\mu C}{\delta^3} + \frac{24\mu D}{\delta^4} + 4(l(l+N-2) + \frac{N^2-4N+3}{4})}\right)^2} \tag{6.4}$$

Table 6.1: The dissociation temperature (T_D) with $T_c = 175MeV$ for the b$\overline{c}$ meson states using $M_c = 1710MeV$ and $M_b = 5050MeV$

State	$1S$	$1P$	$2S$
$T_D(N=3)$	$1.23Tc$	$1.25Tc$	$1.25Tc$
$T_D(N=4)$	$1.24T_c$	$1.26T_c$	$1.26T_c$
$T_D(N=5)$	$1.25T_c$	$1.27T_c$	$1.27T_c$
$T_D(N=3)$[5]	$1.90T_c$	$1.05T_c$	$1.04T_c$

Table 6.2: The dissociation temperature (T_D) with $T_c = 175MeV$ for the c$\overline{s}$ meson states using $M_c = 1710MeV$ and $M_s = 540MeV$

State	$1S$	$1P$	$2S$
$T_D(N=3)$	$1.33Tc$	$1.35Tc$	$1.36Tc$
$T_D(N=4)$	$1.34T_c$	$1.36T_c$	$1.37T_c$
$T_D(N=5)$	$1.35T_c$	$1.36T_c$	$1.38T_c$

6.4 Dissociation temperature of b$\overline{c}$ and c$\overline{s}$ mesons in N-dimensional space

Here we use the condition $E_{bin} = T$ to find out the dissociation temperatures [13] for the different states of b$\overline{c}$ and c$\overline{s}$ mesons. The dissociation temperatures for different states are summarized in Tables 6.1 and 6.2.

6.5 Results and Discussions

Fig. 6.1 and Fig. 6.2 show the variation of binding energy of $b\overline{c}$ and $c\overline{s}$ mesons with temperature. As the temperature increases, the binding becomes weaker. This result agrees with the literature [14]. Fig. 6.3 shows the variation of mass spectra

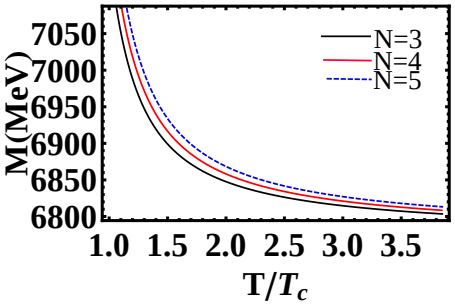

(a) b$\bar{c}$ 1S state

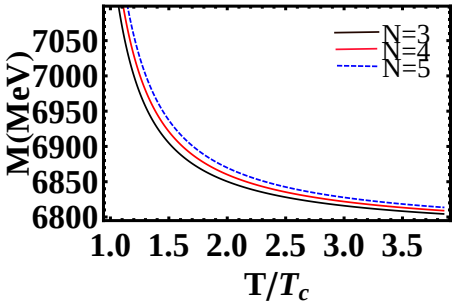

(b) b$\bar{c}$ 1P state

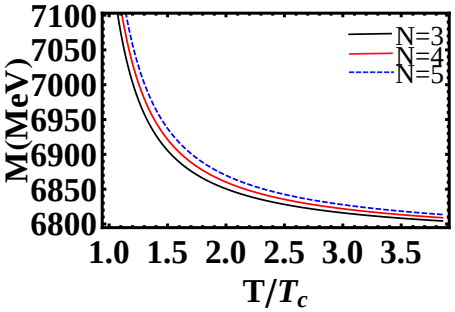

(c) b$\bar{c}$ 2S state

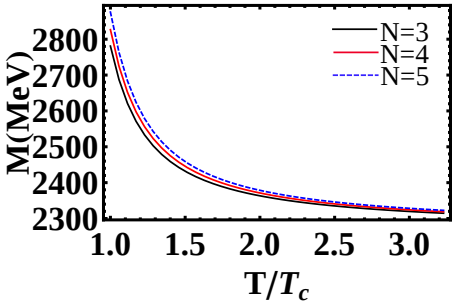

(d) c$\bar{s}$ 1S state

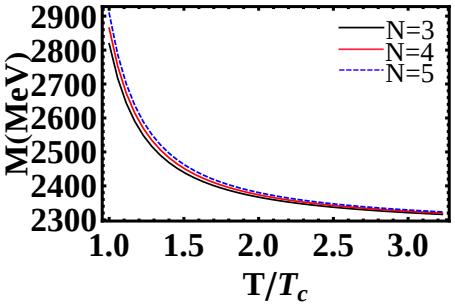

(e) c$\bar{s}$ 1P state

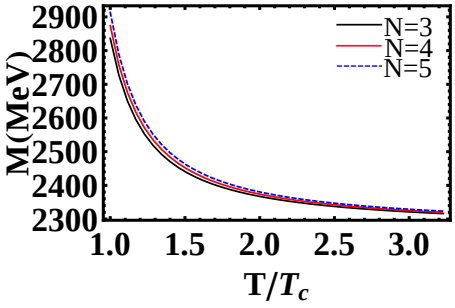

(f) c$\bar{s}$ 2S state

Figure 6.3: The mass spectra of different states of b$\bar{c}$ and c$\bar{s}$ mesons as a function of temperature T for different values of N

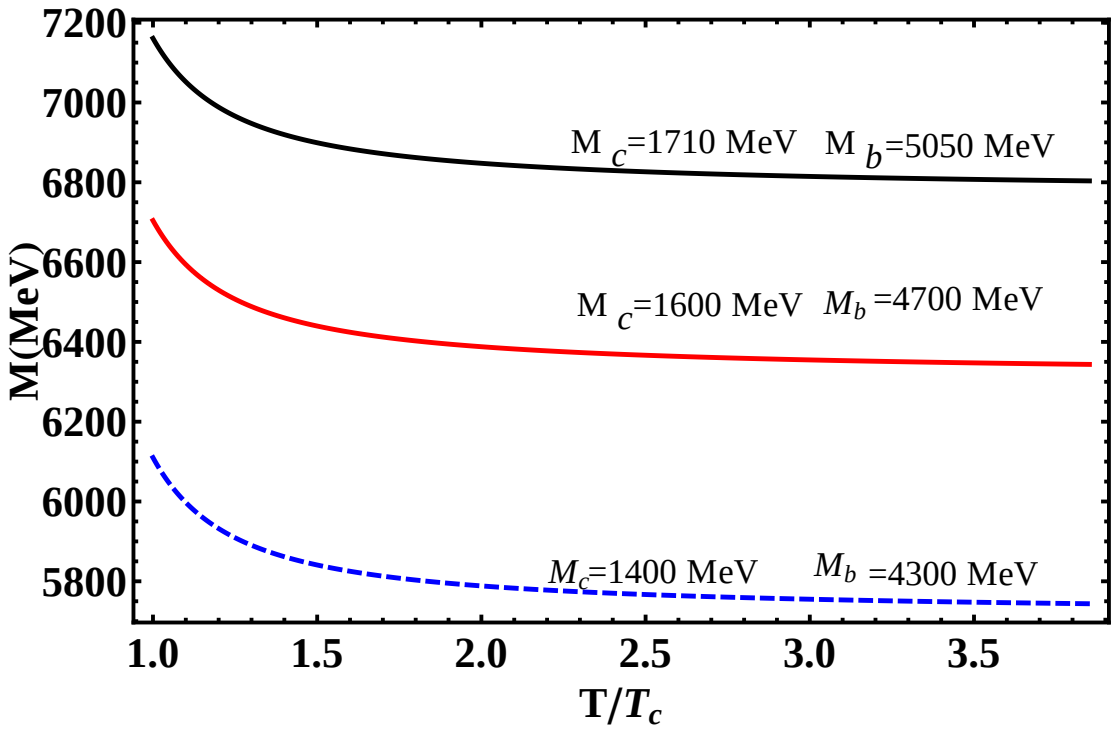

Figure 6.4: The mass spectra of b$\bar{c}$ 1S state as a function of temperature T for different quark mass at N=3

of $b\bar{c}$ and $c\bar{s}$ mesons with temperature for different dimensionality numbers. From the figure, it is clear that the mass spectra decrease with increasing temperature and increase with the increasing dimensionality number. Fig. 6.4 and Fig. 6.5 show the behavior of mass spectra of $b\bar{c}$ and $c\bar{s}$ mesons with temperature for different constituent quark masses. The mass spectra increase with increasing quark mass which is in agreement with the previous findings [14]. In Table 6.1 and Table 6.2, the dissociation temperatures for different states of $b\bar{c}$ and $c\bar{s}$ mesons are summarized. We have found that both $b\bar{c}$ and $c\bar{s}$ mesonic states can dissociate at temperatures above the critical temperature ($T_c < T_D < 2T_c$). Also, the results are compared with [5]. It is clear from the table that the increasing dimensionality number leads to increasing dissociation temperatures of $b\bar{c}$ and $c\bar{s}$ mesonic states.

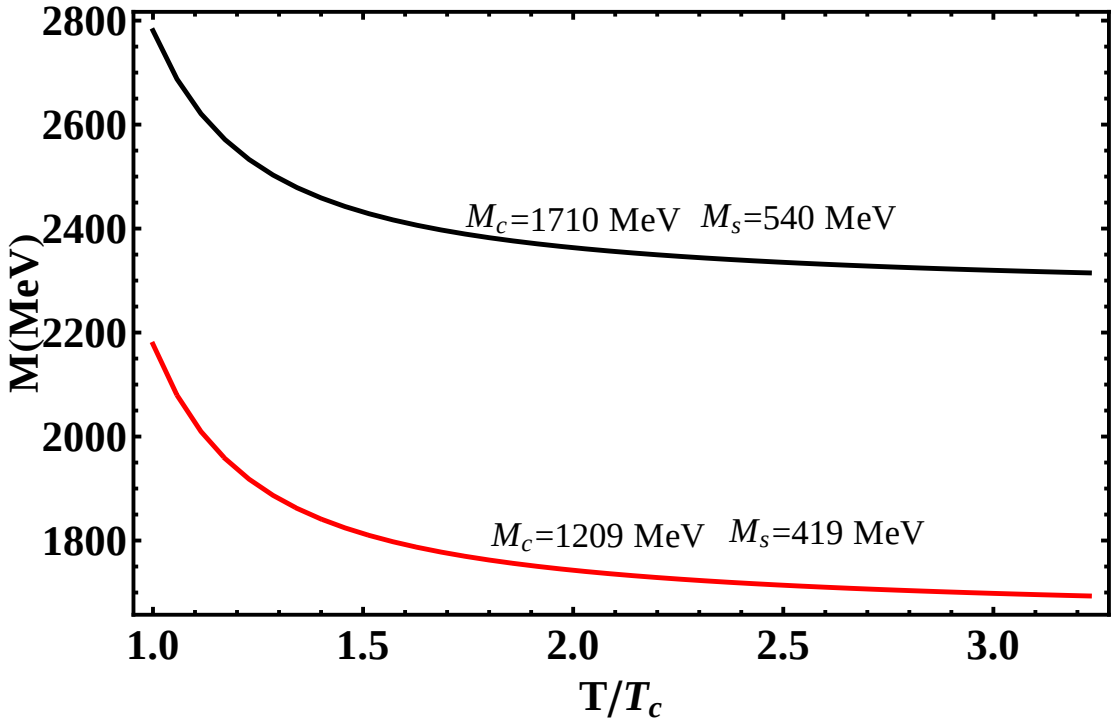

Figure 6.5: The mass spectra of $c\bar{s}$ 1S state as a function of temperature T at N=3 for different component quark mass

Bibliography

[1] T. Matsui and H. Satz, *J/ψ suppression by quark-gluon plasma formation*, Phys. Lett. B 178, 416 (1986).

[2] E. S. Swanson, *The new heavy mesons: A status report*, Phys. Rept. 429, 243 (2006).

[3] S. Godfrey and S. L. Olsen, *The exotic XYZ charmonium-like Mesons*, Ann. Rev. Nucl. Part. Sci. 58, 51 (2008).

[4] F. De Fazio, *New spectroscopy of heavy mesons*, PoS HQL 2012, 001 (2012).

[5] W. M. Alberico, S. Carignano, P. Czerski, A. De Pace, M. Nardi, and C. Ratti , *Survival of B_c mesons in a hot plasma within a potential model*, Cent. Eur. J. Phys. 12 (11), 780 (2014).

[6] C. Chao-Hsi, *Bc meson studies*, Chin. Phys. C 26 (2002).

[7] L.P. Fulcher, J. Rafelski, and R.L. Thews, *B_c Mesons as a signal of deconfinement*, arXiv:hep-ph/9905201 (1999).

[8] B. Aubert et al. [BaBar Collaboration], *Observation of a new D_s meson decaying to DK at a mass of 2.86GeV/c^2* , Phys. Rev. Lett. 97, 222001 (2006).

[9] J. Brodzicka et al. [Belle Collaboration], *Observation of a new D_{sJ} meson in $B^+ \to \overline{D}^0 D^0 K^+$ decays*, Phys. Rev. Lett. 100, 092001 (2008).

[10] B. Aubert et al. [BaBar Collaboration], *Study of D_{sJ} decays to D^*K in inclusive e^+e^- interactions*, Phys. Rev. D 80, 092003 (2009).

[11] M. Albaladejo, P. Fernandez-Soler, J Nieves, and P G. Ortega-, *Contribution of constituent quark model $c\bar{s}$ states to the dynamics of the $D^*_{s0}(2317)$ and $D_{s1}(2460)$ resonances*, Eur. Phys. J. C 78, 722 (2018).

[12] M. Abu-Shady, *Heavy quarkonia and $b\bar{c}$ mesons in the Cornell potential with harmonic oscillator potential in the N-dimensional Schrodinger equation*, Int. J. Appl. Math. Theor. Phys. 2 (2), 16 (2016).

[13] V. Agotiya, V. Chandra, and B. K. Patra, *Dissociation of quarkonium in a hot QCD medium: Modification of the inter quark potential*, Phys. Rev. C 80, 025210 (2009).

[14] M. Abu-Shady, T. A. Abdel-Karim, and E. M. Khokha, *Binding energies and dissociation temperatures of heavy quarkonia at finite temperature and chemical potential in the N-Dimensional space*, Advances in High Energy Physics, Volume 2018, Article ID 7356843 (2018).

Chapter 7

Conclusions and Future plans

Recent experiments show clear evidence for the strongly coupled nature of QGP at temperatures near the transition temperature. In this regime, QGP seems to be close to a strongly coupled Coulombic plasma with an effective coupling constant $\approx$ 0.5-1 and multiple bound states of quasiparticles. These bound states play an important role in the thermodynamics and transport properties of the QGP. Recent lattice works have found that the charmonium states and the mesonic bound states of light quarks can survive upto $T \leq 2T_c$. In this work, we have conducted a study to explore the properties of bound states in strongly coupled quark-gluon plasma.

7.1 Conclusions

The major outcomes of the present work are summarized as follows.

- The screening potential of a color charge entering into the high-density strongly coupled quark-gluon plasma is calculated using the hydrodynamic

approach.

- The screening potential is plotted as a function of r for different values of α. For smaller values of α the attractive potential vanishes. For $\alpha \geq 1$, the screening is remarkable. A minimum in the potential shows the formation of bound states.

- The temperature dependence of the screening potential between quarks in the high density strongly coupled quark-gluon plasma is investigated. A minimum in the potential near T_c shows the formation of bound states. The screening potential may lead to the expected suppression of J/ψ mesons.

- In this work, we have calculated the screening attractive potential to study the formation of bound states of quarks in a simple manner.

- We report the solution of the N-dimensional radial Schrödinger equation in which two-body potential in SCQGP is generalized. The energy eigenvalues have been calculated in N-dimensional space for any state with quantum numbers (n, l). The binding energy for the bound states of quarks is calculated by solving Schrödinger's equation using this attractive potential in three different methods. i.e., analytical exact iteration method (AEIM), power series method (PSM), and Nikiforov-Uvarov (NU) method. Thus three expressions for the binding energy of the bound state of quarks have been obtained.

- Using these results, in this work, we have calculated the masses of diquarks using the attractive screening potential in the high-density strongly coupled quark-gluon plasma.

- The results are applied for studying the properties of quarkonia (charmonium and bottomonium). The effect of temperature on binding energy and mass spectra of heavy quarkonia are studied. The dependence of binding energies of 1S and 1P charmonium and bottomonium on temperature are studied. The result is in agreement with the existing literature.

- The effect of dimensionality number on binding energy and mass spectra is also studied and compared it with previous works.

- We have determined the dissociation temperature for different states of heavy quarkonia at finite temperature and compared with the previous works.

- Also, the variations in binding energy and mass spectra of $b\overline{c}$ and $c\overline{s}$ mesons with temperature are studied and we reported the dissociation temperatures of $b\overline{c}$ and $c\overline{s}$ mesons.

- By comparing the numerical results with experimental values, we can observe that out of the three mathematical methods, the NU method has minimum error.

7.2 Future plans

In the present work, we proposed a new attractive potential and properties of bound states are studied using this potential.

- In this work, only the screening effect is considered. So in future, the present work can be extended to study all the collective effects in strongly coupled quark-gluon plasma including waves and instabilities.

- Recent trends indicate that the properties of heavy and light mesons can be studied by solving the relativistic Schrödinger equation. So in future, the relativistic Schrödinger equation can be solved within the framework of the new screening potential.
- It is possible to investigate the transport coefficients of SCQGP.
- Also, the magnetized QGP can be studied in this model.